A GAP in Form and Function: The Rac-GAP Alpha2-Chimaerin regulates Dendrite Morphogenesis and Synaptic Plasticity

by

Chris Valdez

A dissertation submitted in partial fulfillment
of the requirements for the degree of
Doctor of Philosophy
(Neuroscience)
in the University of Michigan
2016

Doctoral Committee:

Assistant Professor Asim Beg, Chair
Professor Roman Giger
Professor Richard I. Hume
Associate Professor Geoffrey G. Murphy
Professor Jack M. Parent

Dedication

To my grandparents, Daniel S. Valdez and Juanita V. Valdez,
I miss you both dearly

To my wife Yvonne M. Valdez and daughter Nora B. Valdez,
you both are more than I will ever deserve

Acknowledgements

The work presented in this thesis was made possible by the support and encouragement from numerous people. To my thesis mentor, Dr. Asim Beg, I am greatly appreciative of the scientific knowledge you have passed down to me over the years. I believe that your mentorship has made me a more determined person both in the laboratory and in life. I know that my future career as a neuroscientist will be better served having you as my graduate school mentor.

I am very thankful to my thesis committee members, Dr. Roman Giger, Dr. Rich Hume, Dr. Jack Parent and Dr. Geoff Murphy for their scientific input and personal encouragement during my graduate school career. In particular, I am very grateful for Dr. Geoff Murphy who opened up his lab, and dedicated his time to training me in the electrophysiological and behavioral techniques presented in Chapter 2 of this dissertation.

To the past and present members of Dr. Asim Beg's laboratory, I am very appreciative of your support and great conversations. In particular to our lab manager, Georgina Nicholl, you have been such a reliable force in the lab during my time as a graduate student. We have had good laughs and great collaborations, and I am very thankful for your support. In the laboratory, I had the privilege of training Alex Stanczyk, a very talented undergraduate student who provided technical assistance and data analyses to the work presented in Chapter 3 of this thesis.

To our collaborator, Dr. Erik Jorgensen from the University of Utah, I am very thankful to be included in a joint project between your laboratory and Dr. Asim Beg's laboratory. Our joint efforts resulted in a published manuscript described in Appendix 1 of this thesis.

I would like to thank my family for their support during graduate school. To my parent-in-laws, Rick and Yolanda Garcia, our many laughs and great conversations have brought light and encouragement to my journey during graduate school. To my wife, Yvonne Valdez, your support during graduate school has been so instrumental to the completion of my degree, and I look forward to the next step of our life journey. To my daughter, Nora Valdez, you are the light of my life and have kept my spirit high with your laugh and smile. I hope one day you read this dissertation, and can be proud of me. To my parents, Brenda and Steven Zachmeyer, I am thankful for your support and pride you had for me during my pursuit of a graduate education. Lastly, to my grandparents, Daniel and Juanita Valdez, there is not a day that goes by where I don't feel your encouragement and love. I think about you both everyday, during graduate school, my memories of you kept me focused and grateful for the opportunities that I've pursed in my life.

Table of Contents

List of Figures

List of Abbreviations

α1	alpha1-chimaerin
α2	alpha2-chimaerin
aCSF	artificial cerebrospinal fluid
AMPA	α-amino-3-hydroxy-5-methyl-4-isoxazolepropionic acid
APC^{Cdh1}	anaphase-promoting complex-CDC20 homologue 1
AraC	cytosine d-D-arabinofuranoside
ASD	Autism Spectrum Disorder
β-gal	β-galactosidase
BDNF	Brain-derived neurotrophic factor
C1	Diacylglycerol-binding domain
°C	Celsius
CAG	Cytomegalovirus early enhancer element, chicken beta-Actin promoter, and splice acceptor of the rabbit β-Globin gene
C. elegans	*Caenorhabditis elegans*
Caspase-3	cysteine-dependent aspartate-directed proteases
Cdc42	Cdc42-GTPase
CDK5	Cyclin-dependent kinase 5
cDNA	complementary DNA
CHN1	n-chimaerin gene

CNS	central nervous system
CPG	central pattern generator
CRMP-2	Collapsin response mediator protein family-2
CST	corticospinal tract
DAG	diacylglycerol
DCX	doublecortin
DIV	days *in vitro*
DPBS-MC	Dulbecco's phosphate buffer containing $MgCl_2$
DRG	dorsal root ganglion
DRS	Duane's retraction syndrome
EphR	Eph receptors
EPSP	excitatory postsynaptic potentials
fEPSP	field excitatory postsynaptic potential
GAPs	GTPase activating proteins
GCL	granule cell layer
GDP	guanosine diphosphate
GEFs	guanine exchange factors
GFAP	glial fibrillary acidic protein
GRIA1	glutamate receptor ionotropic AMPA 1 subunit
GRIN2B	Glutamate receptor, ionotropic, N-methyl-D-aspartate, subunit 2B
GTP	guanosine triphosphate
H9	human embryonic neural stem cells
HBSS	Hanks-buffered salt solution

HEPES	4-(2-hydroxyethyl)-1-piperazineethanesulfonic acid
LMC	lateral motor column
LTD	long-term depression
LTP	long-term potentiation
MAPs	microtubule-associated proteins
mEPSPs	miniature EPSPs
ML	molecular layer
mRNA	messenger ribonucleic acid
Mutant	gene-trap
NMDA	N-methyl-D-aspartate
NSCs	neural stem cells
Olig2	oligodendrocyte transcription factor-2
OPCs	oligodendrocyte precursor cells
P	postnatal day
PAK1	Protein activated kinase-1
PAR-3	partitioning defective protein-3
PCL	pyramidal cell layer
PFA	paraformaldehyde
PHDN1	phallotoxin
PLC	phospholipase-C_{β}
PP2B	calcineurin/protein phosphate 2B
PSD	post-synaptic density
R.P.M.	Rotations per minute

Rac1	Rac1-GTPase
RhoA	RhoA-GTPase
SGZ	subgranular zone
SH2	Src-homology-2
SSH1	Slingshot 1 phosphatases
SVZ	subventricular zone
TrkB	Tropomyosin receptor kinase B
WT	wild type

Abstract

A remarkable feature of the central nervous system is the highly choreographed wiring of neuronal circuits, which provides the structural and functional framework for cognitive abilities in humans. One critical parameter in this process is the elaboration of axonal and dendritic arbors as their size dictates the number of synaptic inputs a neuron can form. Such exquisite connectivity relies on the morphological complexity of the individual neuron. In neurons, cytoskeletal regulators dictate the extent of axonal and dendritic arborization. At the synapse, molecular mechanisms alter cytoskeletal dynamics in response to extracellular cues, thus linking neuronal morphological plasticity to synaptic activity.

A central goal in Neuroscience is to elucidate the molecular mechanisms that regulate intracellular cytoskeletal rearrangement, which mediates morphological transformations in dendritic spines. Importantly, aberrant dendritic spine morphogenesis and synaptic function are unifying features in neurodevelopmental, neuropsychiatric and neurodegenerative diseases. Defects in EphR/ephrin signaling and Rac1 function at the synapse are implicated in the etiology of neurological disorders that exhibit dendritic spine defects.

My dissertation contains three independent studies that focus on the molecular players that link structural and functional mechanisms at the synapse. First, I identified that the Rac-GAP, α2-chimaerin, is a key regulator of convergent signaling pathways

required for normal dendritic spine morphogenesis and synaptic function. Second, I demonstrate that the loss of α2-chimaerin alters proliferation in the adult dentate gyrus that may correlate to a reduction in basal anxiety in rodents. Third, I characterized an excitatory ionotropic GABA receptor in the nematode *Caenorhabditis elegans*, and determined it plays a role in extrasynaptic spillover transmission. Together, these data shed new insight into the molecular mechanisms that regulate dendritic spine morphogenesis and synaptic function, and demonstrate that α2-chimaerin is poised at the nexus of critical signaling pathways to transduce extracellular synaptic signaling to intracellular regulation of dendritic spines and synapses.

Chapter 1

Introduction

The functional unit of neuronal communication

Neurons are the fundamental computational unit of the brain, and their precise connectivity underlies neurological control over diverse behaviors and functions (Douglas and Martin, 2004; Dumont and Robertson, 1986). Neuronal connectivity and information processing is dependent on proper signaling at subcellular sites called synapses, which are highly specialized structures where electrical and/or chemical signals are communicated between cells. In the human brain, a cubic millimeter of cortex contains approximately 26,000 neurons forming 900 billion synaptic connections (Alonso-Nanclares et al., 2008). Astoundingly, the human brain has ~125 trillion synapses (Micheva et al., 2010; Risi et al., 2014). Cortical function, similar to other regions of the central nervous system (CNS), relies on proper synapse formation and accurate wiring of neuronal circuits during development, which are critical for higher cognitive function (Goodman and Shatz, 1993).

An important parameter for precise circuit assembly is outgrowth and arborization of specialized neuronal processes called dendrites and axons (Goodman and Tessier-Lavigne, 1997; Katz and Shatz, 1996). In fact, the number of synaptic inputs a cell makes and receives is determined by the neuronal arbor size and complexity (Goodman

and Shatz, 1993). Thus, the regulation of axonal and dendritic morphology is critically important for the appropriate formation and function of neuronal circuits.

Principles of axonal development

Axonal arborization is a unique process in that the immature axon must extend and migrate, often up to several feet in length, before it elaborates to form a synapse with a target cell (Dickson, 2002). Axon migration relies on extracellular environmental cues that act like "*traffic signs*" to guide axonal outgrowth to the target cell (Dickson, 2002; Guan and Rao, 2003). The extracellular environment is complex because it contains both attractive and repulsive guidance cues causing axonal outgrowth to be a dynamic process of progressive and regressive events (Huber et al., 2003; Stoeckli and Landmesser, 1998). Processing of the extracellular environment takes place at the axonal growth cone, a highly motile and specialized structure, which is densely populated by guidance receptors that bind to guidance cues present in the extracellular environment (Bashaw and Klein, 2010; Dickson, 2002). Through surface receptor interactions with extracellular signals, the axonal growth cone computationally decodes the extracellular environment, and activates concerted intracellular pathways that steer axonal outgrowth and retraction (Figure 1.1B).

For example, the corticospinal tract (CST) is a group of cortical motor axons whose cell bodies reside in Layer V of the cortex and extend axons to the spinal cord to innervate ventral motor neurons, thereby linking higher brain processing to voluntary skilled-movement (Figure 1.1A) (Canty and Murphy, 2008; Donatelle, 1977). Decades of elegant research have demonstrated that attractive and repulsive extracellular signals

are utilized to appropriately guide the CST axonal trajectory (Canty and Murphy, 2008; Porter and Lemon, 1993).

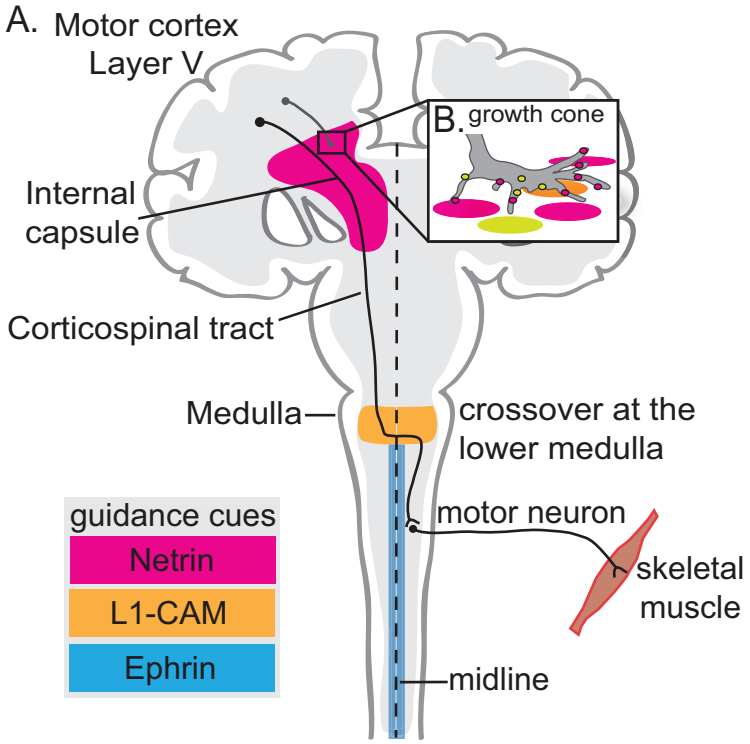

Figure 1.1 Overview of the corticospinal tract

(A) The CST is a pathway that connects cortical motor processing to voluntary skilled-movement. The tract originates from cortical motor axons that migrate into the spinal cord where they innervate interneurons or directly synapse on motor neurons that target skeletal muscle. During development, key guidance signals, Netrin, L1-CAM and Ephrin, guide the developing CST axon to migrate through the internal capsule, decussate at the lower medulla and maintain spinal cord symmetry, respectively. These signaling ligands interact with guidance receptors concentrated on the axonal growth cone.

(B) The magnified image illustrates an axonal growth cone from a developing motor neuron. At the growth cone, different guidance receptors interact with ligands in the extracellular environment. The growth cone decodes the complex extracellular environment, through the combination of guidance receptor signaling and intracellular processing, and steers the migrating axon to its appropriate target.

Initially, the chemoattractant Netrin guides CST motor axons through the internal capsule into deep brain structures (Finger et al., 2002). In the lower medulla, the L1 cell adhesion molecule (L1-CAM) causes the majority of CST migrating axons to cross over to the contralateral side of the spinal cord (Cohen et al., 1998; Dobson et al., 2001;

Jakeman et al., 2006). As CST axons descend the contralateral cord, repulsive ephrin signaling prevents the re-crossing of axons across the midline (Dottori et al., 1998; Kao et al.; Kullander et al., 2001). The CST axons migrate until they are signaled to exit the CST starting at the cervical segment and ending at the lower sacral segments (Porter and Lemon, 1993). As the CST axons exit they enter the spinal cord gray matter; here, the axon arborizes forming synapses with interneurons or anterior horn motor neurons that innervate skeletal muscle (Nudo and Masterton, 1990). Overall, the CST is an example of the elegant coordination that exists between guidance cues and growth cone receptors to precisely guide axonal trajectories and arborization to form functional neuronal circuits.

Despite these seminal discoveries characterizing axon guidance molecules in vertebrate models, only a handful of human neurological disorders have been identified as direct results of primary errors in axon arborization and guidance (Engle, 2010; Nugent et al., 2012; Yüksel et al., 2010). A contributing factor is that guidance molecules play a developmental role in cardiogenesis, angiogenesis and bone formation, and genetic mutations in these systems often lead to embryonic lethality before potential neurological deficits manifest and functional errors can be characterized. (Carmeliet and Tessier-Lavigne, 2005; Serini and Bussolino, 2004).

Principles of dendritic development

The proper formation and long-term maintenance of dendrites are crucial for neuronal connectivity and function (Bourne and Harris, 2008). During early development, dendrites and dendritic spines undergo constant structural rearrangement to facilitate proper wiring in response to synaptic activity (Ethell and Pasquale, 2005; McAllister,

2000). Later, cytoskeletal dynamics become dissociable in that a stable dendritic receptive field can be maintained, yet dendritic spines retain highly plastic properties in response to individual synaptic inputs (Ethell and Pasquale, 2005; Koleske, 2013). Therefore, the precise spatiotemporal regulation of molecules that control dendritic cytoskeletal plasticity is important for the proper formation of dendritic arbors and neuronal function.

Dendritic arborization

The dendritic cytoskeleton is composed of microtubule bundles that are bridged by microtubule-associated proteins (MAPs) (Caceres et al., 1983). Microtubules run parallel to the dendritic shaft to provide structural integrity for long-term maintenance of dendritic arbors (Figure 1.2) (Gray, 1959). Initial contact with immature axonal terminals can stabilize a dendrite and activate cytoskeletal mechanisms that induce the formation of secondary and tertiary dendritic branches (Goodman and Shatz, 1993). Sustained synaptic activity can stabilize these higher order dendritic branches; likewise, the loss/reduction of activity can destabilize the segment simplifying dendritic complexity (Carlisle and Kennedy, 2005; Goodman and Shatz, 1993). As a result of constant outgrowth and retraction, the available area that afferent fibers can sample is determined by the dendritic branch pattern and total length of the dendritic field (Goodman and Shatz, 1993). Following the formation of the dendritic arbor, cytoskeletal plasticity becomes largely refined to dendritic spines allowing the neuron to retain long-term integrity of dendritic arbors while fine tuning individual connections (Carlisle and Kennedy, 2005).

Dendritic spines

Dendritic spines are fine neuronal processes that spatially restrict activity-dependent changes in one spine, while leaving neighboring protrusions unmodified (Yuste, 2010). During the development of neuronal connectivity, spines often arise from dendritic filopodia, which are immature protrusions that densely populate the developing dendrite (Fiala et al., 1998). Upon spinogenesis and synaptogenesis, postsynaptic mechanisms initiated by adhesion/scaffolding proteins at the filopodial-tip, stabilize and enlarge the structure, promoting its conversion to a dendritic spine (Maletic-Savatic et al., 1999; Niell et al., 2004). The dynamic cycling of proteins at the developing postsynaptic surface is coupled to rapid changes in dendritic spine morphology, which underlie the functional/structural cohesiveness of neuronal connectivity. For example, blockade of synaptic receptors can increase spine density and alter spine morphology (Segal and Andersen, 2000). These plastic properties of dendritic spines are considered compensatory mechanisms that maintain normal synaptic transmission. Importantly, dysregulation of dendritic spine density, morphology and function are known to be associated with cognitive pathologies and neurodevelopmental delays (Fiala et al., 2002; Penzes et al., 2011).

From a molecular standpoint, the dendritic spine cytoskeleton is composed mostly of filamentous (F)-actin (Figure1.2A-B) (Carlisle and Kennedy, 2005; Matus, 2000; Zhang and Benson, 2001). In response to cell-surface signaling, F-actin can polymerize forming branched actin filaments that enlarge the spine head to facilitate incorporation of additional synaptic receptors (Korobova and Svitkina, 2010; Zhang and Benson, 2001). The dendritic spine head is connected to the dendritic shaft by a thin

and narrow neck. The spine neck consists mostly of linear F-actin that can elongate or shorten in response to surface signaling (Carlisle and Kennedy, 2005; Matus, 2000).

This form of structural plasticity can regulate Ca^{2+} diffusion kinetics between the dendritic spine head and shaft; thereby affecting Ca^{2+}-mediated pathway activation along a single dendrite (Bloodgood and Sabatini, 2005; Noguchi et al., 2005). The precise regulation of molecules that control the dendritic spine cytoskeleton can have a profound influence on the formation and maintenance of neural circuits and brain function, including learning and memory (Carlisle and Kennedy, 2005; Chen et al., 2007).

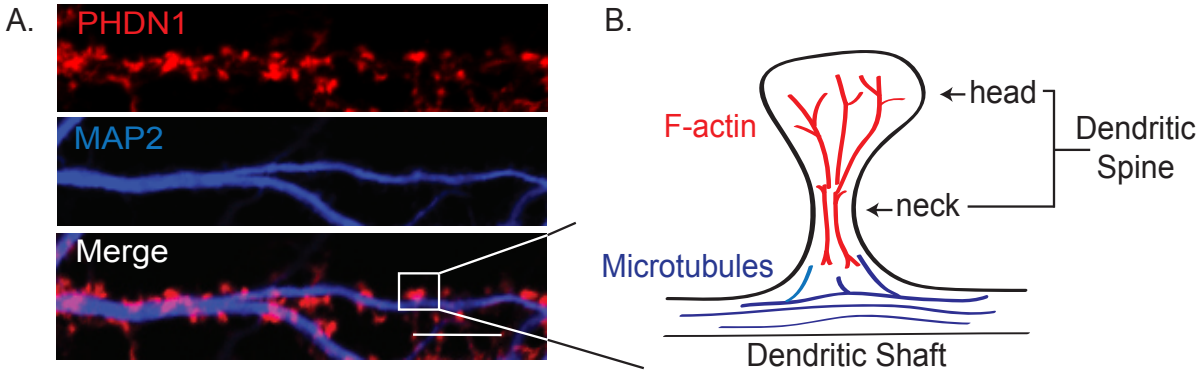

Figure 1.2 The dendritic cytoskeleton

(A) The micrographs illustrate an immunostained dendritic segment from a mouse hippocampal neuron at 18 days *in vitro* (DIV). F-actin is labeled with fluorescently tagged phallotoxin (PHDN1) (red) and is presented as small dense clusters, which are localized to dendritic spines. The MAP2 antibody (magenta) marks microtubules, which are localized in the dendritic shaft. The merged image demonstrates regional-specificity of microtubules and F-actin in dendrites and dendritic spines, respectively; scale bar equals 10μm.

(B) A typical dendritic spine (white box) is schematized demonstrating the compartmentalization of cytoskeleton proteins and key anatomical structures of the dendrite and dendritic spine.

Rho-GTPases

Decades of research have characterized Rho-GTPases as key regulators of the actin cytoskeleton (Hall, 1998; Nakayama et al., 2000; Tashiro et al., 2000). Rho-GTPases are a subgroup of the Ras superfamily of GTPases and consist of three main subclasses: RhoA-GTPase (RhoA), Rac1-GTPase (Rac1) and Cdc42-GTPase (Cdc42). In the cell, Rho-GTPases function as molecular switches cycling between an active and inactive state, the ratio of which, determines their local activity (Figure 1.3) (Etienne-Manneville and Hall, 2002). In general, Rho-GTPase downstream effector activity coordinates multiple signaling pathways that influence synapse formation, gene expression and membrane trafficking (Etienne-Manneville and Hall, 2002; Heasman and Ridley, 2008).

During dendrite outgrowth, extracellular cues activate membrane receptors that engage Rho-GTPases. For example, surface signaling can localize Rac1 and Cdc42 activity to the distal end of the growing neurite and promote F-actin branching, resulting in outgrowth and elaboration of dendritic arbors (Nobes and Hall, 1995). The spatial regulation of Rac1 and Cdc42 activity are required for proper dendritic outgrowth, as exogenous over-expression of constituently active Rac1 abrogates normal physiological dendritic complexity (Aoki et al., 2004; Nakayama et al., 2000). Interestingly, surface signaling that locally induces high Rac1 activity is also associated with a reduction in RhoA activity (Machacek et al., 2009). Conversely, RhoA activation is generally associated with inhibition of neurite initiation and retraction (Tolias et al., 2011). The antagonistic roles between RhoA and Rac1/Cdc42 suggest Rho-GTPases act in a coordinated manner to develop and maintain neuronal arbors (Luo, 2000).

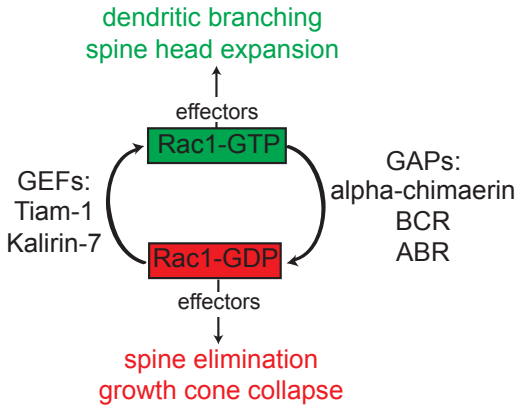

Figure 1.3 Schematic of Rac1 signaling

Rac1 activity engages various effectors that can elaborate or simplify axonal and dendritic arbors. The Rac1-GTPase is a molecular switch that cycles between active GTP-bound and inactive GDP-bound states. GEFs facilitate the active Rac1-GTP form by inducing the release of GDP from Rac1 and promoting GTP binding. GAPs inactivate Rac1-GTP by accelerating the intrinsic GTPase activity of Rac1 thus promoting the Rac1-GDP form.

In dendritic spines, Rho-GTPase activity reorganizes the actin cytoskeleton (Hall, 1998; Luo, 2000). For example, RhoA can promote F-actin depolymerization inducing dendritic spine retraction; whereas, Rac1 and Cdc42 can promote F-actin polymerization causing dendritic spine elongation (Etienne-Manneville and Hall, 2002; Govek et al., 2005; Wiens et al., 2005). To function properly in dendritic spines Rho-GTPases require precise spatiotemporal control, as dysregulation, which results from aberrant F-actin dynamics, manifests as abnormal dendritic spine morphologies and synaptic connectivity often observed in intellectual disabilities (Ramakers, 2002; Schaefer et al., 2014).

GEFs and GAPs

Cell surface receptors can modulate the spatiotemporal activity of Rho-GTPases at dendritic spines (i.e. Rac1, RhoA and Cdc42) (Luo, 2000; Tolias et al., 2011). However, membrane receptors rarely interact directly with Rho-GTPases; instead, they interact with Rho-GTPase modulators such as guanine exchange factors (GEFs) and GTPase activating proteins (GAPs) that regulate the active and inactive state of Rho-

GTPases, respectively (Etienne-Manneville and Hall, 2002; Heasman and Ridley, 2008; Tashiro et al., 2000). GEFs activate Rho-GTPases by promoting their guanosine triphosphate (GTP)-bound form, and GAPs inactivate Rho-GTPases facilitating a guanosine diphosphate (GDP)-bound state (Figure 1.3) (Cherfils and Zeghouf, 2013). Surface signaling along the dendrite and dendritic spine can target GEFs or GAPs to the membrane (Bos et al., 2007). Therefore, to expedite specific control over neuronal morphology, the spatiotemporal cycling of Rho-GTPases and their G-protein modulators (GEFs and GAPs) are critical for proper circuit formation and function.

For example, surface signaling during development can recruit GEFs or GAPs to modulate Rac1 activity at nascent synaptic connections (Figure 1.4). As a result, GEFs induce active cycling of Rac1-GTP, where its interactions with downstream effectors induce actin polymerization in the dendritic spine causing spine head growth. Likewise, GAP protein interactions inactivate Rac1-GTP, which destabilizes polymerized actin causing dendritic spine head collapse. Moreover, synaptic activity in mature circuits can recruit GEFs and GAPs to dendritic spines likely to regulate spine morphogenesis through modulation of Rho-GTPase activity (Liang et al., 2004; Nakayama et al., 2000; Oh et al., 2010; Tolias et al., 2011). However, the molecular logic by which diverse surface receptors uniquely recruit GEFs and GAPs in the context of neuronal connectivity development and adult circuits is largely unknown.

Eph receptors regulate Rho-GTPases

In neurons, mounting evidence suggests that the Eph receptor and ephrin (EphR/ephrin) complex can recruit GEFs and GAPs, to execute precise control over Rac1 essential for local actin rearrangement in dendritic spines observed in the

maturing and adult brain (Kullander and Klein, 2002). Eph receptors are the largest tyrosine kinase receptor family in vertebrates and are divided into two groups, EphA and EphB, determined by their extracellular domain and ligand homology (Gale et al., 1996; Holder et al., 1998). While some exceptions exist, EphA receptors bind to ephrin-A ligands while EphB receptors bind ephrin-B ligands (Kullander and Klein, 2002).

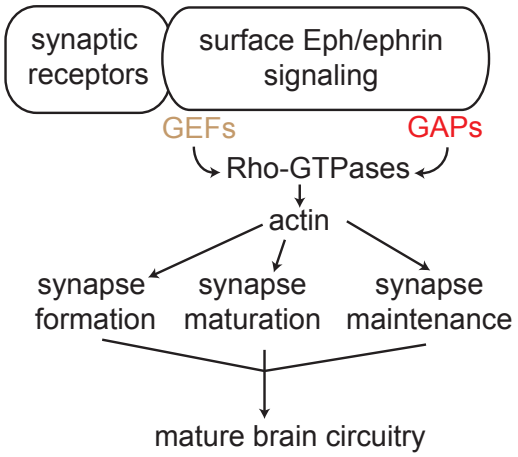

Figure 1.4 The EphR/ephrin complex participates in the formation, maturation and maintenance of synapses in the developing and mature brain

EphR/ephrin signaling can activate GEFs and GAPs to execute precise control over Rho-GTPases, whose downstream activity reorganizes the actin cytoskeleton in dendritic spines and synapses. Additionally, Eph receptors can interact with ion channels to cluster them at the synapse, and induce post-translational modifications that alter their signaling properties.

EphB

During development, highly motile dendritic filopodia sample presynaptic partners and, upon contact, the filopodia can stabilize facilitating initial cell-to-cell contact required for spinogenesis, synaptogenesis and synaptic maintenance (Okabe et al., 2001; Zhang and Benson, 2000). In general, axonal ephrin-B interacts with postsynaptic EphB receptors, whose downstream activity stabilizes initial contact between the immature axonal terminal and dendritic protrusion (Kayser et al., 2008). The EphB tyrosine kinase receptor links dendritic filopodia cytoskeletal motility to the structure's ability to recognize axonal partners, provide trans-synaptic adhesion and initiate synapse formation (Kayser et al., 2008). For example, immature hippocampal neurons

that lack EphB2 exhibit reduced dendritic filopodia motility and synapse formation. The expression of constitutively active Rac1 effectors in EphB2 knockout neurons can reinstate filopodia movement demonstrating that Rac1-mediated actin dynamics drive filopodia motility; however, this manipulation is not sufficient to direct normal synapse formation (Kayser et al., 2008). Instead, exogenously expressed EphB2 can localize at the dendritic filopodial tip and rescue filopodia motility and synapse formation, indicating that EphB signaling links Rac1-mediated filopodia motility to the structure's ability to engage axonal partners (Kayser et al., 2008).

During critical periods of neuronal connectivity, ephrin-B1-treatment of hippocampal neurons can activate the postsynaptic EphB2 receptor to induce clustering of the Rac1-GEF, Kalirin-7 to synaptic membranes, which can activate Rac1 (Rac1-GTP) (Kayser et al., 2008; Penzes and Jones, 2008). As a result, ephrin-B1 treatment leads to downstream phosphorylation and synaptic clustering of the Rac1 effector, Protein activated kinase-1 (PAK1) leading to alterations of F-actin dynamics at the immature dendritic protrusion and inducing filopodia actin rearrangement to form a dendritic spine (Dalva et al., 2000; Dunaevsky et al., 1999; Hall, 1998; Kayser et al., 2008; Penzes and Jones, 2008). On the other hand, the loss of EphB2 signaling negatively impacts spinogenesis causing a reduction in spine density observed in developing neurons and mature dendrites, indicating a critical role of surface EphB2-mediated Rho-GTPase regulation in dendritic spine formation and stability (Dalva et al., 2000; Takasu et al., 2002).

During synaptogenesis and in mature circuits, the ephrin-B1 ligand promotes surface interactions between EphB2 and the N-methyl-D-aspartate receptor (NMDA

receptor) (Dalva et al., 2000; Takasu et al., 2002). EphB2 and NMDA receptors directly interact causing NMDA receptor clustering and phosphorylation of the NMDA receptor subunit, Glutamate receptor, ionotropic, N-methyl-D-aspartate, subunit 2B (GRIN2B) at the developing synapse (Dalva et al., 2000; Takasu et al., 2002). These signaling events are thought to drive intracellular mechanisms that ensure synaptic maturation as opposed to rapid cycling of surface receptors during synaptogenesis (Antion et al., 2010; Henderson et al., 2001; Xu et al., 2011). Overall, dendritic protrusions utilize EphB signaling to engage trans-synaptic adhesion, potentiate Kalirin-7-GEF-mediated regulation of Rac1, and cluster NMDA receptors promoting dendritic spine and synapse maturation.

EphA

In a mature circuit, a synapse will undergo various states of surface receptor remodeling that are coupled to rapid restructuring of dendritic spine morphology (Matus, 2000; Portera-Cailliau et al., 2003). The EphA4 receptor is positioned at the postsynaptic surface and can induce distinct changes to dendritic spine morphology that result in reorganization of the postsynaptic density (Zhou et al., 2012). At the dendritic spine, rapid minute-based EphA/ephrin-A3 signaling activates Cofilin, an actin filament depolymerizing/severing factor that redistributes F-actin from the dendritic spine head to the neck where it interacts with actin-regulatory proteins Slingshot 1 phosphatases (SSH1) and calcineurin/protein phosphatatase 2B (PP2B) leading to dendritic spine elongation (Zhou et al., 2012). If EphA/ephrin-A3 signaling prolongs from minutes to hours it induces synaptic remodeling, resulting in the relocation of the postsynaptic density from the dendritic spine to the dendritic shaft. Concurrently, the dendritic spine

retracts into the dendritic shaft, simplifying the overall protrusion density (Murai et al., 2003; Zhou et al., 2012). Thereby, surface EphA receptor signaling can transiently regulate discrete dendritic spine morphologies, and control synaptic remodeling through intracellular pathways that reorganize the actin cytoskeleton at excitatory synapses.

While EphA4 signaling can engage downstream Rac1-mediated regulation over dendritic spine morphology, emerging evidence demonstrates that EphA4 signaling is important for synaptic plasticity and learning (Fu et al., 2011; Murai et al., 2003). For example, homeostatic plasticity is a synaptic refinement mechanism where neuronal excitability is scaled in response to changes in the strength and number of synaptic connections (Bourne and Harris, 2011; Turrigiano, 1999; Turrigiano and Nelson, 2000). This form of synaptic refinement is thought to prevent unconstrained changes in synaptic strength, and is essential for maintaining the stability of neuronal networks.

Bicuculline treatment of cultured hippocampal neurons blocks inhibitory transmission leading to elevated excitatory synaptic activity (Fu et al., 2011; Jensen et al., 2002). In response to elevated synaptic activity *via* Bicuculline treatment, the EphA4 receptor is phosphorylated, and promotes the removal of the α-amino-3-hydroxy-5-methyl-4-isoxazolepropionic acid receptor (AMPA receptor), a glutamate receptor that generates excitatory postsynaptic potentials (EPSP) at the synaptic surface (Fu et al., 2011). Specifically, EphA4 activation leads to interactions with the ubiquitin ligase anaphase-promoting complex-CDC20 homologue 1 (APC^{Cdh1}) causing the AMPA receptor to undergo ubiquitin proteasomal degradation (Fu et al., 2011). As a result, chronic EphA4 activity results in reduced frequency and amplitude of miniature EPSPs (mEPSPs), an electrophysiological measurement of small spontaneous synaptic activity,

suggesting that EphA4 signaling refines synaptic excitability in response to elevated transmission (Fu et al., 2011). Furthermore, EphA4-knockout neurons treated with Bicuculline, lack the compensatory downregulation of synaptic AMPA receptors, and exhibit a heightened synaptic load of AMPA receptors, as detected by biochemical analysis of the glutamate receptor ionotropic AMPA 1 subunit (GRIA1), in synaptosomal fractions (Fu et al., 2011; Matsuzaki et al., 2001; Murai et al., 2003). Additionally, the loss of EphA4 signaling results in irregular dendritic spine morphologies and negatively affects induced circuit-level plasticity in the hippocampus (Murai et al., 2003). These results demonstrate that postsynaptic EphA4 signaling can induce functional changes at the synapse in response to unconstrained deviations in neuronal transmission. However, unlike the EphB receptor, our understanding of Rho-GTPase regulators that act downstream of EphA4 signaling at the synapse, are largely unknown.

Various GEFs and GAPs are expressed during critical developmental periods of neuronal connectivity, and are also detected in mature neurons where synaptic plasticity is refined in response to afferent input (Etienne-Manneville and Hall, 2002; Govek et al., 2005; Hall, 1998; Luo, 2000). These observations suggest that EphA and EphB receptors may engage different GEFs or GAPs throughout an animal's lifetime. In addition to the functional role of EphA and EphB receptors, the loss of either isoform results in irregular dendritic spine morphologies, suggesting that Eph receptors are required to control dendritic spine morphogenesis (Carlisle and Kennedy, 2005; Henkemeyer et al., 2003; Murai et al., 2003). Our lack of understanding of the molecular interplay between structural/functional synaptic mechanisms that underlie normal cognitive function and the prevalence of spine abnormalities observed in intellectual

disabilities highlights the necessity to identify and characterize downstream EphR effectors in the brain (Figure 1.4) (Gerlai, 2001; Tolias et al., 2011).

The n-chimaerin gene

The n-chimaerin gene (*CHN1*) was discovered in the laboratory of Dr. Louis Lim in 1990 at University College London. N-chimaerin was identified from a complementary DNA (cDNA) screen conducted in human and rat brains (Hall et al., 1990). The messenger ribonucleic acid (mRNA) levels were found to be highest in the cerebral cortex and hippocampus, suggesting a potential role in higher order function such as learning and memory (Hall et al., 1990; Lim et al., 1992). Two gene isoforms, alpha1 (α1)- and alpha2-chimaerin (α2), are produced from the n-chimaerin locus through alternative promoters (Figure1.5) (Hall et al., 1993; Lim et al., 1992). Both α-chimaerin isoforms share identical diacylglycerol-binding (C1) and GTPase-activating protein (GAP) domains, but they differ in that the α2 isoform contains an N-terminal Src-homology-2 (SH2) domain that is absent from the α1 isoform (Hall et al., 1993).

From a signaling perspective, the C1 domain binds diacylglycerol (DAG), causing translocation of α-chimaerins from the cytosol to the plasma membrane (Buttery and Beg et al., 2006; Herrera and Shivers, 1994). The GAP domain is highly selective for Rac1 and, to a lesser extent, Cdc42 (Hall et al., 1993). The SH2 domain in α2-chimaerin binds phosphotyrosine residues, and has been shown to interact with several receptor tyrosine kinases (Beg et al., 2007; Iwasato et al., 2007; Wegmeyer et al., 2007a). Sequence analysis revealed ~97% homology between human and rat α1-chimaerin protein, and ~96% homology between the human and mouse α2-chimaerin protein (Hall et al., 2001; Lim et al., 1992). This striking sequence conservation suggests these

proteins retained a highly conserved function throughout evolution (Hall et al., 1990). Over the last two decades, research from several groups has identified physiological roles for the α-chimaerins, which are summarized below.

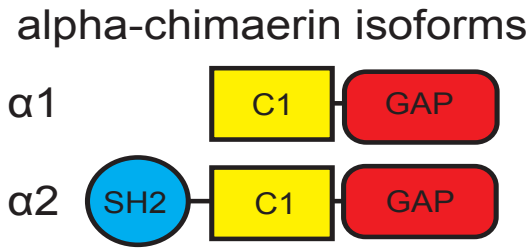

Figure 1.5 Alpha-chimaerin

The α1- and α2-chimaerin isoforms share identical C1 and GAP domains. The C1 domains can bind to diacylglycerol, and the GAP domains exhibit high specificity for Rac1. The α2-chimaerin isoform exhibits a unique N-terminal SH2 domain that can interact with tyrosine kinase receptors.

Alpha1-chimaerin

Rapid changes in dendritic spine structure are coupled to the dynamic cycling of cell surface receptors, whose cooperative activity underlies subcellular facets of synaptic plasticity (Bourne and Harris, 2008; Fischer et al., 1998). Importantly, dysregulation of dendritic spine density, morphology and function are known to be associated with cognitive pathologies and neurodevelopmental delays (Penzes et al., 2011). Alpha1-chimaerin is an essential Rac1-GAP that contributes to dendritic arborization (Buttery and Beg et al., 2006; Van de Ven et al., 2005). In neurons, basal α1-chimaerin is highly regulated and targeted for rapid polyubiquitination-dependent and proteasomal degradation; however, synaptic signaling can stabilize α1-chimaerin preventing its basal degradation (Marland et al., 2011). More specifically, receptor-mediated activation of phospholipase-C_{β} (PLC) increases local diacylglycerol production, which interacts with the C1 domain of α1-chimaerin promoting its translocation to the membrane (Buttery and Beg et al., 2006).

As an essential Rac-GAP protein, too much or too little α1-chimaerin significantly modifies Rac1-GTP levels, and as a result α1-chimaerin can significantly alter the dendritic arbor. The overexpression of α1-chimaerin reduces dendritic branching and prunes dendritic spines simplifying the arbor (Buttery and Beg et al., 2006). The suppression of α1-chimaerin causes spine dysmorphogenesis highlighted by an increase in filopodia-like protrusions and atypical dendritic spines, which exhibit multiple protrusions that emit from the spine head suggesting loss of its precise regulation may prevent proper dendritic arbor maturation (Buttery and Beg et al., 2006).

Alpha2-chimaerin

A decade of research revealed that α2-chimaerin is essential for axon guidance in sensory neurons of the dorsal root ganglion, the corticospinal tract, the spinal cord central pattern generator, and spinal motor neurons. Similar to other systems, axonal guidance in the spinal cord is mediated by attractive and repulsive signals that engage Rho-GTPases for proper axonal outgrowth. As an essential effector, α2-chimaerin interacts with guidance receptors such as the neuropilin-1/Plexin-A receptor complex and EphA and EphB receptor protein tyrosine kinases, which link membrane signaling to actin dynamics at the migrating axon for proper circuit formation.

Alpha2-chimaerin in the dorsal root ganglion

In the spinal cord, dorsal root ganglion (DRG) neurons link sensory afferent information from the periphery to the brain. The Semaphorin-1A and Neuropilin-1/Plexin-A signaling complex maintain proper axon guidance for DRG neurons by preventing irregular axonal outgrowth during development (Figure 1.6) (Nakamura et al., 2000). Intracellular processing of Semaphorin1A leads to phosphorylation of Collapsin

response mediator protein family-2 (CRMP-2) by Cyclin-dependent kinase 5 (CDK5), causing growth cone collapse and retraction of the migrating axon (Huber et al., 2003; Nakamura et al., 2000). Alpha2-chimaerin is essential for Semaphorin signaling in DRG axonal migration, as it interacts with the Neuropilin1/Plexin-A receptor complex, CDK5 and CRMP2. Mutations to the SH2 and GAP domains of α2-chimaerin eliminate CDK5 and CRMP2 interactions, respectively, and as a result block Semaphorin induced growth cone collapse in DRG neurons (Brown et al., 2004). The α2-chimaerin/CDK5 interaction likely localizes the complex to the growth cone where the GAP domain of α2-chimaerin inhibits Rac1-GTP, rearranging the cytoskeleton to induce growth cone collapse. The α2-chimaerin/CRMP2 interaction may place CRMP2 in proximity to CDK5 leading to CRMP2-phosphorylation, which is also required for Semaphorin induced growth cone collapse. Taken together, these data suggest that α2-chimaerin links Semaphorin signaling and actin dynamics at the growth cone in DRG neurons (Figure 1.6) (Brown et al., 2004).

Alpha2-chimaerin signaling in the corticospinal tract

The EphA4 tyrosine kinase receptor controls multiple axon guidance steps in locomotor circuitry such as the corticospinal tract (Beg et al., 2007; Iwasato et al., 2007; Wegmeyer et al., 2007b). The CST is a group of axonal fibers from the motor cortex that largely crossover at the lower medulla and descend the contralateral spinal cord to target ventral motor neurons (Figure 1.1). During CST development, EphA4 receptor signaling triggers axonal growth cone collapse preventing aberrant ipsilateral misprojections (Canty et al., 2006). As a result, the loss of EphA4 activity leads to abnormal bilateral organization of the CST causing synchronous hindlimb movement

(Coonan et al., 2001; Dottori et al., 1998). The intracellular effector that transduces EphA4 signaling in CST axon migration had yet to be identified as several candidates, such as Ephexin and Vav1, failed to phenocopy hindlimb synchrony in EphA4 mutant mice (Bashaw and Klein, 2010; David and Lacroix, 2003; Yoshida et al., 2006). Therefore, an unknown effector was required for EphA4 signaling in CST axonal migration.

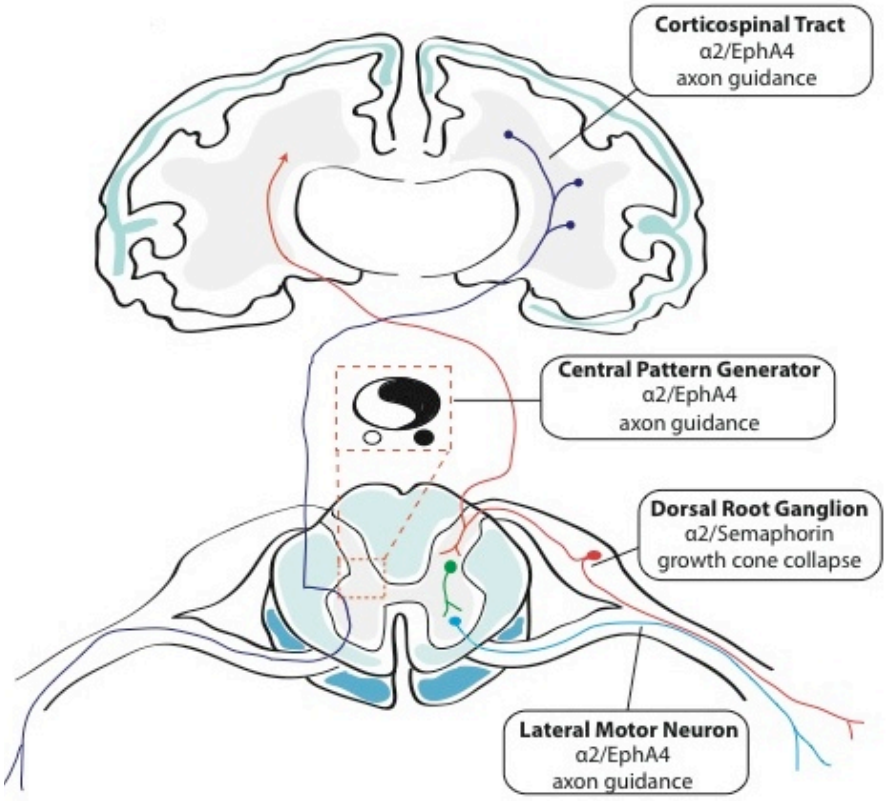

Figure 1.6 Alpha2-chimaerin is an essential effector for locomotor circuit assembly
The schematic illustrates a decade of research that has identified distinct neuronal populations in the motor cortex and spinal cord that utilize α2-chimaerin for axon guidance. Surface receptors such as EphA and Semaphorin utilize α2-chimaerin effector processing to engage rapid changes in actin at the axonal growth cone during the assembly of locomotor circuits.

The α2-chimaerin Rac-GAP was identified to be an essential intracellular EphA4 protein effector in the CST (Beg et al., 2007; Iwasato et al., 2007; Wegmeyer et al., 2007a). Several research groups generated α2-chimaerin knockout mice and observed a synchronous hindlimb gate that phenocopied the EphA4 mutant mouse (Beg et al., 2007; Iwasato et al., 2007; Wegmeyer et al., 2007a). CST pathway analysis in α2-chimaerin mutant mice demonstrated aberrant bilateral organization as previously observed in the EphA4 knockout mouse (Coonan et al., 2001; Dottori et al., 1998). Therefore, α2-chimaerin is a highly dedicated EphA4 effector required for the assembly of CST locomotor circuits, which control voluntary movement (Figure 1.6) (Beg et al., 2007; Evarts, 1981; Iwasato et al., 2007; Wegmeyer et al., 2007a).

Alpha2-chimaerin signaling in the central pattern generator

In contrast to the CST, the central pattern generator (CPG) is an autonomous neuronal network localized within the spinal cord and does not rely on top-down control from the motor cortex (Saint-Amant and Drapeau, 2001). As a result, the CPG is not involved in voluntary movement; instead, it is responsible for rhythmic motor patterns that are independent of sensory and motor feedback (Cazalets et al., 1995; Saint-Amant and Drapeau, 2001). Movements such as swallowing and walking are examples of CPG mediated control over stereotypic locomotion (Lanuza et al., 2004). The CPG network consists of interneurons that project to different ipsilateral and contralateral targets specific to each spinal cord hemisegment. In the medial hemisegments, EphA4 repulsive signaling prevents aberrant midline crossing of CPG axonal fibers (Canty et al., 2006). The EphA4 knockout mice exhibit aberrant midline line crossing of CPG interneurons. Therefore, to determine if α2-chimaerin mutant mice develop a similar

phenotype, the mutant was injected with a fluorescent tracer at the lumbar spinal cord region. Fluorescence analysis revealed that, similar to EphA4, α2-chimaerin mutants exhibit aberrant midline interneuron crossing, providing additional evidence to its role as an essential EphA4 protein effector in locomotor circuit assembly and function (Figure 1.6) (Beg et al., 2007; Borgius et al., 2014; Iwasato et al., 2007; Wegmeyer et al., 2007a).

Alpha2-chimaerin signaling in the lateral motor column motor neurons

Alpha2-chimaerin is an essential effector of EphA4-mediated axon guidance throughout the motor cortex and local spinal cord circuitry. It was unknown if α2-chimaerin was a class-specific Eph receptor signaling intermediate, or acted downstream of both EphA and EphB subfamilies. The spinal lateral motor column (LMC) motor neurons utilize both Eph subfamilies to guide lateral and medial motor axons, which innervate dorsal and ventral limb muscles, respectively (Hollyday and Hamburger, 1977; Kao et al.). Specifically, EphA-expressing lateral LMC axons target the dorsal limb in response to ventral limb ephrin-A. Likewise, EphB-expressing medial LMC motor axons migrate to the ventral limbs in response to dorsal limb ephrin-B (Eberhart et al., 2004; Klein, 2004). This binary axon paradigm was utilized to test the specificity of α2-chimaerin as a functionally relevant effector for Eph receptor subfamilies.

Stripe assays demonstrate that ephrin-A5 and ephrin-B2 prevented axonal migration when incubated on alternating stripes seeded with LMC motor neuron explants (Kao et al., 2015). When the LMC motor neurons were electroporated to overexpress or suppress α2-chimaerin, the results revealed a selective defect in ephrin-

A5 repulsive axonal signaling but not in ephrin-B2. Specifically, chick LMC motor axons ignored the ephrin-A5 repulsive cue, extending axons on ephrin-A5- and Fc (control)-treated stripes. However, the axons maintained ephrin-B2 repulsiveness, as migration was not detected on ephrin-B1-treated stripes (Kao et al., 2015). The *in vitro* data demonstrated the gain or loss of α2-chimaerin yields similar axonal defects, suggesting EphA receptor repulsive signaling accuracy is critically dependent upon spatially restricted pools of activated α2-chimaerin (Kao et al., 2015).

The functional role of α2-chimaerin was further tested in an *in vivo* experimental model (Kao et al., 2015). Here, chick LMC neurons were electroporated with EphA or EphB expressing cDNA plasmids to redirect LMC motor axonal trajectories to ventral muscular targets (upon EphB electroporation) or dorsal muscular targets (upon EphA electroporation). The results demonstrated that EphA ectopic expression drives LMC motor axons to the dorsal hindlimb, and EphB ectopic expression drives LMC motor axons to the ventral hindlimbs (Kao et al., 2015). However, when LMC motor neurons were co-electroporated to suppress α2-chimaerin and ectopically express either EphA or EphB, loss of redirection was only observed in EphA co-expression experiments, while EphB redirection remained unmodified (Kao et al., 2015). These data corroborate the *in vitro* findings that intracellular α2-chimaerin levels, and downstream activity, may be a *"bottleneck"* for EphA-mediated cell surface axonal guidance.

In α2-chimaerin mutant animals, lateral (EphA4-mediated) LMC misprojections are detected in the ventral nerve, demonstrating that subsets of lateral LMC motor neurons maintain abnormal axonal projections into adulthood (Kao et al., 2015). The lateral LMC motor axon misprojections result in *"hyperflexion"* of the hindlimb

characterized as uncoordinated antagonistic muscle contraction (Kao et al., 2015). Overall, these data reveal that α2-chimaerin/EphA signaling mediates accurate embryonic motor axon guidance which is critical for optimal neuromuscular function in adulthood (Figure 1.6) (Kao et al., 2015).

The neurological role of α2-chimaerin

Alpha2-chimaerin protein is distributed throughout the neuronal layers of the developing and adult hippocampus (Hall et al., 1993; Iwata et al., 2014; Wegmeyer et al., 2007a). Biochemical analysis from hippocampal neurons has revealed that α2-chimaerin is enriched in postsynaptic protein fractions and is likely a core postsynaptic protein (Shi et al., 2007). Taken together, the ubiquitous hippocampal neuronal expression and subcellular distribution in synaptic compartments, suggest α2-chimaerin may play a prominent role in regulating dendritic spine morphology in response to synaptic activity within the hippocampus (Bourne and Harris, 2008; Eichenbaum et al., 1999; Izquierdo and Medina, 1997). However, only a few studies have begun to unravel the role of α2-chimaerin in the hippocampus.

Alpha2-chimaerin modulates cognitive abilities in adulthood

A recent report evaluated the function of α2-chimaerin in hippocampal dependent behaviors (Iwata et al., 2014). The group utilized a mutant mouse that lacks α2 in the dorsal telencephalon (α2KO-DT), thereby knocking out α2 expression in the hippocampus, amygdala and cerebral cortex (Iwata et al., 2014). To evaluate the role of α2-chimaerin in hippocampal-dependent behaviors, the group conducted contextual fear conditioning to evaluate if a neutral context or tone could elicit a fear response as a result of a pairing with an electric foot shock (McEchron et al., 1998). Alpha2KO-DT

mice demonstrated a higher percentage of freezing when placed in the context of the electric foot shock but not from the tone presentation alone. The authors propose that heightened freezing in the α2 mutant is indicative of enhanced cognition (Iwata et al., 2014). Interestingly when α2 was selectively silenced in the adult dorsal telencephalon (Adult-α2KO-DT), leaving early perinatal and adolescent expression unaltered the animal performed similar to controls in contextual fear conditioning and context discrimination (Iwata et al., 2014). The data indicate that α2 plays a critical role during perinatal development to shape cognition in the adult brain, and expression in mature circuitry is dispensable for hippocampal function (Iwata et al., 2014).

Alpha2-chimaerin and disease

Hyperactive α2-chimaerin mutation in Duane's Retraction Syndrome

Duane's retraction syndrome (DRS) is a congenital eye movement disorder caused by aberrant motor axon innervation to extraocular muscles (Hotchkiss et al., 1980). DRS patients exhibit strabismus resulting in abnormal eye movement preventing inward and outward ocular mobility (DeRespinis et al., 1993). Genetic analysis from individuals with variant forms of DRS revealed dominant nucleotide substitutions common in the α-chimaerin gene located on chromosome *2q31* (Chan et al., 2011) (Miyake et al., 2008). Three of the seven mutations altered amino acids specific to the α2-chimaerin isoform and four altered amino acids that reside in both the α1 and α2-chimaerin isoforms. Structural modeling of the amino acid substitutions determined that the missense nucleotide mutations negatively affected the closed configuration of α2-chimaerin. Recombinant α2-chimaerin cDNA encoding wild type and the mutant isoforms were expressed in HEK293T cells to evaluate α2-chimaerin Rac-GAP activity

(Miyake et al., 2008). The results demonstrated that human DRS α2-chimaerin mutants exhibited an enhanced reduction in Rac-GTP levels, suggesting that the mutants generate a hyperactive α2-chimaerin isoform (Miyake et al., 2008).

To investigate the functional consequence, the α2-chimaerin point-mutant cDNAs were electroporated in embryonic chick midbrains, and the oculomotor nerve axonal projection pattern was analyzed. (Miyake et al., 2008). Expression of the α2-chimaerin mutant constructs resulted in oculomotor nerve stall, and axons terminated prematurely adjacent to the dorsal rectus muscle that controls eye movement. Furthermore, previous clinical findings in humans with the same α2-chimaerin mutations support the observed primary defect in oculomotor nerve development (Yüksel et al., 2010). Overall α2-chimaerin mutations identified in DRS patients confer hyperactive Rac-GAP activity that lead to an ocular motor phenotype as a result of errors in cranial nerve development (Chan et al., 2011; DeRespinis et al., 1993).

A potential role in Autism Spectrum Disorder

Autism Spectrum Disorder (ASD) is a developmental psychiatric condition where cellular abnormalities in synaptic structure and function are prominent (Penzes et al., 2011). Many ASD patients display social impairment, communication difficulties and altered behavioral patterns that begin at infancy and persist throughout adulthood (Zoghbi and Bear, 2012). Human studies have implicated more than 284 candidate genes in ASD (IMGSAC, 2001; Williams et al., 1980). A whole-genome screen of ASD children revealed that the familial autism susceptibility genomic region with the greatest maximum likelihood score contains *CHN1* (Bacchelli et al., 2003; IMGSAC, 2001).

A leading hypothesis is that neurons control the spatial and temporal parameters of redundant developmental factors to different subcellular compartments and timepoints (Govek et al., 2005). For this reason, a mutation or loss to one or more of these molecules may have deleterious effects on neuronal function. Functionally, α2-chimaerin interacts with EphB receptors and is an essential EphA4 receptor tyrosine kinase protein effector, both of which exhibit altered synaptic signaling in psychiatric disorders (Beg et al., 2007; Iwata et al., 2014; Pasquale, 2008; Wegmeyer et al., 2007b). Early work demonstrated that suppression or overexpression of α-chimaerins alters Rac1-GTP levels, and generates abnormal dendritic spine morphologies similar to the unique phenotypes often observed in ASD (Buttery and Beg et al., 2006; Durand et al., 2011; Van de Ven et al., 2005; Williams et al., 1980). Perhaps the lack of dynamic control over Rac1-mediated pathways by α-chimaerins could be a contributing cause of structural and functional defects in ASD at the synapse (Buttery and Beg et al., 2006; Iwata et al., 2014; Shi et al., 2007).

Looking Forward

The motivation behind this dissertation was inspired by work from Donald Hebb who suggested that coordinated changes in the structural and functional efficacy of individual synapses could alter neuronal connectivity and ultimately affect neurological behavior (Hebb, 1949). In Chapter Two, I address this central hypothesis by evaluating the structural and functional role of α2-chimaerin in the mouse hippocampus. Accordingly, I tested if α2-chimaerin is required for dendritic arbor and synapse formation. Furthermore, I conducted electrophysiological and behavioral experiments to ask if the loss of α2-chimaerin alters hippocampal function. I hypothesized that the loss

of α2-chimaerin would affect neuronal connectivity and dendritic arbor formation by uncoupling the coordination between structural and functional mechanisms at the synapse. In Chapter 5, I discuss my findings in the context of normal brain function, and in neurological disorders characterized by aberrant synaptic connectivity.

In Chapter Three, I expanded my investigation of α2-chimaerin by evaluating its potential role in subgranular zone proliferation, and oligodendrocyte precursor cell division throughout the dentate gyrus. Additionally, I mapped the spatial and temporal expression profile of α2-chimaerin in the hippocampus, which revealed dynamic control over α2-chimaerin in different neuronal populations. Lastly, I discuss the potential role of α2-chimaerin in oligodendrocytes, and in neuronal subsets that express α2-chimaerin in the adult hippocampus.

Chapter Four addresses a collaborative project that identified a novel GABA-mediated receptor in the nematode *Caenorhabditis elegans*. Under most circumstances, GABA-activated channels conduct chloride ions resulting in inhibition of neuronal activity. On the contrary, this novel GABA-activated receptor, LGC-35, conducts cations and is therefore excitatory (Jobson and Valdez et al., 2015). Phylogenetic analysis suggest that the pore-forming domain of LGC-35 contains molecular determinants that confer cation selectivity, but that channel has evolved from GABA-A receptors. Overall, the data presented in this chapter demonstrate that both direct and indirect excitatory GABA signaling plays important roles in regulating neuronal circuit function and behavior in *C. elegans.*

In Chapter Five, I summarize the main contributions of my thesis work on α2-chimaerin to our understanding of structural and functional plasticity at the synapse. I

discuss unanswered questions that address the role of α2-chimaerin in dendritic spines, and elaborate on key cell-surface mechanisms that may recruit α2-chimaerin to activated synapses. From a physiological prospective, I discuss the role of α2-chimaerin in the development of neuronal connectivity, and mature synapses in the adult brain. Moreover, I explain how my dissertation work challenges current published data describing α2-chimaerin's role in the mouse hippocampus.

Chapter 2

The Rac-GAP alpha2-chimaerin regulates hippocampal dendrite and spine morphogenesis

Abstract

Neurons possess a dynamic cellular morphology that can be modulated by synaptic transmission. In particular, dendritic spines are fine neuronal processes where spatially restricted input can induce activity-dependent changes in one spine while leaving neighboring spines unmodified. Rapid changes in spine morphology are coupled to the dynamic cycling of cell-surface receptors, which underlie aspects of synaptic plasticity. Dysregulation of synaptic receptors can result in an increase in spine density and alterations in morphology. These plastic properties of dendritic spines are considered to be compensatory mechanisms that maintain normal synaptic transmission. Importantly, alterations in dendritic spine density, morphology and function are known to be associated with cognitive pathologies and neurodevelopmental delays. From a molecular standpoint, the Rho-GTPase, Rac1 is associated with the recruitment of synaptic receptors and exerts dynamic control over dendritic spines, thus contributing to their architecture and function. However, the key molecules and mechanisms that regulate Rac1-dependent pathways at the synapse are not well understood. We have identified a Rac-GTPase activating protein, α2-chimaerin, that is a

negative modulator of Rac1 in hippocampal neurons. The loss of α2-chimaerin increased active Rac1-GTP levels and induces the formation of polymorphic and polysynaptic dendritic spines. Using a combination of cellular, electrophysiological and behavioral analyses, our data demonstrate that α2-chimaerin is a critical regulator of spine morphogenesis and synaptic connectivity.

Introduction

Nervous system function relies on the precise wiring of neuronal circuits during development (Goodman and Shatz, 1993). A key parameter in this process is the elaboration of axonal and dendritic arbors, as their size and complexity determines the number of synaptic connections a neuron makes and receives, respectively (Cline, 2001; Goodman and Tessier-Lavigne, 1997). With billions of neurons in the brain, individual axons and dendrites have the momentous task of locating the appropriate partner in which to form synaptic connections. The majority of excitatory synaptic neurotransmission occurs at dendritic spines, tiny F-actin rich protrusions that emanate from the dendritic shaft (Harris, 1999; Matus, 2000). A typical dendritic spine contains a single glutamatergic synapse, thus spine density reflects the amount of excitatory drive a neuron receives (Fiala et al., 2002). Moreover, spines are highly modifiable and exhibit tremendous structural and functional plasticity. Structural plasticity involves cytoskeletal rearrangement that affects spine morphology; whereas, functional plasticity leads to changes in glutamate receptor dynamics (Fischer et al., 2000; Segal and Andersen, 2000). These changes in spine shape and number can last for weeks *in vivo* and are thought to reflect cellular mechanisms underlying cognitive processes like learning and memory (Bhatt et al., 2009). Not surprisingly, mutations in signaling

pathways that regulate F-actin cause abnormalities in dendritic spine shape, density and function; pathological hallmarks highly correlated with neurodevelopment, neuropsychiatric and neurodegenerative disorders (Penzes et al., 2011).

In response to physiological stimuli, a complex network of signaling events can trigger changes in dendritic spine number and morphology. Rho-GTPases are key proteins that regulate actin cytoskeletal dynamics by coupling upstream signals with the correct downstream effector proteins (Hall, 1998; Luo, 2000). Rho-GTPases control diverse cellular processes, thus signaling specificity is achieved through regulatory proteins that modulate Rho-GTPase activity (Cherfils and Zeghouf, 2013). Like all Rho-GTPases, Rac1 acts as a molecular switch cycling between a GDP-bound inactive form and a GTP-bound active form. Rac1 is activated by guanine nucleotide exchange factors (GEFs) and inactivated by GTPase-activating proteins (GAPs) (Bos et al., 2007). Despite the importance of these regulatory factors, it is unclear how GEFs and GAPs coordinately act to regulate Rac1 signaling in dendrites and spines.

Here, we demonstrate that the Rac-GAP α2-chimaerin plays an important role in hippocampal dendrite arborization and spine morphogenesis. Our findings reveal that α2-chimaerin is a major negative regulator of Rac1, and loss of α2-chimaerin simplifies dendritic arbor complexity, decreases dendritic spine protrusion density, alters spine morphology, and increases the density of polysynaptic dendritic spines. Together, these data provide important insight into the molecular repertoire that shapes dendrites, spines and synapses. Importantly, our data identify α2-chimaerin as a novel Rac-GAP protein that plays a key role in counterbalancing GEF activation of Rac1 in spines and synapses.

Results

Alpha2-chimaerin is localized to dendrites and spines in the hippocampus

The Rac-GAP α2-chimaerin is essential for the proper guidance of corticospinal, oculomotor, spinal interneuron and spinal motor neuron axons (Aoto et al., 2007; Beg et al., 2007; Iwasato et al., 2007; Shi et al., 2007; Wegmeyer et al., 2007a). To determine if α2-chimaerin plays a role in regulating the structural and functional plasticity of dendrites and spines, we co-transfected wild type (WT) mouse hippocampal neurons with soluble mCherry and low levels of EGFP-tagged α2-chimaerin. We found that EGFP-α2-chimaerin was expressed throughout the neuron with robust expression in dendrites and spines (Figure 2.1A). The subcellular localization of EGFP-α2-chimaerin to dendritic spines suggests the protein is expressed at synapses, which is supported by biochemical studies demonstrating that α2-chimaerin is a tightly associated with core components of the post-synaptic density (PSD) (Shi et al., 2007). Taken together, the expression data suggest that α2-chimaerin may play a pivotal signaling role in hippocampal dendrites and spines.

Alpha2-chimaerin is a major negative regulator of Rac1 in the hippocampus

Several groups including ours have used recombinant expression systems to assay the Rac-GAP activity of α2-chimaerin (Buttery et al., 2006; Kao et al., 2015; Shi et al., 2007). Given α2-chimaerin's spatial distribution in hippocampal dendrites, we sought to investigate if it's loss altered active Rac1 levels in mature hippocampal neurons (Buttery and Beg et al., 2006; Iwata et al., 2015; Iwata et al., 2014). Primary hippocampal neurons cultured for 18-20 DIV were lysed, and a quantitative spectrophotometric assay was used to detect the cellular levels of active Rac1-GTP.

The results from the small GTPase-activation assay (G-LISA) demonstrated that α2-chimaerin gene-trap (mutant) neurons had significantly increased Rac1-GTP levels compared to controls, suggesting that α2-chimaerin is a major negative regulator of Rac1 in hippocampal neurons (Figure 2.1C). In dendrites and spines, active Rac1 can promote F-actin polymerization by initiating several downstream signaling effector pathways (Nakayama et al., 2000). Thus, we investigated if the heightened Rac1-GTP levels led to changes in polymerized F-actin in dendrites and spines. Primary hippocampal neurons were fixed and stained with fluorescently labeled phalloidin, which binds selectivity to polymerized F-actin. Quantification revealed a significant 9% increase in baseline levels of polymerized F-actin intensity, selectively, in the dendritic spine head but not the dendritic shaft in α2-chimaerin mutants.

Alpha2-chimaerin regulates dendritic arborization and spine morphogenesis

To examine the role of α2-chimaerin in dendritic arborization and spine morphogenesis, we cultured primary hippocampal neurons from WT and α2-chimaerin mutant mice and transfected cells with a pCAG-EGFP plasmid to assess dendrite morphology. Morphological assessment at 18 DIV revealed α2-chimaerin mutant neurons exhibited a simplified dendritic arbor (Figure 2.2A). To further confirm our *in vitro* findings, we crossed α2-chimaerin mutants to Thy1-GFP-M animals in which a subset of CA1 pyramidal cells express GFP. Dendritic complexity was similarly simplified in α2-chimaerin; Thy1-GFP-M+ mutants corroborating our *in vitro* findings and identifying α2-chimaerin as a key player in shaping dendritic arbor complexity (Figure 2.2B-C).

Endogenous α2-chimaerin is a core component of the PSD (Iwasato et al., 2007; Shi et al., 2007) and EGFP-α2-chimaerin can localize to dendritic spines, thus we asked if its loss altered dendritic spine density and morphology. Loss of α2- chimaerin both *in vitro* and *in vivo* resulted in a significant decrease in the number of protrusions

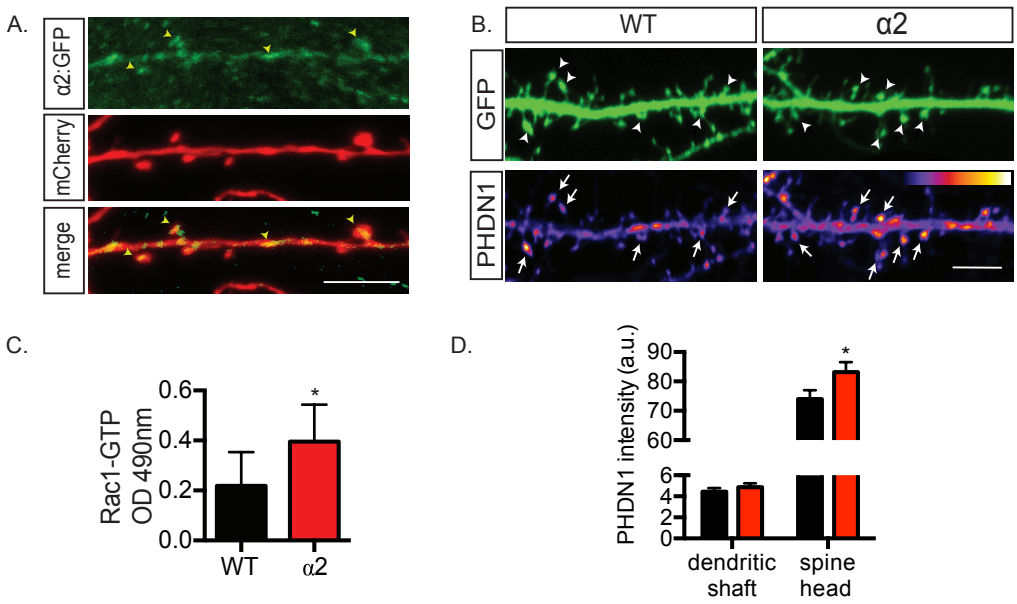

Figure 2.1, Alpha2-chimaerin is localized to hippocampal dendrites and is a regulator of Rac1 in dendritic spines

(A) WT primary hippocampal neurons at DIV 16 were co-transfected with 50ng of EGFP-α2-chimaerin and 550ng of mCherry to resolve fine dendritic structures. Scale bar equals 5μm.

(B) Representative dendritic segments from WT and α2-chimaerin mutant hippocampal neurons at DIV 18. The cells have been transfected with GFP to resolve fine dendritic structures, and treated with phalloidin, a fluorescently tagged phallotoxin to label polymerized F-actin. The white arrowheads identify dendritic spines, and the white arrows delineate polymerized F-actin in these dendritic spines. Scale bar equals 10μm.

(C) Rac1-GTP G-LISA activation assay from hippocampal lysate of WT and α2-chimaerin hippocampal neurons at DIV 18. Optical density measurements of Rac1-GTP (mean±SEM): WT = 0.218 ± 0.134 and α2 = 0.395 ± 0.148; N = 4 per genotype; paired two-tailed *t-test*, **p* = 0.0331, absorbance was read at 490nm

(D) Quantification of phallotoxin intensity (a.u.) in the spine head (mean ± SEM): WT = 74.03 a.u. ± 3.0; N=7 cells and α2 = 83.17 a.u. ± 3.38; N=8 cells; unpaired two-tailed *t-test*, **p* = 0.0444. Quantification of phallotoxin intensity in the dendritic shaft (mean ± SEM): WT = 4.434 a.u. ± 0.36; N = 7 cells and α2 = 4.863 a.u. ± 0.38; N = 8 cells.

emanating from secondary and tertiary dendritic shafts (Figure 2.3A-C).

To determine if specific classes of spines were affected, we quantitated spine shape frequency. Examples of our categorical classification of dendritic protrusions are shown in Figure 2.3D: 1) Filopodia: thin and narrow protrusions that lack a bulbous head; 2) Stubby spines: a short bulbous head with an unresolved neck; 3) Mushroom spines: a defined narrow neck terminating to a bulbous head; and 4) Atypical spines: bifurcated in which two spine heads share a common neck, or branched where secondary and tertiary spine heads branch from the primary spine head (Bourne and

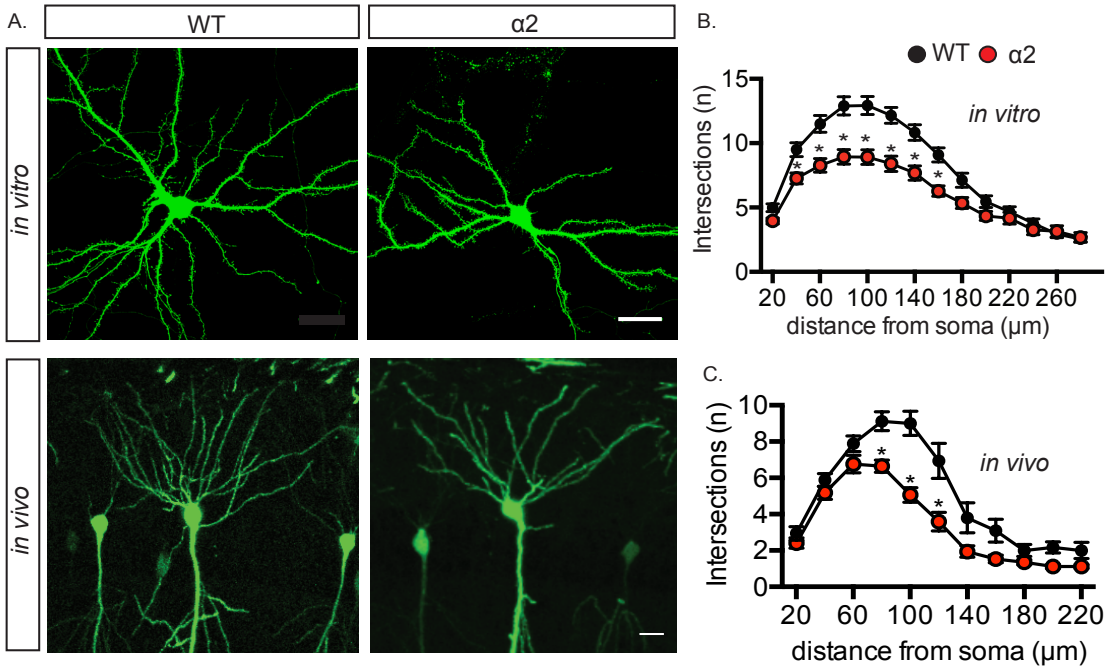

Figure 2.2, Alpha2-chimaerin mutant neurons exhibit a simplified dendritic arbor

(A) *In vitro*, representative images of WT and α2-chimaerin mutant hippocampal primary neurons at DIV 16. *In vivo*, representative images of CA1 apical dendrites from WT;Thy1-GFP-M+ and α2-chimaerin;Thy1-GFP-M+ hippocampal slices. Scale bar equal 30μm

(B-C) Alpha2-chimaerin mutant neurons exhibit a significant reduction in dendritic complexity both *in vitro* and *in vivo*; *In vitro* sholl analysis: *t-test*, $\alpha = .05$, Holm-Sidak method, $^*p < 0.001$, N = 75 cells per genotype. *In vivo* sholl analysis: *t-test,* $\alpha = .05$, Holm-Sidak method, $^*p < 0.004$, N = 17 cells per genotype.

Harris, 2008; Harris et al., 1992). Confocal imaging of cultured hippocampal neurons revealed the reduction in protrusion density was due to a selective loss of mushroom shaped spines, whereas stubby spines and filopodia were unchanged compared to controls (Figure 2.3E). Furthermore, the reduced mushroom spine population in the α2-chimaerin exhibited an overall increase in spine length and head area (Figure 2.2G-H). One possibility is that the heightened levels of polymerized F-actin (Figure 2.1D) may drive the significant increase in dendritic spine head area observed in α2-chimaerin mutant hippocampal neurons (Figure 2.3H). Analysis of atypical spine types revealed a significant increase in irregular branched spines, but no change in bifurcated spines in α2-chimaerin mutants (Figure 2.3F).

Given the presence of irregular dendritic spine morphology in several neuropsychiatric diseases, we next used acute shRNA-mediated knockdown of α2-chimaerin to determine if cell-autonomous neuronal loss also caused a similar increase in irregular branched spines observed in the constitutive gene-trap mutants (Penzes et al., 2011). Wild type neurons were transfected with α2-chimaerin specific shRNAs at DIV 10, and analyzed at 16-18 DIV (Figure 2.4A). Similar to the *in vitro* and *in vivo* findings, acute cell-autonomous knockdown resulted in significantly increased atypical spine density compared to scrambled shRNA (control) expressing neurons (Figure 2.4A-B). Furthermore, we demonstrated that the increased irregular branched spine density was specifically due to loss of α2-chimaerin, as re-expression of a EGFP-α2-chimaerin into α2-chimaerin mutant neurons at 10 DIV rescued the irregular dendritic spine defects. (Figure 2.4D-F). Together, these data strongly argue that α2-chimaerin is

a cell-autonomous determinant of spine density, and key regulator of mature spine morphology (Figure 2.4H-I).

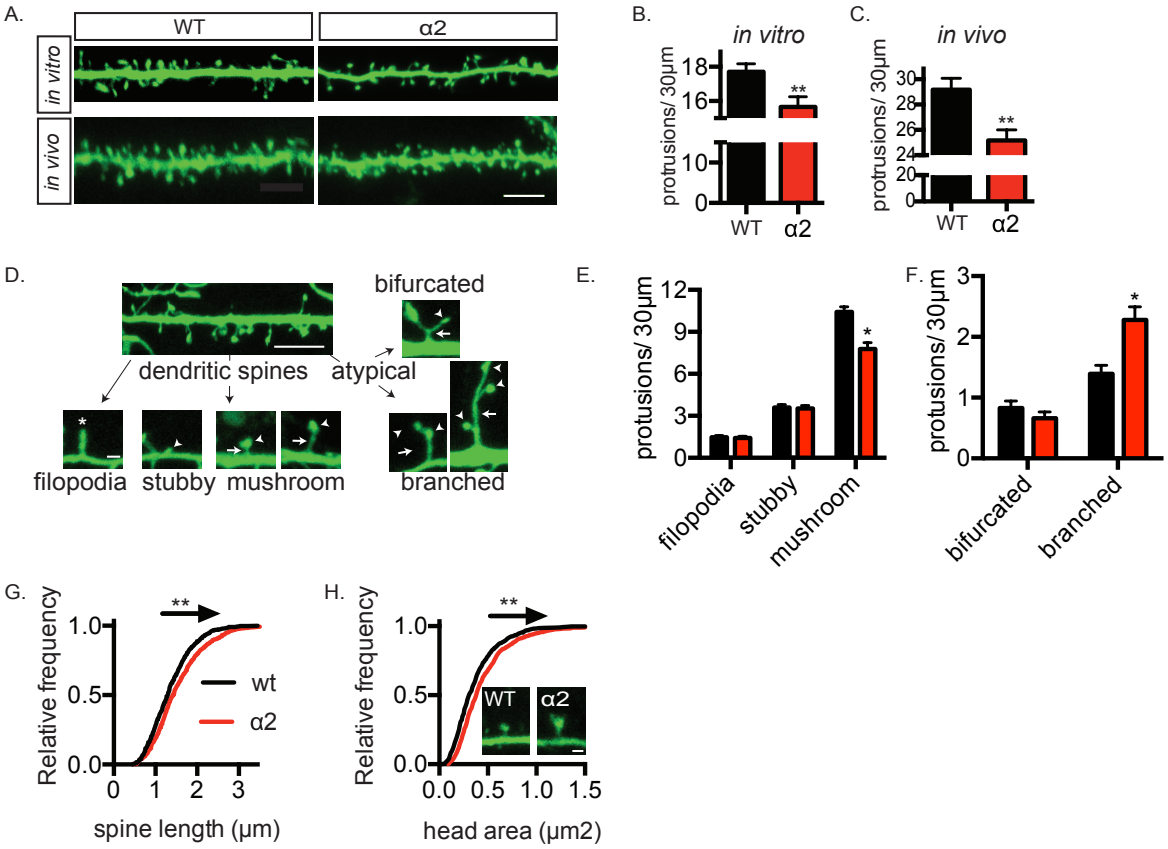

Figure 2.3, Alpha2-chimaerin is a key regulator of mature spine morphology

(A) *In vitro* and *in vivo* representative images of WT and α2-chimaerin mutant hippocampal dendrites. Scale bar equals 5μm

(B-C) Alpha2-chimaerin dendrites exhibit a reduction in protrusion density. *In vitro* quantification of dendritic protrusion density (mean ± SEM): WT = 17.71 ± 0.46; N = 33 cells and α2 = 15.66 ± 0.58; N = 35 cells; unpaired two-tailed *t-test*, $^{**}p = 0.0068$. *In vivo* quantification of CA1 apical dendritic protrusion density: WT = 29.17 ± 0.91; N = 8 cells and α2 = 25.17 ± 0.84; N = 7 cells; unpaired two-tailed *t-test,* $^{**}p = 0.0019$.

(D) Dendritic spines were categorized based on their morphological structures. In brief, filopodia protrusions lack a bulbous head (white asterisk); stubby, mushroom, bifurcated, and branched spines exhibit a spine neck (white arrows) and spine head (white arrow-heads). Dendritic scale bar equals 5μm and protrusion image scale bar equals 1μm.

(E) Alpha2-chimaerin mutant hippocampal neurons exhibit a reduction in mushroom spine density, *in vitro*. Protrusion shape density quantification (mean ± SEM): mushroom-shaped spines: WT = 10.42 ± 0.36; N = 32 cells and α2 = 7.77 ± 0.46; N = 35 cells; *t-test,* $\alpha = .05$, Holm-Sidak method, $^{*}p < 0.0001$.

(F) Alpha2-chimaerin mutant hippocampal neurons exhibit an increase in atypical dendritic spines, *in vitro*. Atypical dendritic spine density quantification (mean ± SEM): revealed a significant difference in branched spine density between WT = 1.39 ± 0.13; N = 32 cells and α2 = 2.28 ± 0.21; N = 35 cells; *t-test,* $\alpha = .05$, Holm-Sidak method, $^{*}p < 0.0001$.

(G) Alpha2-chimaerin mutant hippocampal neurons exhibit an increase in the length of mushroom spines. Quantification of mushroom spine length (mean ± SEM): WT = 1.35 ± 0.017, N = 32 cells, n = 819 mushroom spines and α2 = 1.54 ± 0.0219, N = 35 cells, n = 813 mushroom spines; unpaired two-tailed *t-test,* $^{**}p < 0.0001$.

(H) Alpha2-chimaerin mutant hippocampal neurons exhibit an increase in mushroom spine head area. Quantification of mushroom spine head area (mean ± SEM): WT = 0.36μm^2 ± 0.00813, N = 32 cells, n = 819 mushroom spines and α2 = 0.45μm^2 ± 0.00981, N = 35 cells, n = 813 mushroom spines; unpaired two-tailed *t-test,* $^{**}p < 0.0001$. Inserted are representative images of WT and α2-chimaerin mutant mushroom dendritic spines. Scale bar equals 1μm.

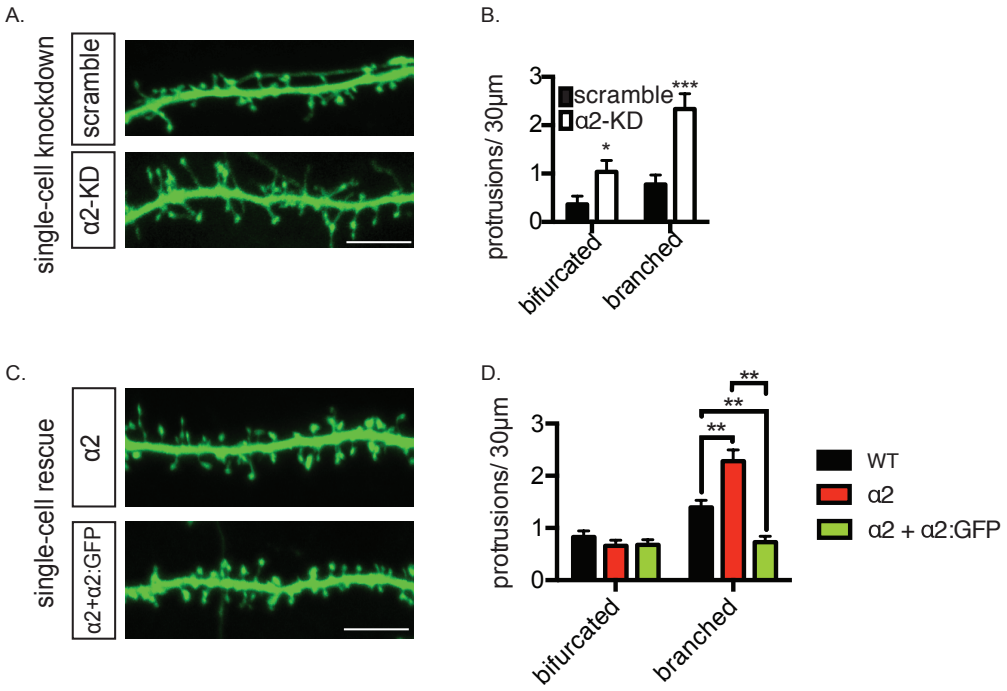

Figure 2.4 Alpha2-chimaerin is a cell-autonomous determinant of dendritic spine morphology

(A) Representative images of DIV 16 dendritic segments from WT primary neurons transfected at DIV 10 with scramble or alpha2-chimaerin shRNA, respectively. Scale bar equals 5µm

(B) Alpha2-chimaerin suppression increases the density of atypical bifurcated and branched dendritic spines. Quantification of bifurcated dendritic spines (mean ± SEM): scramble = 0.36 ± 0.16 and α2-KD= 1.037 ± 0.23; N = 8 cells per genotype; *t-test, α* = .05, Holm-Sidak method, **p* = 0.0307 and **p* < 0.0001. Quantification of branched dendritic spines (mean ± SEM): scramble = 0.77 ± 0.19 and α2-KD = 2.33 ± 0.320; N = 8 cells per genotype; *t-test, α* = .05, Holm-Sidak method, **p* = 0.0307 and ****p* = 0.000278.

(C) Representative images of DIV 16 dendritic segments from wt primary neurons transfected at DIV 10 to express GFP or co-transfected to express GFP plus α2:GFP, respectively. Scale bar equals 5µm

(D) Exogenous expression of α2-chimaerin rescues the altered atypical branched spine density in α2-chimaerin mutant hippocampal neurons. Quantification of atypical branched spine density (mean ± SEM): WT = 1.39 ± 0.13; N = 33, α2 = 2.28 ± 0.22; N = 35 and α2+α2:GFP = 0.73 ± 0.11; N = 25; ordinary one-way ANOVA F(2,274) = 20.6; ***p* < 0.001.

Alpha2-chimaerin regulates monosynaptic innervation

The hallmark of mature dendritic spines is that they form a single synapse with a presynaptic axon (Ethell and Pasquale, 2005). The selective loss of mature mushroom shaped spines coupled with increased atypical spines in α2-chimaerin mutants suggests that synaptic connectivity and function may be altered. To quantitate synapse density, 18 DIV hippocampal neurons were immunostained with the presynaptic marker synaptophysin and the excitatory postsynaptic marker PSD-95 (Figure 2.5A). In comparison to controls, α2-chimaerin mutants exhibited a significant increase in synapse density along secondary and tertiary dendrites (Figure 2.5B). To determine if the increased synapse density was due to synaptic changes in specific spine classes, we counted the total number of synapses formed across dendritic segments and assigned each synapse to one of the categorical classes of spines described above. In control neurons, mushroom (72.9%) and stubby (14.41%) spines accounted for the majority of synapses. In α2-chimaerin mutants, mushroom-shaped spines also accounted for the majority of synapses (59.6%) (Figure 2.5C). Strikingly, atypical branched spines (20.7%) accounted for the second highest percentage of synapses, which was significantly increased compared to controls (6.04%) (Figure 2.5C). Thus, loss of α2-chimaerin shifts the distribution of synapse-to-spine type from mature mushroom synapses to atypical branched synapses.

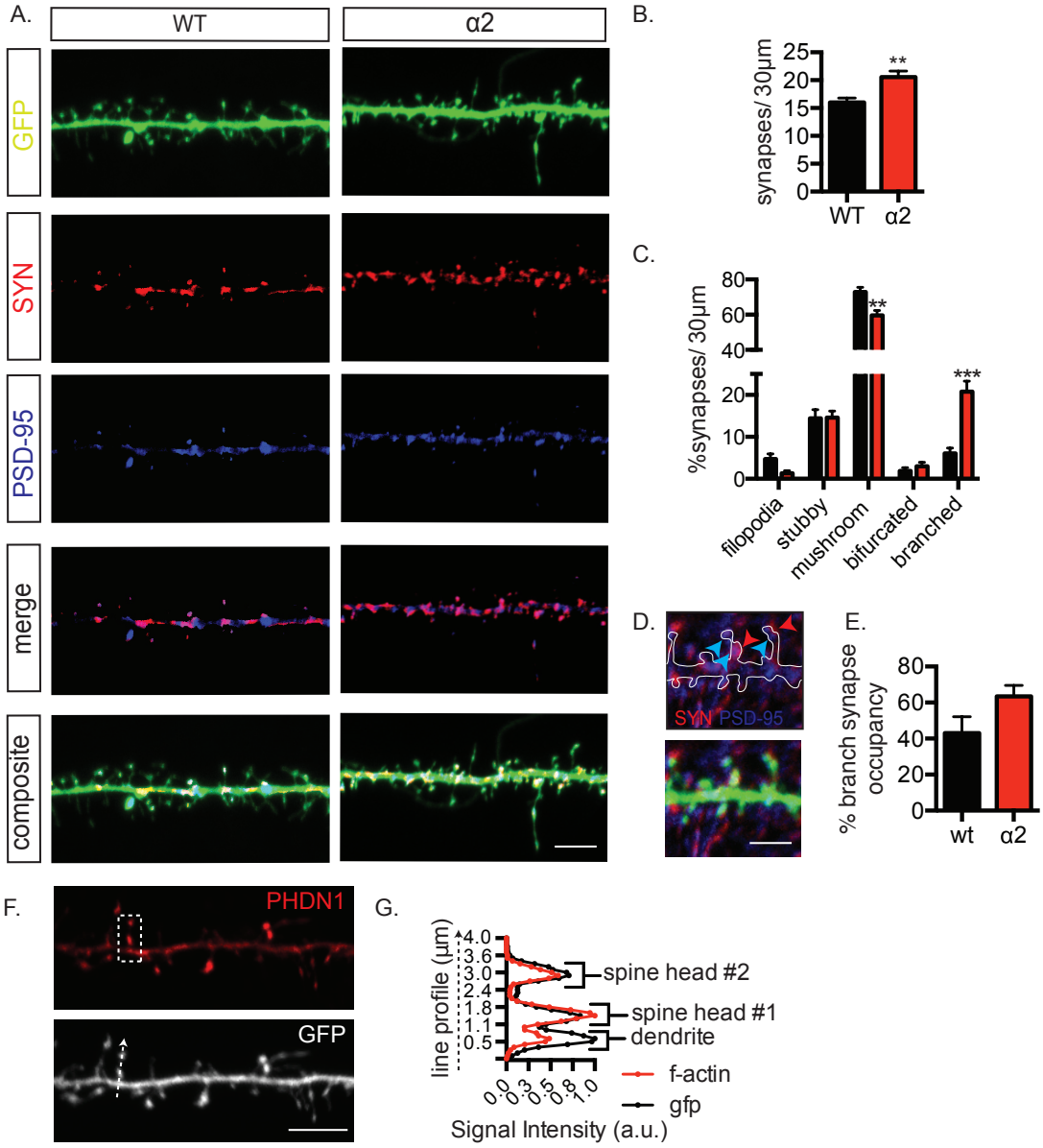
A.
WT
α2
GFP
SYN
PSD-95
merge
composite
B.
synapses/ 30µm
25
20
15
10
5
0
**
WT
α2
C.
%synapses/ 30µm
80
60
40
20
10
0
**
***
filopodia
stubby
mushroom
bifurcated
branched
D.
SYN PSD-95
E.
% branch synapse occupancy
80
60
40
20
0
wt
α2
F.
PHDN1
GFP
G.
line profile (µm)
4.0
3.6
3.0
2.4
1.8
1.1
0.5
spine head #2
spine head #1
dendrite
f-actin
gfp
0.0
0.3
0.5
0.8
1.0
Signal Intensity (a.u.)

Figure 2.5 The loss of α2-chimaerin alters spine-to-synapse dynamics

(A) Representative images of DIV 16 WT and α2-chimaerin dendritic segments expressing GFP, and immunostained with synaptophysin (red) and PSD-95 (blue). Scale bar equals 5μm

(B) Alpha2-chimaerin mutant hippocampal neurons exhibit an increase in synapse density. Quantification of synapse density (mean ± SEM): WT = 16.00 ± 0.0877; N = 18 cells and α2 = 20.56 ± 1.069; N = 14 cells; unpaired two-tailed *t-test*, ***p* = 0.0011

(C) Alpha2-chimaerin exhibit an increase in the percent of synapses formed on branched dendritic spines. Quantification of the percent of synapses formed on mushroom-shaped dendritic spines: WT = 72.94 ± 2.66, N = 18 cells and α2 = 59.64 ± 2.81, N = 14 cells; *t-test, α* = .05, Holm-Sidak method, ***p* = 0.001. Quantification of the percent of synapses formed on branched-shaped dendritic spines: WT = 6.04% ± 1.29; N = 18 cells and α2 = 20.77% ± 2.5; N = 14 cells; *t-test, α* = .05, Holm-Sidak method, ****p* < 0.0001.

(D). Representative image of multiple synapses depicted in red arrowheads (SYN) and blue arrowheads (PSD-95) where spine heads are positive for both synaptophysin and PSD-95. Even on the same spine, some branched spine heads are only positive for PSD-95 suggesting the potential for synaptic integration. Scale bar equals 2.5μm

(E) Alpha2-chimaerin mutant neurons exhibit an increase in the density of synapses formed on branched dendritic spines. Quantification of the percentage of synapses formed on multiple dendritic spines heads (mean ± SEM): WT = 42.95% ± 9.00, N = 18 cells and α2 = 63.51% ± 6.00; N = 14 cells; unpaired two-tailed *t-test*; *p* = .0615

(F) Representative image of a DIV 16 hippocampal dendritic segment that exhibits an irregular branched spine. The cell was treated with Alexa 594-phallotoxin to fluorescently label polymerized F-actin. Scale bar equals 5μm.

(G) A line profile spine revealed polymerized F-actin in the multiple spine heads across an atypical branched spine.

Atypical branched spines have multiple spine heads, suggesting these polymorphic protrusions may be poly-innervated (Figure 2.5D). Thus, we quantitated the number of synapses a single atypical branched spine receives to determine the extent of poly-innervation. In control neurons 42% of atypical branched spines received more than one synapse (Figure 2.5E). In contrast, 63% of atypical branched spines from α2-chimaerin mutants were associated with more than one synapse (Figure 2.5E). Finally, the bulbous secondary and tertiary heads on atypical branched spines are morphologically reminiscent of mature mushroom shaped spine heads. To determine if these structures contain hallmark cytoskeletal features of spines, we stained neurons with Alexa594-phalloidin, revealing these supernumerary spine heads are highly enriched in F-actin (Figure 2.5F-G). Together, these data suggest that atypical branched spine heads are structurally similar to mature spines, and are capable of receiving multiple synaptic inputs.

Alpha2-chimaerin is dispensable for long-term potentiation and fear conditioning

The morphological and synaptic alterations in dendrites and spines suggest that α2-chimaerin may be a critical regulator of hippocampal network connectivity and function. A recent study reported that α2-chimaerin functions during development to adjust cognitive ability in adulthood (Iwata et al., 2014). Specifically, loss of α2-chimaerin during early development was reported to increase contextual fear conditioning, a hippocampal-dependent behavior (Iwata et al., 2014). Our cellular findings of reduced dendritic complexity, decreased protrusion density, altered spine

morphologies, and increased synapse density suggest these key structural changes may account for the altered behavioral changes previously reported.

We conducted fear conditioning experiments and assessed long-term potentiation in the α2-chimaerin mutant mouse. In brief, fear conditioning is a form of learning where a neutral stimulus (tone/context) is paired with an aversive stimulus (i.e. foot shock). After pairing, the once neutral variable becomes a conditioned stimulus that elicits fear (conditioned response) in the animal. Fear conditioning relies on LTP-dependent mechanisms in the amygdala and hippocampus (Anagnostaras et al., 2001; Maren, 2001; Rogan et al., 1997). These circuits exhibit an increase in synaptic strength that presumably transmits information about the conditioned stimulus to neurons that have previously processed the neutral tone/context, suggesting LTP is an underlining component of memory encoding and storage (Schafe et al., 2001; Stevens, 1998).

However, we found that the α2-chimaerin mutants, either males or females, exhibited no difference in contextual fear conditioning to either the conditioning tone or context (Figure 2.6). Due to the failure to observe an effect in hippocampal-dependent contextual fear conditioning, we next assayed the functional consequence of ablating α2-chimaerin. Changes in spine number, morphology and plasticity are associated with long-term potentiation (LTP), a cellular model for learning and memory (Chen et al., 2007; Martinez and Tejada-Simon, 2011). We assessed network connectivity and synaptic plasticity by inducing LTP at Schaffer collateral afferents in area CA1. Recording and stimulating electrodes were placed in the stratum radiatum and input-output curves were constructed showing that loss of α2-chimaerin resulted in no change between the presynaptic fiber volley and slope of the field excitatory postsynaptic

potential (fEPSP), demonstrating that basal transmission was not modified compared to controls (Figure 2.7A).

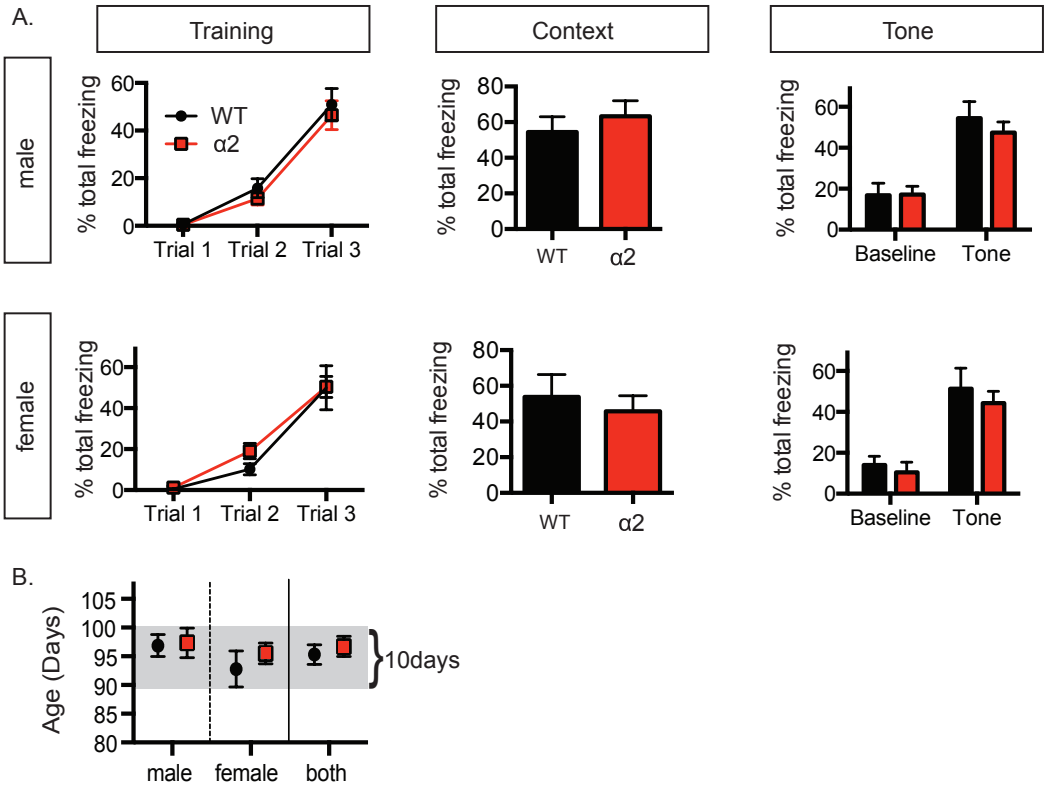

Figure 2.6 The loss of α2-chimaerin does not impair Pavlovian fear conditioning

(A) On Day One, the WT and α2-chimaerin mutant mice, from both sexes, were trained in three sequential training trials, and exhibited an increased level of freezing as training progressed. However both genotypes revealed no significant difference in their performance during training. On Day Two, the mice were re-exposed to the conditioning chambers, and the male α2-chimaerin mutant mice responded with an 8% increase in freezing, but the increase was not significantly different compared to wildtype. On the other hand, α2-chimaerin mutant female mice exhibited an 8% reduction in total freezing, but the percentage was not statistically significant. On Day Three, we tested the mice for tone conditioning in a novel context, and the α2-chimaerin mutant exhibited a 6% decrease in freezing compared to WT, but the difference was not statistically significant. The female cohort exhibited a 7% reduction in total freezing that was also not statistical significant.

(B) Pavlovian fear conditioning was completed on age-matched male and female mice. Females: WT = 96.88 days ± 1.90; N=8 and α2 = 97.36 days ± 2.58; N=11. Males: WT = 92.88 days ± 3.12; N = 5 and α2 = 95.50 days ± 1.82; N = 6. Mixed sexes: WT = 95.31 days ± 1.69; N = 13 and α2= 96.71 days ± 1.76; N=17.

Theta burst stimulation (100Hz, 4 pulses) of CA3 Schaffer collaterals revealed no difference in the induction or maintenance of LTP in CA1 in α2-chimaerin mutants compared to controls (Figure 2.7B). Taken together, these functional data demonstrate that CA3-CA1 hippocampal synaptic efficacy is neither compromised nor potentiated in α2-chimaerin mutants. However, the morphological and synaptic changes we identified may underlie defects in other forms of synaptic signaling that mediate the cognitive defects previously reported in α2-chimaerin knockout mice (Iwata et al., 2014).

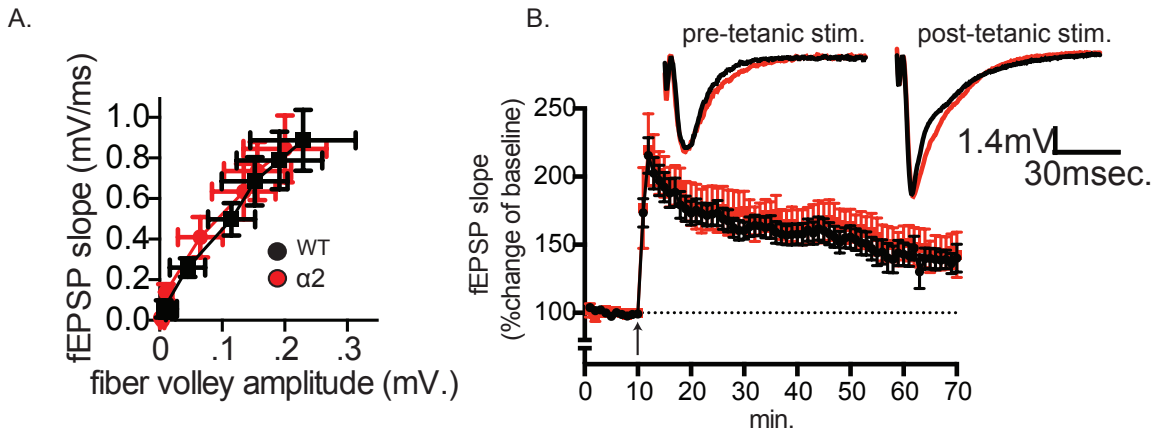

Figure 2.7 CA3-CA1 hippocampal synaptic efficacy is neither compromised, nor potentiated in α2-chimaerin mutants

(A) The loss of α2-chimaerin does not alter synaptic transmission. Input and Output curve plotting the fEPSP against fiber volley amplitude (mean ± SEM). Recording derived from four 5-6 old mice: WT N = 7 animals, n = 12 slices and α2 N = 7 animals, n = 18 slices.

(B) LTP is not affected in α2-chimaerin mutant mice. LTP was induced by theta burst stimulation (black arrow) at 100Hz (4 pulses) in the CA1 region of acute hippocampal slices from α2-chimaerin mutant and WT mice. Representative fEPSP recordings before and 60 minutes after LTP induction are displayed for WT (black) and α2-chimaerin mutants mice (red). The fEPSP slope (mean ± SEM) is graphed for the completion of the time course. Recording derived from 5-6 month old mice: WT N = 5 animals, n = 10 slices and α2 N = 6 animals, n = 12 slices.

Discussion

The function of α2-chimaerin has been studied predominantly in the context of axonal guidance in locomotor circuit assembly (Beg et al., 2007; Iwasato et al., 2007; Kao et al., 2015; Wegmeyer et al., 2007a). Here, we identify a novel function for α2-chimaerin in regulating dendrite arborization and spine morphogenesis in hippocampal neurons. Cellular, electrophysiological and behavioral data reveal that loss of α2-chimaerin (1) simplifies dendritic arbor complexity, (2) decreases dendritic protrusion density, (3) induces atypical branched spine formation, (4) augments neuronal Rac1-GTP levels and increases spine head F-actin content, (5) increases the incidence of co-innervated atypical branched spines, but (6) α2-chimaerin is dispensable for hippocampal LTP. We discuss these findings in the context of the regulatory mechanisms of Rho-GTPase activity and the role of actin-based structural and functional plasticity in neurological disorders associated with aberrant dendritic spine morphogenesis and plasticity.

The ability of dendritic spines to rapidly change shape is due to their highly enriched and labile F-actin cytoskeleton (Matus, 2000). As central regulators of actin cytoskeletal dynamics, the Rho-GTPases are critical determinants of spine morphogenesis and synaptic plasticity (Hall, 1998; Luo, 2000). The regulated cycling between active and inactive states is critically important as gain- and loss-of-function mutations in Rac1, RhoA and Cdc42 impact dendrite arborization and spine density, morphology and plasticity (Tolias et al., 2011). Furthermore, several disease-associated mutations have been identified in genes that regulate Rho-GTPase activity, underscoring that tight control of Rho-GTPase activity is imperative given its diverse

roles in a plethora of cellular processes (Bacchelli et al., 2003; De Rubeis et al., 2014; Ebert and Greenberg, 2013; Penzes et al., 2011; Zoghbi and Bear, 2012). Although, the molecular logic of GEF/GAP regulation of Rho-GTPases in response to synaptic activity is not well understood, the precise spatiotemporal activity of these modulatory proteins is likely to be highly choreographed and context-dependent (Duman et al., 2015). Thus, the cellular expression, subcellular localization, developmental regulation and protein interactions of GEFs and GAPs are major factors that contribute to the spatiotemporal regulation and signaling specificity of Rho-GTPases (Tolias et al., 2011)

Rac-GEF and Rac-GAP regulation of dendrites and spine morphogenesis

Several Rac-GEF proteins are known to localize at synapses and play critical roles in synaptogenesis (Penzes and Jones, 2008; Tolias et al., 2005). An emerging model is that Rac-GEFs play specific spatiotemporal roles in Rac1-dependent dendritic spine formation, maturation, maintenance and activity-dependent plasticity (Bai et al., 2015). For example, mice lacking the Rac-GEF, Kalirin-7, exhibit decreased spine density and neurocognitive defects (Penzes et al., 2003). Kalirin-7 expression occurs later during development and is maintained throughout adulthood, suggesting that it's role may be important in spine maturation/maintenance as opposed to early synapse development (Cahill et al., 2009; Ma et al., 2008; Xie et al., 2007). Furthermore, RNA interference knockdown of the Rac-GEF Tiam1 results in dendritic arbor simplification and a reduction in spine and synapse density (Tolias et al., 2005). Tiam1 interacts with the partitioning defective (PAR) protein PAR-3, which may act to spatially restrict Tiam1 to modulate a specific subpool of Rac1 within the dendritic spine head (Tolias et al., 2011; Zhang and Macara, 2006). While several other Rac-specific GEFs (i.e. a/b-PIX,

Vav2/3, Farp1) are known to play important roles in dendrite arborization and spine morphogenesis, relatively few Rac-GAP proteins have been characterized whose loss of function affects dendrites and spines (i.e. BCR, ABR, srGAP, Rich2) (Luo, 2000). We and others have shown that the shorter α1-chimaerin isoform plays a role in the pruning of dendrites and spines, suggesting that as a family, the α-chimaerins are important regulators of neuronal arborization (Buttery and Beg et al., 2006; Van de Ven et al., 2005). Importantly, our data demonstrate that dendritic dysmorphogenesis caused by loss of α2-chimaerin is not compensated for by α1-chimaerin, suggesting these two isoforms play unique and non-overlapping roles in dendritic arborization and spine morphogenesis. Taken together, these examples highlight that Rac-GEF/GAP protein localization, developmental regulation, and protein-protein interactions are critically important in modulating the spatiotemporal activity of Rac1 in dendrites and spines.

Cell surface regulation of GEF and GAPs in dendrites and spines

Activity-dependent signal transduction pathways need to be tightly controlled to ensure that individual dendritic spines respond appropriately to local signals. Coupling upstream receptor activation to the correct downstream effector proteins permits signaling specificity and is essential for driving morphological and functional plasticity in activated spines. In this context, α2-chimaerin is known to interact with several receptor tyrosine kinases that have important roles in dendritic spine morphogenesis and synaptic plasticity. The cell surface Eph receptors (EphR) play essential roles in dendritic spine morphogenesis (Gerlai, 2001). Activation of EphA4 causes spine retraction and shortening, whereas EphB2 promotes spine formation, maintenance and clustering of NMDA receptors (Dalva et al., 2000; Zhou et al., 2012). An outstanding

question is whether EphA4 and EphB1/2 receptors share common molecular pathways in differentially sculpting spines, or if they use distinct molecular pathways. Mounting evidence suggests that EphR regulate spine morphogenesis and synaptic plasticity by modulating Rho-GTPase activity (Calo et al., 2006). Significantly, the Rac-GEFs Kalirin-7, Tiam1 and Intersectin-L are required for EphB-induced spine remodeling (Tolias et al., 2007). We have previously demonstrated that α2-chimaerin interacts with both EphA4 and EphB1/2 receptors, and our data demonstrate that the loss of α2-chimaerin results in significant spine abnormalities (Beg et al., 2007). Together, these data suggest that the Rac-GAP α2-chimaerin may be a critical mediator of EphR-dependent spine morphogenesis and synaptic plasticity. However, it remains unclear what role α2-chimaerin plays in EphR-dependent spine morphogenesis. Is α2-chimaerin: 1) a dedicated EphA4 effector required for spine pruning; 2) required for EphB-mediated spine maturation and maintenance; or 3) a global EphR effector in spine morphogenesis? Given the lack of Rac-GAP proteins that have been characterized in spine morphogenesis, one possibility is that α2-chimaerin is recruited to synapses in response to EphR activation to counterbalance GEF activation of Rac1. Intriguingly, the similar dysmorphic spine phenotypes shared between EphA4 and α2-chimaerin mutant mice suggest that α2-chimaerin may be a critical downstream mediator of EphA4-dependent spine morphogenesis, which remains to be determined (Murai et al., 2003). Moreover, although α2-chimaerin can biochemically interact with EphB1/2, we have yet to identify a phenotype linked to these signaling pathways resulting from the loss of α2-chimaerin. Adding to the complexity of GEF/GAP regulation, a recent and elegant study revealed that GEFs and GAPs can form regulatory

complexes that modulate spine morphogenesis and synaptic plasticity (Um et al., 2014). Specifically, in response to Brain-derived neurotrophic factor- Tropomyosin receptor kinase B (BDNF-TrkB) signaling, a GEF/GAP complex comprised of Tiam 1 and BCR has been demonstrated to dynamically regulate the spatiotemporal activity of Rac1 within spines (Um et al., 2014). This intriguing example suggests that α2-chimaerin may form a similar regulatory complex with other GEF proteins to dynamically regulate spine morphogenesis and synaptic plasticity, but experimental evidence supporting this model remain to be determined.

Why are LTP and hippocampal-dependent behavior unaffected in α2-chimaerin mutants?

Actin cytoskeletal reorganization is critical for synaptic plasticity such as LTP (Chen et al., 2007). The effects of α2-chimaerin on the loss of F-actin organization, spine morphology and dendrite arborization suggest that α2-chimaerin-dependent signaling may contribute to activity-dependent synaptic plasticity. Given that disruption of other Rac-GAPs such as BCR, ABR and Rich2 result in decreased LTP maintenance, it is surprising that the loss of α2-chimaerin, which increases neuronal active Rac1-GTP and spine head F-actin, had no effect on LTP induction or maintenance (Oh et al., 2010; Raynaud et al., 2013). Our data suggests that α2-chimaerin may function to maintain the mature morphological hallmarks of dendritic spines, but may not be critical for functional changes within the spine. Accordingly, it has been reported that different pools of F-actin within the spine serve distinct functions in hippocampal LTP induction and maintenance (Honkura et al., 2008). Moreover, distinct molecular pathways can modulate Rho-GTPase signaling in spines, which are required for either the induction or

maintenance phases of LTP (Kennedy et al., 2005; Martinez and Tejada-Simon, 2011). An important observation from our results is that loss of α2-chimaerin dissociates morphological form and function. Specifically, the structural abnormalities in the dendritic receptive field and at the single spine level are not reflected as functional deficits within the hippocampus. A possible explanation is that the high basal levels of active Rac1 caused by loss of α2-chimaerin may invoke compensatory mechanisms that homeostatically inhibit downstream pathways associated with LTP. Alternatively, upregulation or enhanced activity of other Rac-GAPs such as BCR and ABR, or reduced activity of Rac-GEFs may compensate for loss of α2-chimaerin.

Mature mushroom-shaped spines are autonomous units that compartmentalize synaptic activity and restrict the diffusion of postsynaptic signaling molecules (Dailey and Smith, 1996; Harris, 1999). One possibility is that the dysmorphic spines in α2-chimaerin mutants may permit the spread of activity from one synapse to another, thereby compensating for alterations at the neuronal level to balance network activity. Alternatively, the increased occurrence of poly-innervated spines may compensate for the reduced protrusion density and simplified dendritic arbor. Accordingly, although α2-chimaerin loss results in decreased protrusion density, the number of synapses per unit length is increased, which may be a compensatory mechanisms that equalizes synaptic drive in α2-chimaerin mutant neurons.

Loss of α2-chimaerin during development has recently been reported to increase hippocampal-dependent contextual fear conditioning (Iwata et al., 2014). Our behavioral experiments are inconsistent with those reported by Iwasato et al, which suggested loss of α2-chimaerin early in development affects cognitive abilities in

adulthood. A possible explanation is that our behavioral experiments were performed on age-matched, mixed-gender P90 animals. Alternatively, the nature of the gene-trap mutation may be subtly different than the knockout strategy used by Iwasato et al (Stanford et al., 2001). However, both strains are phenotypically identical and exhibit similar axonal guidance and locomotor defects (Beg et al., 2007; Iwata et al., 2014). Regardless, the functional data strongly argue that hippocampal (CA3-CA1) LTP is unaffected by loss of α2-chimaerin, suggesting the reported changes in cognitive ability may be due to alterations in other forms of hippocampal synaptic plasticity.

In conclusion, our study provides the first evidence that α2-chimaerin is a critical regulator of Rac1 signaling in dendrites and spines. Elucidating the molecular mechanisms of how α2-chimaerin integrates and transduces cell-surface receptor activation to downstream effector pathways that alter dendritic spine cytoskeletal regulation are pressing questions for future studies.

Methods

Animal strains

Mice containing a gene-trap insertion in the a-chimaerin gene were obtained from Lexicon Genetics. For in vivo imaging, α2-chimaerin gene-trap mice were bred with Thy1-GFP-M transgenic mice (Feng et al., 2000).

Primary cell cultures

P0-1 C57BL/6J (WT) and α2-chimaerin homozygous mutant pups were utilized to prepare primary hippocampal neuronal cultures (Kaech and Banker, 2006). In short, hippocampi were isolated in Hanks-buffered salt solution (HBSS) without $MgCl_2$ and $CaCl_2$ containing 10mM 4-(2-hydroxyethyl)-1-piperazineethanesulfonic acid (HEPES).

The isolated hippocampi were washed once with HBSS + 10mM HEPES to remove small tissue debris then the solution was replaced with 1% Tyrpsin + 0.01% DNaseI in HBSS + 10mM HEPES. The hippocampi were exposed to the trypsin solution for 15 minutes at 37°C. Next, the solution was removed, and the tissue was washed with 5mLs of culture media containing DMEM (Gibco 11995-065), 0.8% D(+)Glucose, 1% Glutamax and 10% FBS. We then triturated the hippocampi in 1mL of this media with 10 pipette strokes from a 9" glass pipette. The tissue was again triturated with a 9" glass pipette that was 50% (eight triturations) and 25% (five triturations) of the original opening. We added 4mLs of DB1 to the triturated tissue and placed the tube on ice for 15 minutes. Afterwards we transferred the middle layer of the cell suspension (~4.5mLs) to a new tube. The cell suspension was pelleted *via* a spin at 1,500 rotations per minute (r.p.m.) for three minutes. We removed the culture media and re-suspended the cells in 1mL of fresh culture media *via* 10 triturations from a 9" glass pipette, and five triturations from a 9" glass pipette that was fire-polished to 50% of the original opening. The cells were then counted in Trypan Blue to exclude dead cells from the quantification. We plated 120,000 cells in culture media on 10mm poly-D-lysine coated coverslips placed individually in a 24-well cluster plate. After three hours the media was aspirated and replaced with Neurobasal media containing 1x B27 and 1x Glutamax. After two days, we treated the neurons with 10uM cytosine d-D-arabinofuranoside (AraC). Every 4 days we removed 50% of the media, which was replaced with fresh neural growth media.

Transfections

To analyze dendritic arborization and dendritic spines we transfected WT and α2-chimaerin mutant hippocampal neurons at 10 DIV with 600ng of β-actin GFP. All transfections were completed with 0.5μLs of Lipofectamine 2000 per well.

Rac1-GTP G-LISA

Primary hippocampal cultures were plated at a density of 500,000 cells per 35mm dish. After 17-19 DIV, cells were lysed and protein concentration was determined. We utilized equivalent amounts of protein lysate between the WT and α2-chimaerin mutant neurons to access basal Rac-GTP levels from the G-LISA colorimetric assay. A detailed protocol can be found at www.cytoskeleton.com/bk128.

Immunocytochemistry

Between 16-17 DIV, primary neurons were fixed with 4% paraformaldehyde (PFA) / 4% Sucrose in Dulbeco's phosphate buffer containing $MgCl_2$ and $CaCl_2$ (DPBS-MC) for 15 minutes at room temperature (RT). The coverslips were washed three times in DPBS-MC, for five minutes per wash and permeabilized in 0.01% TritonX-100 for ten minutes at RT. The cells were then washed three times for five minutes per wash at RT then incubated in 5% Donkey serum for 30 minutes at 4°C in a humidifying chamber. Afterwards, the coverslips were incubated with primary antibodies overnight at 4°C in a humidifying chamber. The next day the coverslips were washed three times with DPBS-MC for five minutes each at RT. The coverslips where incubated in secondary antibodies for 30 minutes at RT in a humidifying chamber. The coverslips were then washed three times for five minutes each at RT and mounted on glass slides.

Antibodies

PSD-95 (NeuroMab clone K28/43); Synaptophysin (Millipore 04-1019); anti-CHN1(abcam156869); GluR1 (Millpore MAB2263); GAPDH (GeneScript A00191-40); GFP (NeuroMab N86/38)

Image analysis

To analyze dendritic arborization in primary WT and α2-chimaerin mutant hippocampal neurons, we imaged GFP positive cells with a 20x objective on a wide-field fluorescence microscope. We utilized a semi-automated approach to trace dendritic segments from a single neuron with a NeuroJ Plugin in ImageJ (Meijering, 2010). From the generated binary image, we analyzed dendritic complexity by counting the number of proximal to distal dendritic intersections on concentric circles placed in a 20μm fixed radius around the soma via the Sholl Analysis Plugin in ImageJ (Longair et al., 2011). For *in vivo* dendritic arborization analysis, we utilized the same process and quantitative approaches; however, single cell images were collected from Z-series confocal micrographs that were Z-projected with a 20x objective.

Dendritic spine images were collected from Z-series confocal micrographs under the 60x objective plus a 3x digital zoom at 1024 pixel^2. The images were Z-projected and then we utilized the segmented line function to straighten 30μm segments of secondary and tertiary dendrites. The 30μm straightened dendritic segments were used to analyze spine density and protrusion shape frequencies. The protrusion shapes were binned into three categories: 1) Filopodial-like protrusions that exhibit a thin protrusion and lack a bulbous-shaped head; 2) dendritic spines, which are divided into; a) stubby spines that are stocky bulbous shaped protrusions and b) mushroom spines

that exhibit a narrow neck with a bulbous-like head; and 3) atypical spines are either bifurcated spines that exhibit a split spine neck and two separate bulbous-like protrusion heads, or branched spines, that resemble mushroom spines with a single or multiple mushroom-shaped protrusions emanating from the primary spine head. For *in-vivo* protrusion analysis, we counted secondary and tertiary dendritic protrusions on CA1 neurons from WT;GFPm+ and α2-chimaerin mutant;GFPm+ mice. The image acquisition parameters and processing of the 30μm dendritic segments were similarly collected as in our *in-vitro* approach.

For synapse analysis, we immunostained primary neurons that were previously transfected to express GFP with synaptophysin to label all pre-synaptic sites and PSD-95 to label the protein dense post-synaptic structures. We collected Z-series confocal micrographs of secondary and tertiary dendrites under the 60x objective plus a 3x digital zoom at 1024 pixel^2, and similarly we straightened 30μm dendritic segments from the collected images. The combination of the synaptic marker staining and the EGFP-expressing cells allowed for quantification of synapse density and synapse localization per protrusion-type.

Fear Conditioned Learning

Individual animals were placed into a conditioning chamber constructed of aluminum sides and clear acrylic backs and doors. The floor consisted of a stainless steel grid, spaced 1/8 inches apart with a stainless steel drop pan. A 120-Watt fluorescent bulb, placed ~10 feet away from the conditioning chambers, generated the ambient lighting, and we used 70% ethanol to clean the chambers between animal exposures. On Day One we trained squads of 4 animals that were individually placed in

the conditioning chambers and cameras mounted above each chamber monitored the animal's movement. We monitored 120 seconds (sec.) of baseline movement followed by a 30 sec. tone (2.8kHz and 75Db) that co-terminated with a 2 sec. electric shock (0.75 milliAmp.) to the stainless steel grid floor. The training protocol was repeated three times before the animal was removed from the chamber.

The shock was delivered through a solid-state shock scrambler, and an electronic constant current shock source. A desktop PC running Actimetrics Freeze-Frame software controlled the electric source and live-camera footage. On Day Two (Context Test), we monitored the animal's movement for five minutes in the conditioning chamber with the same context as Day One, but in the absence of tone or electric shock. On Day Three (Tone Test) the animals were placed in conditioning chambers but in a novel context. The new environment consisted of opaque white acrylic tiles placed over the stainless steel grid, and white walls producing a semicircular chamber. The light source was switched to a red fluorescence bulb (60 Watts), and chambers were cleaned with 2% acetic acid between animals. Once the animal was placed in the chamber we monitored 120 sec. of baseline movement followed by six, 30-second tones with a 30 sec. inter-tone interval for a total exposure of 7.5 minutes. From Day one through three, we recorded the animal's movement in conditioning chambers to analyze the percentage of time spent freezing. We defined freezing as the lack of motion, except for movement acquired during respiration that lasted longer than one second. We obtained the data from a sensitive global motion-detection algorithm to calculate the percentage freezing, and used GraphPad Prim 6.0 for statistical analysis.

Slice Preparation

Mice were anesthetized with isoflurane followed by decapitation to isolate the brain. We removed the cerebellum and glued the posterior end of the brain to a cutting stage that was immediately placed in ice-cold oxygenated artificial cerebrospinal fluid (aCSF: 125 NaCl, 25 NaHCO3, 2.5 KCl, 1.25 NaH2PO4, 2 CaCl2, 1 MgCl2, 0.4 ascorbic acid, and 25 D-glucose). From a vibrating blade microtome (VT1000S, Leica Microsystems), we prepared 400μm coronal sections at a slicing speed of 0.14mm/sec. and 1.00mm amplitude. Brain slices containing the hippocampus were cut at the mid-sagittal line and transferred to a holding chamber filled with oxygenated-aCSF. After one hour the brain slices were individually transferred to a submersion chamber and continuously perfused with oxygenated aCSF at 31°C.

Electrophysiology

To examine LTP in the CA3-CA1 hippocampal circuit, we placed recording and stimulating electrodes in the Schaffer Collateral region of CA1. The recording electrode was constructed from a Clark Borosilicate Standard Wall glass pipette pulled from a P-97 Flaming-Brown pipette puller and filled with aCSF. The recording electrode was connected to an amplifier and subsequent recordings were digitized. The stimulating electrode was purchased from WPI (WPI, TST33C05KT) and current was generated from a stimulus isolator. The digitized tracings were acquired to a Dell PC with pClamp 9.8. To collect field recordings, we first examined the fEPSP response to different stimulating current amplitudes to obtain an input-output curve. The fEPSP response was recorded from stimulus steps from 0-60 μA at 10 μA intervals. We evaluated the recordings and selected a stimulus intensity that produced 50% of the max fEPSP

response, and exhibited a symmetrical geometry related to the downward and upward slope of the fEPSP. The selected stimulus intensity was delivered to the slice every 15 seconds to collect ten minutes of basal synaptic activity followed by a theta burst stimulation at 100Hz (4 pulses) where we recorded the fEPSP response to the same baseline stimulus for one hour every 15 seconds.

Acknowledgements

Chris Valdez and Asim Beg designed the work presented in this chapter. Chris Valdez completed the experimental work and data analysis, and Dr. Geoff Murphy contributed scientific training and analytic tools to the behavioral and electrophysiological experiments.

Chapter 3

Alpha2-Chimaerin Alters Proliferative Properties in the Adult Mouse Hippocampus

Abstract

The subventricular zone (SVZ) of the lateral ventricle and subgranular zone (SGZ) in the hippocampal dentate gyrus are two neural regions that exhibit ongoing proliferation in the adult brain. In particular, the SGZ contains neural stem cells (NSCs) that divide to generate neurons and glial cells, or self-renew by generating progenitor cells to maintain the NSC population within the hippocampus. On a cellular level, the molecular players that regulate NSC cell division, and physically maintain the SGZ niche, remain elusive. Eph receptor signaling regulates proliferation of NSCs within the SGZ, and suppresses stem cell division outside this neurogenic region. The Rac1-GAP α2-chimaerin can interact with EphA4 and EphB1 receptors, and is a well-characterized protein effector that transduces EphA4 surface signaling. Our preliminary findings suggest α2-chimaerin expression may be targeted to the SGZ in the adult hippocampal dentate gyrus, where EphR/ephrin signaling modulates aspects of NSC proliferation. Our goal was to elucidate the potential role of α2-chimaerin in the adult SGZ. Here, we demonstrate that α2-chimaerin may contribute to the formation and cell cycle progression of proliferative cells in the adult SGZ. Further, we identified a previously uncharacterized role of α2-chimaerin in oligodendrocyte precursor cell proliferation

throughout the dentate gyrus. Given that the loss of α2-chimaerin produced similar cellular phenotypes in the SGZ as EphB1 receptor knockout mice, our research supports further testing of α2-chimaerin's activity as an Eph protein effector in the adult SGZ.

Introduction

The SVZ of the lateral ventricle and SGZ in the hippocampal dentate gyrus are two neural regions that exhibit proliferative capabilities in the adult brain (Alvarez-Buylla and García-Verdugo, 2002; Eriksson et al., 1998). Unlike other brain regions that actively suppress proliferation, the SVZ and SGZ contain neural stem cells (NSCs) that actively divide, and give rise to neurons and glia, or self-renew by generating progenitor cells to maintain the NSC population within the hippocampus (Gage, 2002). On a functional level, a reduction of adult-born neurons has been correlated to an increase in basal anxiety in rodents (Revest et al., 2009). Administration of anti-depressants (ADs) increases the rate of adult neurogenesis, and presumably the efficacy of ADs is affected by the increased incorporation of these adult-born neurons into the existing granule layer circuitry (Revest et al., 2009). While adult hippocampal proliferation may be subjected to modulation from pharmacological stimuli, the molecular players that regulate NSC cell division and preserve the SGZ niche under physiological conditions remain elusive (Ming and Song, 2011).

The EphR/ephrin signaling complex has been shown to regulate neural proliferation within the SGZ, and prevent stem cell division in non-neurogenic areas throughout the brain (Chumley et al., 2007; Khodosevich et al., 2011). For example, mice that lack EphB1 receptors exhibit a significantly reduced population of NSCs, and

neuronal progenitors exhibit defects in polarity and cell positioning within the SGZ (Chumley et al., 2007). Additionally, ephrin-A2 and ephrin-A3 signaling in astrocytes can suppress stem cell division outside the SGZ region (Mori et al., 2005). In these non-neurogenic areas, the loss of ephrin-A2 and ephrin-A3 signaling can induce presumably quiescent NSCs to generate adult-born neurons and glia (Jiao et al., 2008). Furthermore, mice that lack EphA4 exhibit a reduction in self-renewal of NSCs and have cell-cycle defects in neuronal progenitors, causing premature differentiation (Khodosevich et al., 2011). Taken together, these data suggest that EphR/ephrin signaling is important for various aspects of adult hippocampal proliferation. However, the protein effectors that transduce EphR/ephrin-mediated signaling are largely unknown.

We have previously demonstrated that the Rac1-GAP α2-chimaerin can interact with EphA4 and EphB1/2 receptors and is a well-characterized effector protein that transduces EphA4-mediated surface signaling in axonal guidance (Beg et al., 2007; Iwasato et al., 2007; Kao et al., 2015; Wegmeyer et al., 2007a). Here, we show that α2-chimaerin is expressed in SGZ primary neurospheres, an *in vitro* free-floating culture derived from NSCs in the adult hippocampus. In α2-chimaerin mutant mice, there was a significant increase in proliferative cells within the SGZ, and primary neurosphere formation was increased compared to controls. Intriguingly, the loss of α2-chimaerin increased oligodendrocyte precursor cell (OPC) proliferation throughout the adult mouse dentate gyrus. Taken together, our preliminary results suggest that α2-chimaerin may contribute to the formation and cell cycle progression of proliferative cells in the adult SGZ, which may affect basal anxiety levels in rodents.

Results

Alpha2-chimaerin is selectively expressed in the adult hippocampus

We first evaluated α2-chimaerin protein expression in neural tissues throughout the body. In adult WT mouse tissue lysates, we detected strong α2-chimaerin protein expression in the brain and testis and minimal levels in the heart and lungs (Figure 3.1A). We focused our analysis on the hippocampus because of its well-characterized role in learning and memory (Izquierdo and Medina, 1997; Squire, 1992). Currently, there is no commercially available α2-chimaerin antibody that is effective for immunohistochemical analysis. Thus, we took advantage of the lacZ reporter cassette in the α2-chimaerin mutant mouse to determine the spatial distribution, and temporal onset of α2-chimaerin expression in the early postnatal and adult hippocampus (Beg et al., 2007). Using this approach, we observed the onset of α2-chimaerin transcription in the pyramidal cell layer at P1 and expression in the granular cell layer at P5 (Figure 3.1B). From P5-P25, β-galactosidase (β-gal)+ cells were observed in the pyramidal and granular neuronal cell layers (Figure 3.1B). In P60-P90 hippocampi we observed a reduction of β-gal+ cells within the dentate gyrus; however, expression remained in the pyramidal cell layer (PCL). High magnification images revealed that β-gal+ cells were selectivity lost in the granule cell layer (GCL), but remained in the SGZ and hilus region of P60 and P90 adult hippocampi (Figure 3.1B). These data suggest that the temporal reduction of the α2-chimaerin protein in adult animals, relative to early postnatal stages, may be due to a spatially distinct and a selective loss of α2-chimaerin in adult granule neurons as opposed to an overall reduction throughout the hippocampus.

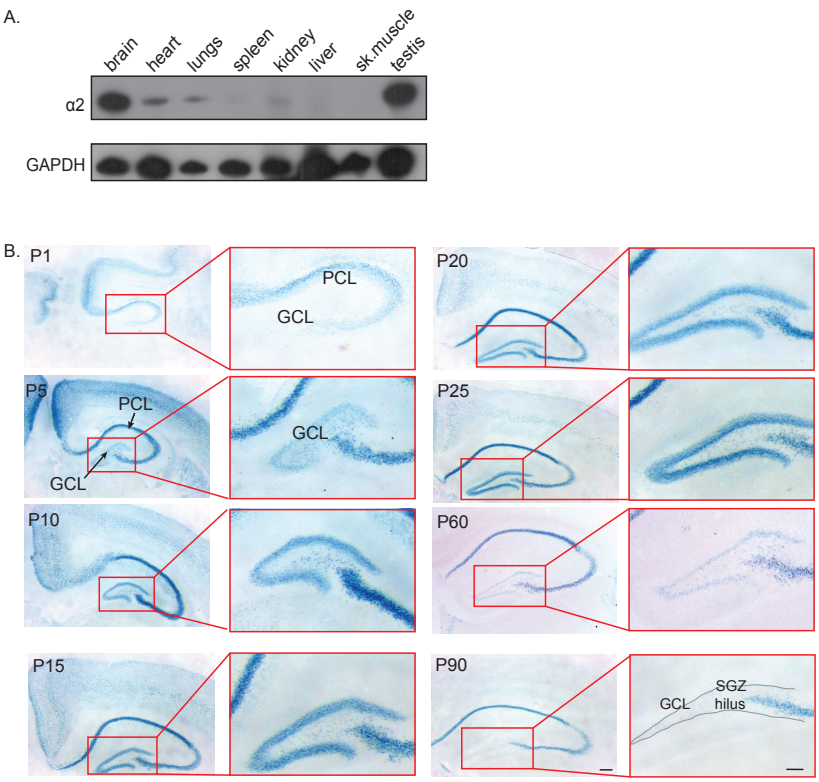

Figure 3.1 The spatial distribution of β-gal+ cells in the α2-chimaerin mutant mouse hippocampus

(A) Tissue was harvested from WT mice at 5-weeks of age, and 20μg of protein were loaded per well

(B) β-gal+ cells are present in the PCL from P1-P90. In the dentate, β-gal+ cells are observed at P5 and continue to P25. However, at P60 and P90 β-gal+ cells are present in the PCL, but are mostly cleared from the dentate. At higher magnification, β-gal+ cells are visible in the P60 and P90 dentate, but only in the SGZ and hilus, and are no longer visible in the GCL. Scale bar equals 120μm

Alpha2-chimaerin protein is expressed in proliferative cells

Given that α2-chimaerin transcription perdures in the adult SGZ, a stem cell niche in the adult hippocampus, we next utilized several *in vitro* approaches to determine if α2-chimaerin protein is expressed in neural stem cells. To this end, we cultured human embryonic neural stem cells (H9) and primary SGZ neurospheres, and demonstrated that α2-chimaerin protein was expressed in these cell types (Figure 3.2A-B). Next, we generated and probed primary SVZ neurospheres, a stem cell niche lining

the lateral wall of the lateral ventricle, revealing that α2-chimaerin protein is also expressed in this NSC-enriched population (Figure 3.2B). Overall, the results suggest that the α2-chimaerin protein is expressed in embryonic neural stems cells, and adult SGZ and SVZ primary neurospheres, which are distinct cellular populations enriched in adult neural stem cells as compared to whole tissue lysates.

To further characterize α2-chimaerin expression, we generated SGZ primary neurospheres from adult α2-chimaerin mutant mice and, using the β-gal reporter within the gene trap cassette, observed that a subset of β-gal+ cells distributed throughout the neurosphere (Figure 3.2C). At the single cell level β-gal+ and β-gal- cells were detected that co-localized with the proliferative cell marker, Ki67 (Figure 3.2E).

Since α2-chimaerin is expressed in Ki67+ cells in SGZ primary neurospheres, we next asked if the loss of α2-chimaerin affects the number of primary hippocampal neurospheres. We quantified the number of free-floating primary SGZ neurospheres in α2-chimaerin mutant mice and the α2-chimaerin mutant generated significantly more SGZ neurospheres compared to WT (Figure 3.2D). These data indicate that the loss of α2-chimaerin may increase the number neural stem cells capable of generating neurospheres, and suggests that, *in vivo*, the α2-chimaerin mutant hippocampus may exhibit altered levels of proliferative neural stem or progenitor cells.

Postnatal hippocampal proliferation in the α2-chimaerin mutant mouse

To assay SGZ proliferation, *in vitro*, we injected postnatal day (P)15 and 60 WT and α2-chimaerin mutant animals with 5-bromo-2'-deoxyuridine (BrdU) with a two-hour pulse before the animals were scarified and brains were isolated. From P15 animals, we quantified the number of BrdU+ cells in the SGZ, and observed no significant difference

between α2-chimaerin mutants and WT (Figure 3.3A-B). Additionally, we assayed P60 animals, and observed no significant difference in the number of BrdU+ cells in the SGZ between genotypes (Figure 3.4A-B). We further evaluated SGZ proliferation by immunostaining hippocampal slices for Ki67. At P15, we observed a significant reduction in the number of Ki67+ cells in the α2-chimaerin mutant (Figure 3.3A and E); however, the observation was transient, as we detected a significant increase in the total number of Ki67+ cells in the α2-chimaerin mutant hippocampus at P60 (Figure 3.4A and E). Taken together, these data suggest that the α2-chimaerin mutant SGZ does not display altered cell proliferation rates, as deduced by incorporation of BrdU over a two-hour pulse. However, the α2-chimaerin mutant SGZ displayed altered levels of proliferation, as measured by the number of Ki67+ cells. Given that α2-chimaerin mutants and WT controls exhibit equivalent numbers of BrdU+ cells in the SGZ, but that only the α2-chimaerin mutants display changes in numbers of Ki67+ cells, it is possible that the loss of α2-chimaerin alters cell cycle progression in proliferative cells within the hippocampus (See Discussion for details pg. 84).

Intriguingly, we observed increased numbers of BrdU+ and Ki67+ cells in the granule cell layer and molecular layer of the α2-chimaerin mutant dentate gyrus (Figure 3.3A and Figure 3.4A). Thus, we calculated the total number of proliferative cells localized throughout the dentate including the SGZ, GCL and ML. At P15 and P60, there was no significant difference in total BrdU+ cells localized throughout the α2-chimaerin mutant and WT dentate gyrus (Figure 3.3C and Figure 3.4C). We next quantified the total number of Ki67+ cells localized throughout the dentate gyrus.

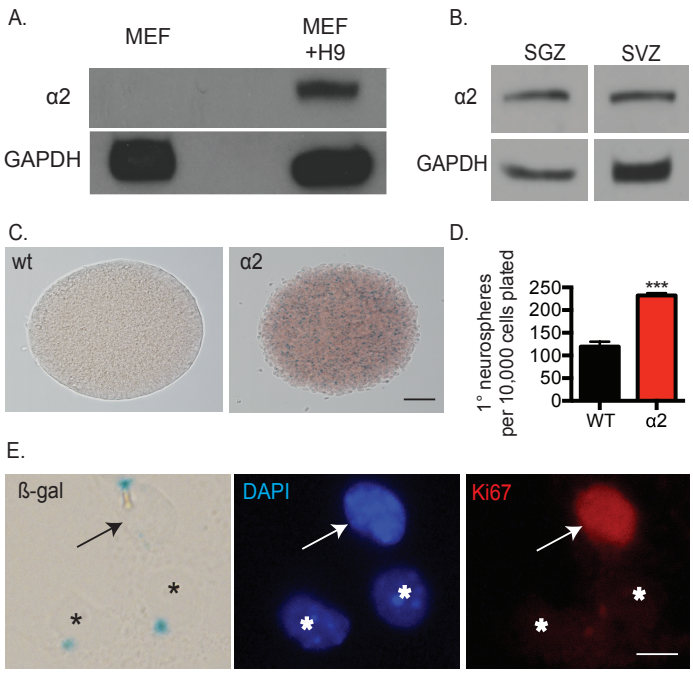

Figure 3.2 Alpha2-chimaerin expression in proliferating cells

(A) Western blot of H9, embryonic stem cells, grown on MEFs. Alpha2-chimaerin protein was detected in human embryonic neural stem cells grown on a bed of MEFs but not in MEFs grown alone as a control. Twenty micrograms of protein were loaded per well, and GAPDH protein was used as a loading control.

(B) Western blots demonstrating that α2-chimaerin protein is present in neurospheres derived from the adult mouse SGZ and SVZ. Fifty micrograms of protein were loaded per well, and GAPDH protein was utilized as a loading control.

(C) Upon X-gal exposure, we identified β-gal+ cells in neurospheres derived from the α2-chimaerin mutant hippocampus indicating α2-chimaerin transcription in primary neurospheres. The WT neurospheres were utilized as a negative control. Scale bar equals 25μm.

(D) Alpha2-chimaerin mutants formed significantly more primary neurospheres per well as compared to WT. Primary neurospheres formed (mean ± SEM): WT = 119.4 ± 64.75 and α2 = 232.3 ± 28.8; N = 3, n = 18 per strain; unpaired two-tailed *t-test*, $^{**}p < 0.0001$. Scale bar equals 100μm

(E) Immunostaining combined with X-gal treatment revealed α2-chimaerin expression on a single cell level in primary neurospheres grown on glass coverslips in self-renewal media for 7 DIV. The arrow indicates a Ki67+ proliferative cell that is β-gal+; while the asterisks specify β-gal+ cells that are not co-localized with Ki67. Scale bar 5μm

At P15, we observed a significant reduction in Ki67+ cells in the α2-chimaerin mutant dentate gyrus followed by a significant increase at P60 compared to WT (Figure 3.3F and Figure 3.4F). Importantly, these data demonstrate that loss of α2-chimaerin alters the number of Ki67+ cells throughout the hippocampus and not just the SGZ.

Next, we evaluated the percent distribution of total BrdU+ and Ki67+ cells in the SGZ, GCL and ML in the α2-chimaerin mutant and wild type hippocampus. At P15, we calculated that 96% of total BrdU+ cells in the WT dentate gyrus were localized in the SGZ in WT (Figure 3.3D); whereas, 88% of the total BrdU+ cells in the α2-chimaerin mutant dentate gyrus were localized in the SGZ (Figure 3.3D). In the α2-chimaerin mutant 11% of the total BrdU+ cells were localized in the GCL and ML as opposed to 4% in WT (Figure 3.3D). At P60 we observed a similar trend, in that 93% of the total BrdU+ cells were localized to the SGZ in control animals, and 84% were localized in the SGZ of the α2-chimaerin mutant, leaving 15% of the total BrdU+ cells in the GCL and MCL (Figure 3.4D) (control = 7% of total BrdU+ cells in the GCL and ML). Similar analyses were performed using Ki67 immunostained hippocampal slices. At P15, control animals exhibited 96% of total Ki67+ cells in the SGZ and 4% were localized in the GCL and ML (Figure 3.3G). α2-chimaerin mutants displayed 85% of total Ki67+ cells in the SGZ and 15% in the GCL and ML (Figure 3.3G). At P60, control animals expressed 96% of total Ki67+ cells in the SGZ and 4% in the GCL and ML (Figure 3.4G). In P60 α2-chimaerin mutants, 88% of the total Ki67+ cells were localized in the SGZ, and 12% were localized in the GCL and ML (Figure 3.4G). These data suggest that the loss of α2-chimaerin disrupts the distribution of BrdU+ and Ki67+ cells in the young and adult hippocampus.

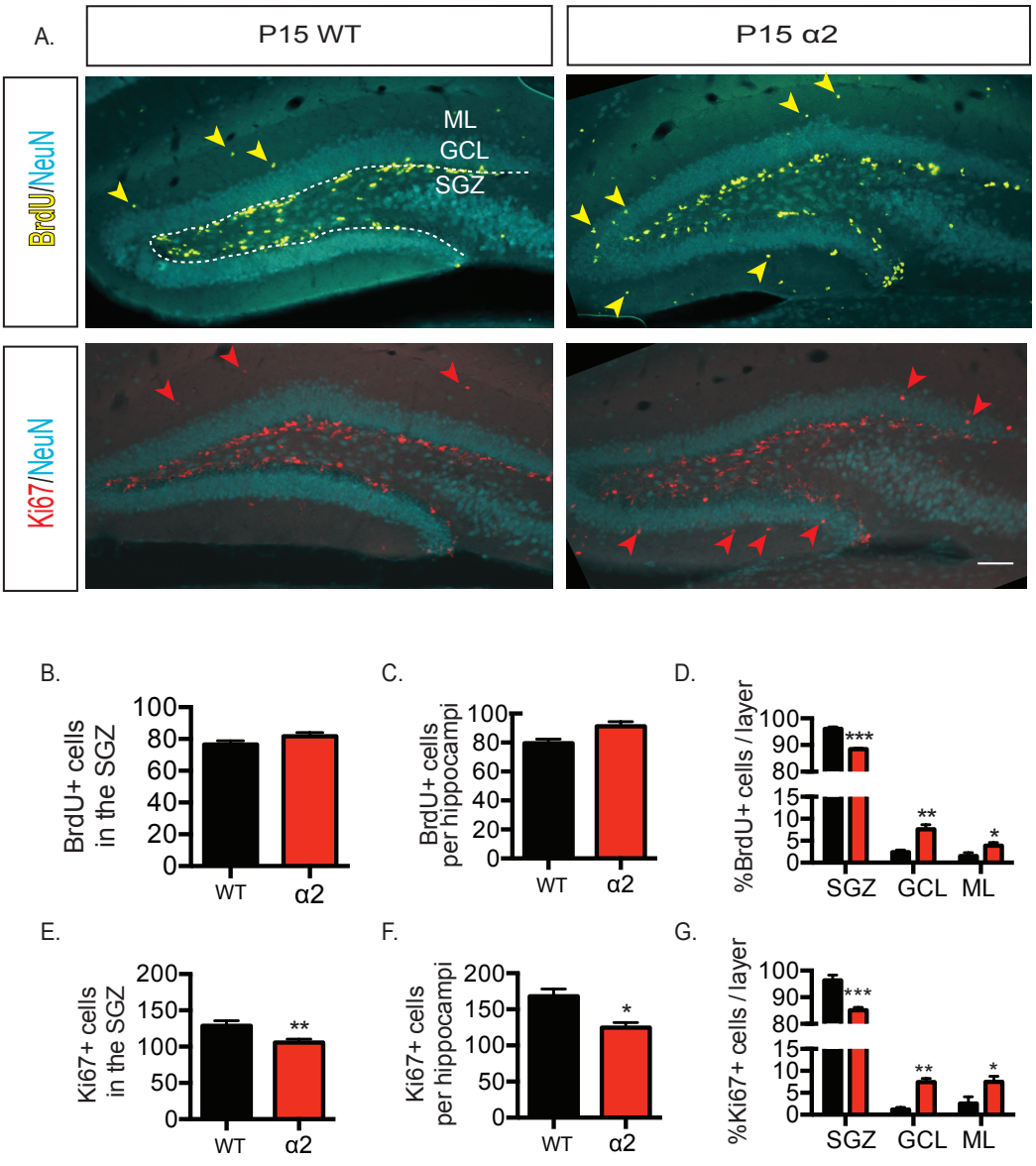
A.
P15 WT
P15 α2
BrdU/NeuN
Ki67/NeuN
ML
GCL
SGZ
B.
BrdU+ cells in the SGZ
100
80
60
40
20
0
WT
α2
C.
BrdU+ cells per hippocampi
100
80
60
40
20
0
WT
α2
D.
%BrdU+ cells / layer
100
90
80
15
10
5
0
***
**
*
SGZ
GCL
ML
E.
Ki67+ cells in the SGZ
200
150
100
50
0
**
WT
α2
F.
Ki67+ cells per hippocampi
200
150
100
50
0
*
WT
α2
G.
%Ki67+ cells / layer
100
90
80
15
10
5
0
***
**
*
SGZ
GCL
ML

Figure 3.3 P15 hippocampal proliferation

(A) Representative images of P15 wild type and α2-chimaerin mutant hippocampi immunostained to identify BrdU+ and Ki67+ cells. The dashed line delineates the GCL that contains mature neurons and the SGZ that houses neural progenitors. The ML contains dendrites from the granule neurons in the GCL. The yellow and red arrows identify BrdU+ and Ki67+ cells localized outside the SGZ, respectively. Scale bar 100μm

(B) Quantification of BrdU+ cells localized in the SGZ (mean ± SEM): WT = 76.61 ± 2.2; N = 3, n = 31 and α2 = 81.67 ± 2.4; N = 3, n = 27

(C) Quantification of BrdU+ cells localized throughout the hippocampus (SGZ+GCL+MCL) (mean ± SEM): wt = 79.95 ± 2.86; N = 3, n = 31 and α2 = 91.17 ± 3.32; N = 3, n = 27

(D) Quantification of the percentage of BrdU+ cells that reside in the GCL, SGZ and ML (mean ± SEM): WT: 96.1 ± 0.39%(SGZ), 2.40 ± 0.28%(GCL) and 1.49 ± 0.44%(ML); N = 3,n = 31 and α2 = 88.5 ± 0.19%(SGZ), 7.62 ± 0.58%(GCL) and 3.87 ± 0.42%(ML); N = 3,n = 27; *t-test, α* = .05, Holm-Sidak method; ****p < 0.0001* (SGZ), ***p* = 0.001 (GCL), and **p* = 0.017 (ML)

(E) Quantification of Ki67+ cells localized in the SGZ (mean ± SEM): WT = 128.7 ± 7.1; N = 3, n = 31 and α2 = 105 ± 4.7 N = 3, n = 27; unpaired two-tailed *t-test*, ***p* = 0.0083

(F) Quantification of Ki67+ cells localized throughout the hippocampus (SGZ+GCL+MCL) (mean ± SEM): WT = 168.1 ± 10; N = 3, n = 31 and α2 = 124.9 ± 6.9; N = 3, n = 27; unpaired two-tailed *t-test*, **p* = 0.0347

(G) Quantification of the percentage of Ki67+ cells that reside in the GCL, SGZ and ML (mean ± SEM): WT: 96.30 ± 1.56%(SGZ), 1.16 ± 0.30%(GCL) and 2.52 ± 0.91%(ML); N = 3, n = 31 and α2 = 85.07 ± 0.65%(SGZ), 7.44 ± 0.488%(GCL) and 7.47 ± 0.73%(ML); N = 3, n = 27; *t-test, α* = .05, Holm-Sidak method; ****p* = 0.0004 (SGZ), ***p* = 0.001 (GCL), and **p* = 0.013 (ML)

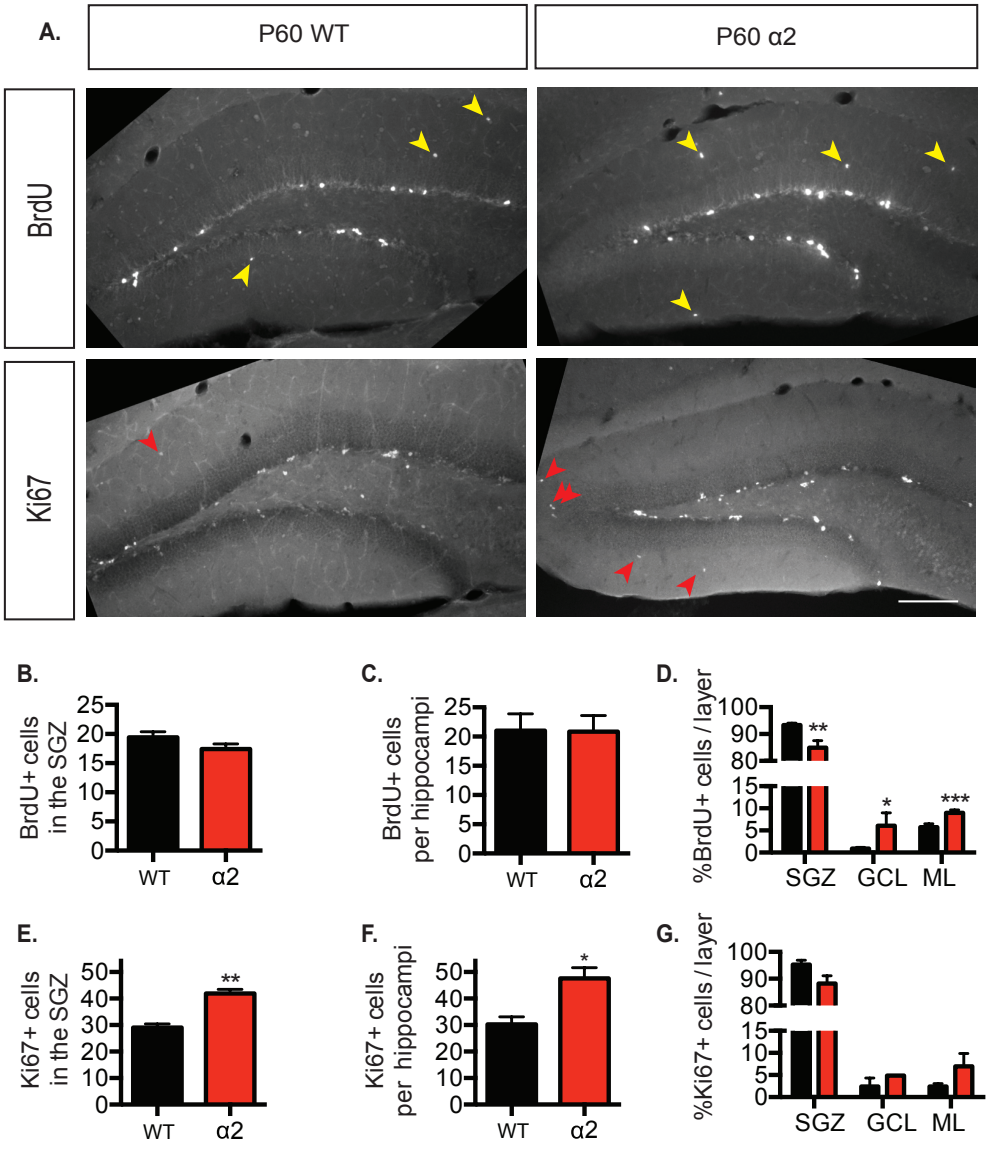
A.
P60 WT
P60 α2
BrdU
Ki67
B.
BrdU+ cells in the SGZ
25
20
15
10
5
0
WT
α2
C.
BrdU+ cells per hippocampi
25
20
15
10
5
0
WT
α2
D.
%BrdU+ cells / layer
100
90
80
15
10
5
0
**
*
***
SGZ
GCL
ML
E.
Ki67+ cells in the SGZ
50
40
30
20
10
0
**
WT
α2
F.
Ki67+ cells per hippocampi
50
40
30
20
10
0
*
WT
α2
G.
%Ki67+ cells / layer
100
90
80
15
10
5
0
SGZ
GCL
ML

Figure 3.4 P60 hippocampal proliferation

(A) Representative images of P60 wildtype and α2-chimaerin mutant hippocampus immunostained to reveal BrdU+ and Ki67+ cells. The yellow and red arrows identify BrdU+ and Ki67+ localized outside the SGZ, respectively. Scale bar equals 120μm

(B) Quantification of BrdU+ cells localized in the SGZ (mean ± SEM): WT = 19.43 ± 2.9; N = 3, n = 28 and α2 = 17.43 ± 0.83; N = 3, n = 28

(C) Quantification of BrdU+ cells localized throughout the hippocampus (SGZ+GCL+MCL) (mean ± SEM): WT = 21.03 ± 4.9; N = 3, n = 28 and α2 = 20.84 ± 4.75; N = 3, n = 28

(D) Quantification of the percentage of BrdU+ cells that reside in the GCL, SGZ and ML (mean ± SEM): WT: 93.34 ± 0.43% (SGZ), 0.92 ± 0.462% (GCL) and 5.73± 0.14% (ML); N = 3, n = 28 and α2 = 84.93 ± 1.53% (SGZ), 6.07 ± 1.67% (GCL) and 8.98 ± 0.38% (ML); N = 3, n = 28; *t-test, α* = .05, Holm-Sidak method; ***p* = 0.006 (SGZ), **p* = 0.03 (GCL), and ****p* = 0.005 (ML)

(E) Quantification of Ki67+ cells localized in the SGZ (mean ± SEM): WT = 29.2 ± 1.7; N = 3, n = 26 and α2 = 41 ± 1.5; N = 3, n = 28; unpaired two-tailed *t-test*, ***p* < 0.0001

(F) Quantification of Ki67+ cells localized throughout the hippocampus (SGZ+GCL+MCL) (mean ± SEM): WT 30.3 ± 2.72; N = 3, n = 26 and α2 = 47.62 ± 3.98; N = 3, n = 28; unpaired two-tailed *t-test*, **p* = 0.0234

(G) Quantification of the percentage of Ki67+ cells that reside in the GCL, SGZ and ML (mean ± SEM): wt: 95.21 ± 0.94%(SGZ), 2.38 ± 1.11%(GCL) and 2.40 ± 0.34%(ML); N = 3, n = 26 and α2 = 88.20 ± 1.67%(SGZ), 4.84 ± 0.02%(GCL) and 6.94 ± 1.68%(ML); N = 3, n = 28

Assessment of neurogenic defects in the dentate gyrus of the α2-chimaerin mutant mouse

Our data suggest that loss of a2-chimaerin results in increased number of proliferative cells localized outside the SGZ. This unique phenotype is also observed in EphB1 knockout mice, as they exhibit ectopically localized BrdU+ proliferative cells in the granule cell layer and molecular layer of the dentate gyrus (Chumley et al., 2007). Given the shared phenotype, we next assessed if the α2-chimaerin mutant mouse exhibited additional phenotypes observed in the EphB1$^{-/-}$ or the EphB1/2$^{-/-}$double

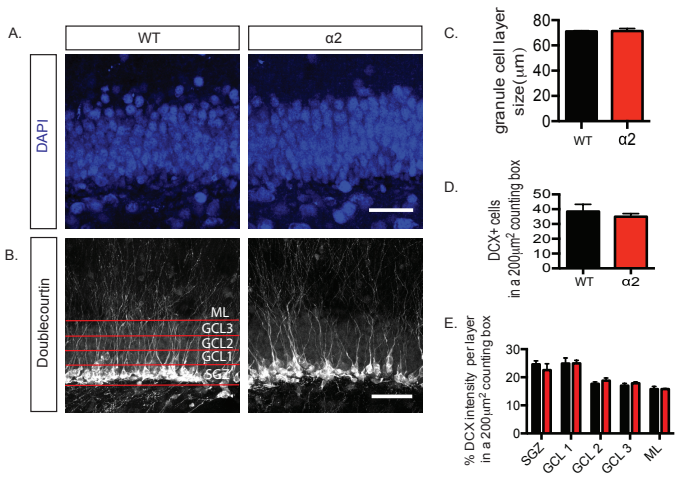

Figure 3.5 The loss of α2-chimaerin does not alter the size of the granule cell layer, or number and dendritic complexity of DCX+ neurons in the SGZ

(A) Representative Dapi stained images of the granule cell layer from P60 WT and α2-chimaerin mutant animals. Scale bar equals 50μm

(B) Representative images of DCX+ cells from the P60 WT and α2-chimaerin SGZ. The rectangle boxes delineate the subgranular zone (SGZ); the granule cell layer (GCL), which was divided into three sections from beginning at GCL 1 (proximal to the SGZ) to GCL 3 (distal to the SGZ) and the molecular layer (ML). Scale bar equals 50μm

(C) Quantification of the granule cell layer size in WT and α2-chimaerin (mean ± SEM): WT = 71.17 ± 0.52μm and α2 = 71.39 ± 1.95μm; N = 4, n = 30 per genotype

(D) Quantification of DCX+ cells in a 200μm^2 quantification box (mean ± SEM): WT = 38.40 ± 4.87 and α2 = 34.93 ± 2.08; N = 3, n = 15 per genotype.

(E) Quantification of the percentage of DCX+ fluorescence intensity distributed across the SGZ, GCL1-3 and ML in wt and α2-chimaerin mice (mean ± SEM): WT = 24.61 ± 0.61%(SGZ), 24.92 ± 0.97%(GCL1, 17.66± 0.33%(GCL2), 17.00 ± 0.41%(GCL3) and 15.79 ± 0.46 %(ML); N = 4, n = 20 and α2 = 22.53 ± 1.13%(SGZ), 24.97 ± 0.54%(GCL1, 18.82 ± 0.46%(GCL2), 17.87 ± 0.22%(GCL3) and 15.78 ± 0.10%(ML); N = 4, n = 20.

knockout animal. For example, the EphB1$^{-/-}$ and EphB1/2$^{-/-}$ double-knockout mice exhibit a reduction in granule cell layer size and volume. While EphB1 knockout animals do not have a reduced granule cell layer volume, suggesting an EphB2-specific deficit, they do exhibit a decrease in the number and dendritic complexity of immature neurons in the SGZ (Catchpole and Henkemeyer, 2011; Chumley et al., 2007).

To assess granule cell layer morphology, we measured the size of the granule cell layer by utilizing DAPI staining to label all cells within the section. We did not observe a difference in granule cell layer size in the α2-chimaerin mutant as compared to WT (Figure 3.5A). Additionally, we assessed the number and complexity of immature neurons by immunostaining hippocampal sections with an anti-doublecortin (DCX) antibody, and observed no significant difference in these metrics (Figure 3.5B). The partial phenocopy observed between EphB and α2-chimaerin mutants suggests that EphB signaling may utilize α2-chimaerin as a protein effector for distinct mechanisms, but that some EphB activity may be independent of α2-chimaerin activity.

Identifying proliferative cells in the α2-chimaerin mutant hippocampus

We next aimed to determine the cellular identity of the BrdU+ and Ki67+ cells localized in the GCL and ML in the α2-chimaerin dentate gyrus using the following markers: immature neuronal marker, doublecortin (DCX); neuronal precursor marker, Nestin; neural stem cell marker, glial fibrillary acidic protein (GFAP) and apoptotic marker, cysteine-dependent aspartate-directed proteases (Caspase-3). From the immunostained hippocampal sections, we did not detect co-localization of GFAP, DCX, Nestin or Caspase with BrdU+ or Ki67+ cells localized in the α2-chimaerin mutant GCL and ML (Figure 3.6E-F). The results from the antibody screen suggest that the proliferative cells present in the granule cell layer and molecular layer of the α2-chimaerin dentate gyrus are not immature neurons (DCX), astrocytes (GFAP), apoptotic cells (Caspase-3) or Nestin/GFAP expressing neural stem cells (Figure 3.6F-G). As expected, we did observe co-localization of the aforementioned cell markers with BrdU+ and Ki67+ cells in the SGZ of both α2-chimaerin mutant and WT (Figure 3.6A-D).

To date, α2-chimaerin is thought to be exclusively expressed in CNS neurons (Hall et al., 2001). To determine if other CNS cell types express α2-chimaerin protein, we probed purified cell type lysates with a specific α2-chimaerin antibody. Using this approach, we identified that α2-chimaerin is robustly expressed in oligodendrocyte precursor cells (OPCs), but largely absent in Schwann cells, microglia and astrocytes (Figure 3.6G). Due to the robust expression in OPCs, we sought to determine if the ectopic proliferative cells in the α2-chimaerin dentate gyrus were positive for OPC markers.

The loss of α2-chimaerin induces proliferation of oligodendrocyte precursor cells in the hippocampus

To identify OPCs, we utilized an antibody against the oligodendrocyte transcription factor-2 (Olig2), a protein expressed in OPCs that is a multifunctional regulator of proliferation throughout the CNS, and a key-determinant for OPC maturation to oligodendrocytes (Takebayashi et al., 2000). Confocal Z-series images of the α2-chimaerin mutant dentate gyrus revealed BrdU+/Olig2+ cells localized outside the SGZ in the α2-chimaerin mutant (Figure 3.7A). We further analyzed the images by counting the number of BrdU+ cells localized outside the SGZ (Figure 3.7B-D). From these cells, we quantified the number of BrdU+/Olig2+ and BrdU+/Olig2- cells in the

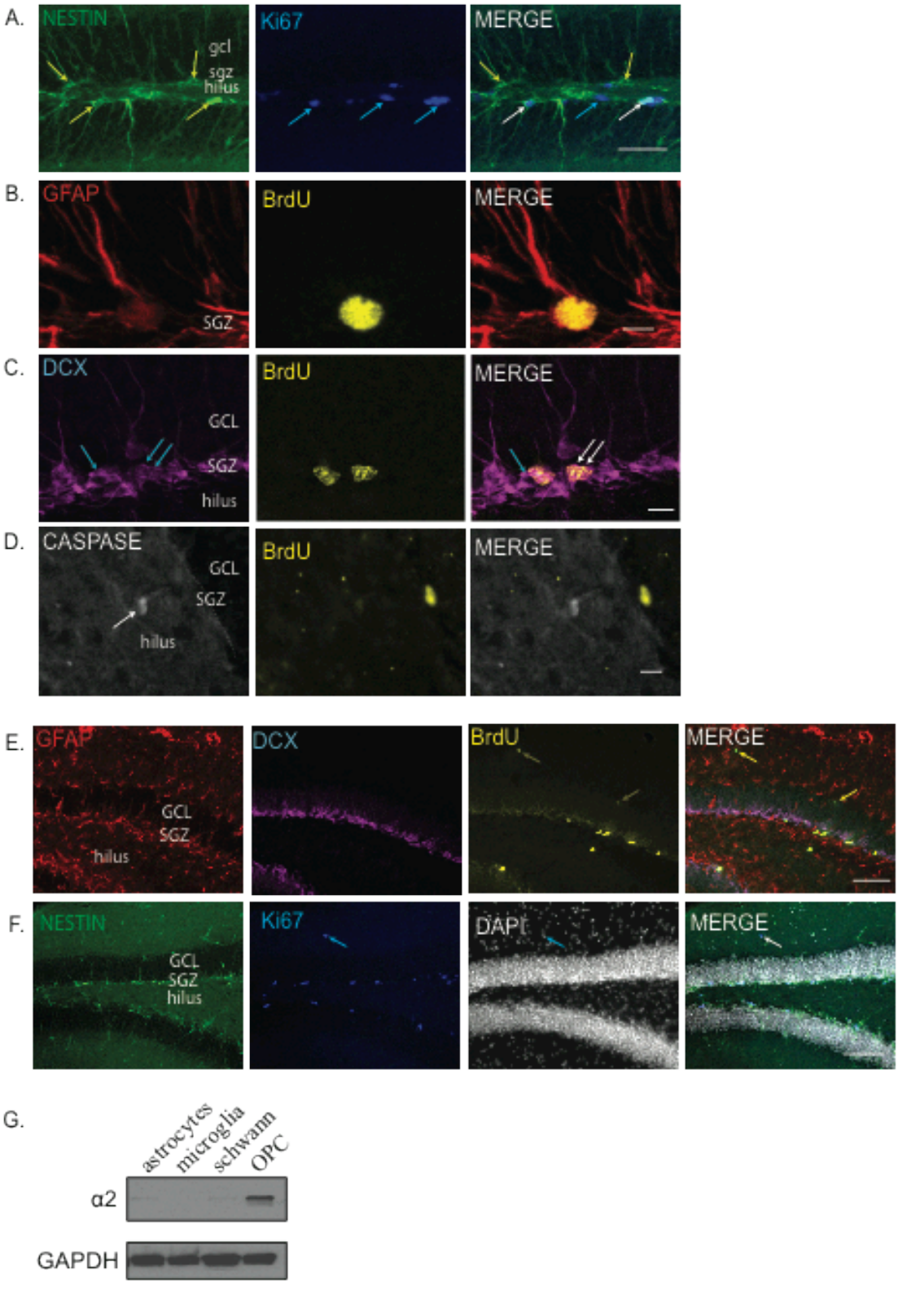
A.
NESTIN
gcl
sgz
hilus
Ki67
MERGE
B.
GFAP
SGZ
BrdU
MERGE
C.
DCX
GCL
SGZ
hilus
BrdU
MERGE
D.
CASPASE
GCL
SGZ
hilus
BrdU
MERGE
E.
GFAP
GCL
SGZ
hilus
DCX
BrdU
MERGE
F.
NESTIN
GCL
SGZ
hilus
Ki67
DAPI
MERGE
G.
astrocytes
microglia
schwann
OPC
α2
GAPDH

Figure 3.6 Cell marker screen to identify aberrant proliferative cells in the α2-chimaerin hippocampus

(A). Representative images demonstrating the specificity of cell markers utilized in the antibody screen: Nestin antibodies label Type 1-2b stem cell/progenitor cells in the SGZ of the adult hippocampus. As expected, we observed Ki67+ (magenta arrows) and Nestin+ cells (green arrows) throughout the SGZ. The white arrows mark co-labeled Nestin+/Ki67+ cells. Scale bar equals 80μm

(B). GFAP antibodies label Type 1 neural stem cells and the cytoskeleton of mature astrocytes. The representative image reveals a BrdU+/GFAP+ Type 1 stem cell in the SGZ. Scale bar equals 4μm.

(C) DCX antibodies label the cytoskeleton of immature neurons. The representative image reveals DCX+ immature BrdU+ and BrdU- neurons in the adult SGZ. The BrdU+ cells localized to the SGZ that display DCX+ extensions (white arrows) indicate newly generated immature neurons. Scale bar equals 4μm

(D) Caspase-3 antibodies label cells that are targeted for apoptosis. The representative images capture a Caspase-3+ cell (white arrow) and a BrdU+/Caspase- cell in the dentate hilus. Scale bar equals 4μm

(E) Aberrant BrdU+ cells in the α2-chimaerin mutant dentate gyrus. The yellow arrows delineate BrdU+ cells localized outside the SGZ. In this brain section, we do not observe co-labeling with DCX or GFAP. Scale bar equals 100μm

(F) An aberrant Ki67+ cell in the α2-chimaerin mutant dentate gyrus. The magenta arrows mark a Ki67+ cell outside the SGZ that is not co-labeled with Nestin antibodies. The DAPI staining is used as a control to label cellular DNA. Scale bar equals 100μm

(G) Western blot analysis demonstrates that, in addition to being expressed in neurons, the α2-chimaerin protein is expressed in OPCs, but not in astrocytes, microglia or Schwann cells; purified cell lysates were derived from human samples and loaded at 30μg/well.

GCL and ML, respectively. In the GCL, we observed a significant increase in BrdU+ cells, and a significant number of these cells were Olig2- in the α2-chimaerin mutant (Figure 3.7C). In the ML, the α2-chimaerin mutant exhibited an overall increase in BrdU+ cells, and exhibited both a significant increase in Olig2+ and Olig2- cells compared to control (Figure 3.7D). The data suggest that OPC proliferation in the ML is increased by the loss of α2-chimaerin.

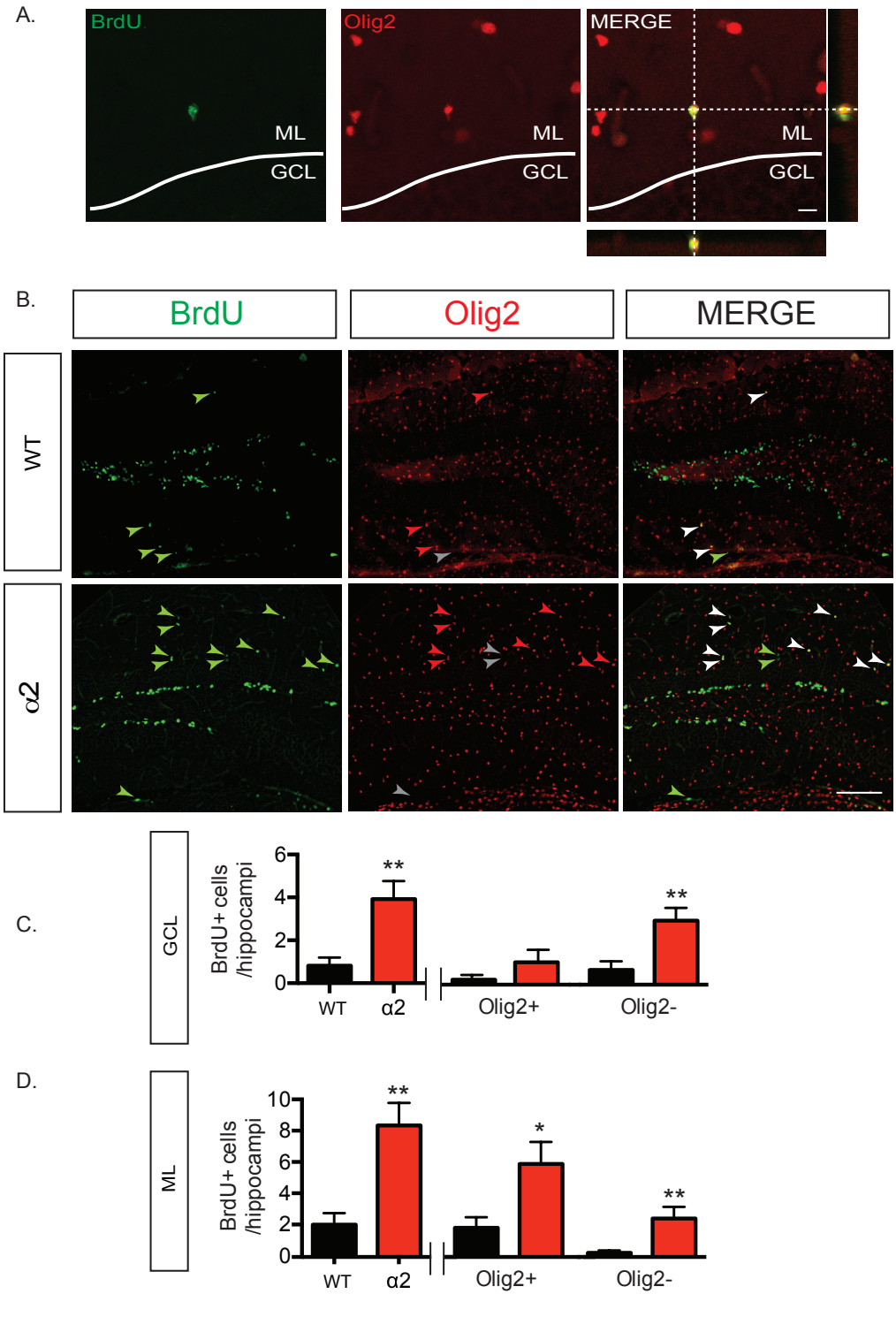
A.
BrdU
Olig2
MERGE
ML
GCL
B.
BrdU
Olig2
MERGE
WT
α2
C.
GCL
BrdU+ cells /hippocampi
WT
α2
Olig2+
Olig2-
D.
ML
BrdU+ cells /hippocampi
WT
α2
Olig2+
Olig2-

Figure 3.7 The loss of α2-chimaerin results in aberrant proliferation of oligodendrocyte precursor cells

(A) Aberrant BrdU+ cell localized in the ML of the α2-chimaerin dentate gyrus co-localizes with Olig2. Scale bar equals 5μm

(B) Representative images of the α2-chimaerin mutant and WT dentate gyrus immunostained to label BrdU+ and Olig2+ cells. The green arrowheads highlight BrdU+ cells outside the SGZ and red arrowheads mark Olig2+ cells. In the Olig2 panel, the gray arrowheads mark BrdU+/Olig2- cells. In the Merge panel, white arrowheads label BrdU+/Olig2+ cells. Scale bar equals 200 μm

(C) Quantification of BrdU+ cells in the GCL (mean ± SEM): WT = 0.81 ± 0.37; N = 3,n = 11 and α2 = 3.91 ± 0.84; N = 3,n = 12; unpaired two-tailed *t-test*, $^{**}p = 0.004$. Quantification of BrdU+/Olig2+ cells in the GCL (mean ± SEM): WT = 0.18 ± 0.18; N = 3,n = 11 and α2 = 1.00 ± 0.53; N = 3,n = 12. Quantification of BrdU+/Olig2- cells in the GCL (mean ± SEM): WT = 0.63 ± 0.36; N = 3,n = 11 and α2 = 2.91 ± 0.55; N = 3,n = 12; unpaired two-tailed *t-test*, $^{**}p = 0.003$

(D) Quantification of BrdU+ cells in the ML (mean ± SEM): WT = 2.00 ± 0.61; N = 3,n = 11 and α2 = 8.33 ± 1.32; N = 3,n = 12; unpaired two-tailed *t-test*, $^{**}p = 0.0004$. Quantification of BrdU+/Olig2+ cells in the ML (mean ± SEM): WT = 1.81 ± 0.61; N = 3,n = 11 and α2 = 5.91 ± 1.37; N = 3,n = 12; unpaired two-tailed *t-test*, $^{*}p = 0.0153$. Quantification of BrdU+/Olig2- cells in the ML (mean ± SEM): WT = 0.18 ± 0.122; N = 3,n = 11 and α2 = 2.41 ± 0.70; N = 3,n = 12; unpaired two-tailed *t-test*, $^{**}p = 0.0067$

Behavioral defect in α2-chimaerin mutant mouse

The marble-burying test has been postulated to measure basal anxiety in rodents (Deacon, 2006). Experimentally, animals that are injected with anxiolytics such as diazepam, chlordiazepoxide or pentobarbitone bury fewer marbles than control-treated rodents suggesting that a reduction in basal anxiety attenuates marble burying behavior in mice (Handley, 1991). In the brain, anxiolytics have been demonstrated to influence adult neurogenesis in the hippocampus presumably by causing an increase in adult-born neuron proliferation, survival and incorporation into existing neuronal circuitry (Deng et al., 2010; Huang et al., 2008; Ming and Song, 2011). Given the altered proliferation levels in the α2-chimaerin mutant hippocampus, we sought to determine if basal anxiety was altered in the α2-chimaerin mutant mouse.

After a 30-minute exposure to a 3x4 grid of equally spaced marbles (12 marbles total), we observed that α2-chimaerin mutants buried significantly fewer marbles as compared to WT controls (Figure 3.8A-B). Furthermore, we extended the assay for 90 minutes and α2-chimaerin mutants buried approximately the same number of marbles as compared to the 30-minute examination. A potential confounding factor is that α2-chimaerin mutant mice exhibit a rabbit-like hopping gait locomotor phenotype, thus the inability to bury marbles might be due to decreased overall movement. Live video tracking during these tasks revealed that α2 mutant mice explore the environment equally as well as controls, demonstrating that reduced movement is unlikely to explain this phenotype (Figure 3.8B). Our behavioral assessment provides preliminary data suggesting that α2-chimaerin mutants may exhibit a reduction in basal anxiety, which maybe mediated through altered dynamics in hippocampal proliferation or other brain areas such as a the cortex (Davidson, 2002).

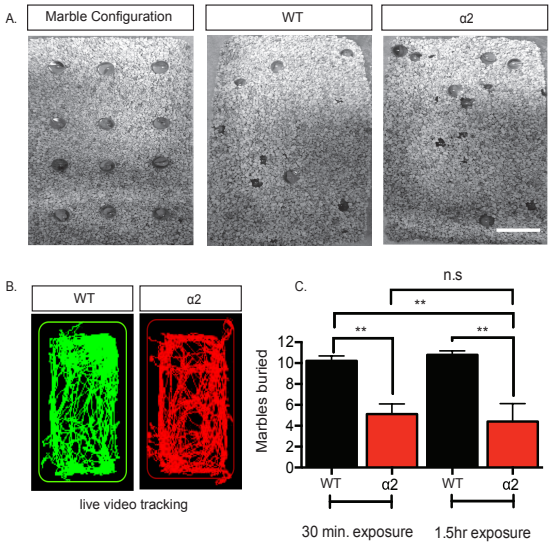

Figure 3.8 Marble-burying test

(A) The left image is a representation of the 3x4 marble grid at the start of the marble burying examination. The center and right images represent marble burying activity of wt and α2-chimaerin mutant mice after a 30-minute exposure. Scale bar equals 5cm

(B) Live video tracking of mice during the marble burying text. The tracer tracks core body movement. Scale bar equals 5cm

(C) Quantification of marbles buried (mean ± SEM): After 30 minutes: WT = 10.2 ± 0.46; N = 9 and α2 = 5.1 ± 0.98; N = 9. After 1.5 hours: WT = 10.80 ± 0.37 and α2 = 4.4 ± 1.7; N = 5 per genotype; one-way *ANOVA* $F(3,25) = 11.29$, $^{**}p < 0.0001$.

Discussion

The state of SGZ proliferation in the α2-chimaerin mutant mouse

We assessed neural proliferation in the α2-chimaerin mutant by quantifying the number of Ki67+ and BrdU+ proliferative cells in the SGZ. Unlike BrdU, Ki67 is an endogenous protein that is expressed during all proliferative stages of the cell cycle (G_1, S, G_2 and Mitosis), and therefore identifies the proliferative fraction of cells within the SGZ (Figure 3.9) (Kee et al., 2002; Taupin, 2007). For example, progeny of adult born neurons will express Ki67 during all proliferative stages, and will incorporate BrdU only during DNA replication (S-phase). However, as the neuron matures it will suppress Ki67 expression and enter the post-mitotic, G_0 cell cycle phase (Endl and Gerdes, 2000; Eriksson et al., 1998). Although the loss of α2-chimaerin altered the number of Ki67+ cells in the SGZ, we did not observe a significant difference in the level of proliferative neural progenitor cells that incorporated BrdU. Taken together, the altered level of Ki67+ cells, but relatively equivalent incorporation of BrdU between α2-chimaerin mutants and WT mice suggest; 1) that the rate of neural proliferation in the SGZ is unaffected by the loss of α2-chimaerin, and 2) that the loss of α2-chimaerin may alter cell cycle dynamics/progression in the adult SGZ as heightened levels of Rac1-GTP, observed in the alpha2-chimaerin mutant animal, can affect cell-cycle progression both, *in vitro* and

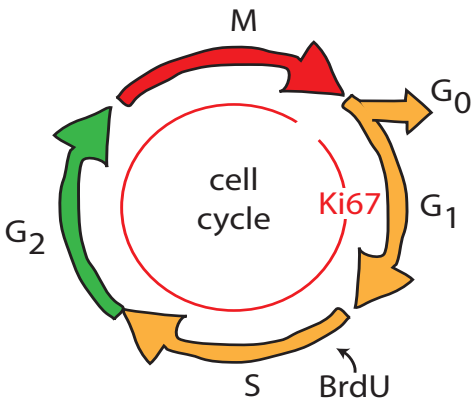

Figure 3.9 Cell cycle schematic
BrdU is incorporated into cells undergoing DNA replication in the S-phase, while Ki67 marks all proliferative stages of the cell cycle.

in vivo (Michaelson et al., 2008). For example, cancerous cells exhibit high levels of Rac1-GTP, which has been found to contribute to aggressive growth and metastasis (Dokmanovic et al., 2009; Kamai et al., 2004; Schnelzer et al., 2000). In the α2-chimaerin mutant SGZ, elevated Rac1-GTP may modulate temporal aspects of cell cycle progression in neural progenitor cells, and delay/accelerate progression out of the proliferative stages of the cell cycle (Michaelson et al., 2008).

Is there a potential role of α2-chimaerin in oligodendrocytes?

Our results reveal a previously uncharacterized role for α2-chimaerin in oligodendrocytes. We have identified that the loss of α2-chimaerin results in an increase in oligodendrocyte precursor proliferation throughout the postnatal dentate gyrus, and that α2-chimaerin is expressed in human OPCs. In the vertebrate brain and spinal cord, OPCs generate oligodendrocytes that myelinate axons. The insulation provided by the myelin increases the speed and efficiency of axonal signal propagation affecting neural network communication (Jackman et al., 2009). In diseased states, such as Multiple Sclerosis (MS), axons in the brain and spinal cord are demyelinated causing a disruption of nervous signal propagation resulting in a wide range of physical, mental and, sometimes, psychiatric problems (Alonso and Hernán, 2008; Ferguson et al., 1997). Current research has pointed to an autoimmune deficiency that destroys myelin, and another possibility is that genetic mutations in oligodendrocyte and/or oligodendrocyte precursor cells fail to establish or maintain proper axonal myelination (Franklin, 2002; Kuhlmann et al., 2008). The future direction of this work is to determine if the elevated OPC proliferation observed in the α2-chimaerin mutant results in the increased formation of oligodendrocytes. Likewise, α2-chimaerin may be involved in the

morphological maturation of oligodendrocytes where it could play a role in Rho-GTPase-dependent regulation of cytoskeletal proteins that establish oligodendrocyte arbors (Jackman et al., 2009). Previous reports also suggest α2-chimaerin may be involved in oligodendrocyte maturation, as α-chimaerin was 11 among 21 actin cytoskeletal genes that were upregulated more than two fold during oligodendrocyte differentiation (Nielsen et al., 2006). Given these preliminary findings, a detailed assessment of α2-chimaerin function in oligodendrocytes/OPCs will be important in elucidating mechanisms that may combat the cellular disruption in MS.

Is α2-chimaerin involved in EphA or EphB control over SGZ proliferation?

Mounting evidence suggests that EphR/ephrin signaling is an important regulator of adult neurogenesis (Ming and Song, 2011; Zhao et al., 2008). For example, loss of EphA or EphB signaling reduces the number of adult SGZ neural stem cells and produces prematurely differentiated neuronal progenitors (Chumley et al., 2007; Khodosevich et al., 2011). Additionally, ephrin-A/B presenting cells that surround the SGZ have been observed to influence aspects of neurogenesis such as polarity, migration and proliferation (Jiao et al., 2008). Our lab, along with others have demonstrated that α2-chimaerin interacts with EphA4 and EphB1/2 receptors, and one possibility is that α2-chimaerin acts downstream of select EphA or EphB signaling in the SGZ niche (Beg et al., 2007; Iwasato et al., 2007; Shi et al., 2007; Wegmeyer et al., 2007a). Interestingly, the loss of EphB1 results in BrdU+ proliferative cells ectopically localized to the granule cell layer and molecular layer (Chumley et al., 2007). Similarly, our results demonstrate that the loss of α2-chimaerin results in BrdU+ cells present in the granule cell layer and molecular layer of the dentate gyrus, suggesting that α2-

chimaerin may act downstream of EphB1 signaling in the SGZ. However, unlike EphB1 receptor studies thus far, we conducted a cell-marker antibody screen and identified that a percentage of the BrdU+ cells are OPCs. It would be interesting to evaluate if EphB1 knockout mice also display altered OPC proliferation similar to the α2-chimaerin mutant mouse. A future goal would be to test the potential role of EphB1 and α2-chimaerin in cell cycle progression of neural stem cells in the adult SGZ.

Marble burying defects in the α2-chimaerin mutant animal

The marble-burying test has been used to measure basal anxiety in rodents (Handley, 1991). Administration of anxiolytics reduces basal anxiety in mice resulting in a reduction of buried marbles (Handley, 1991; Huang et al., 2008). Anti-anxiety drugs have been found to increase adult neurogenesis, which may be the cellular correlate to the reduction of basal anxiety (Eriksson et al., 1998; Huang et al., 2008; Ming and Song, 2011). Our assessment of the α2-chimaerin mutant mouse reveals that the mutant buries less marbles compared to WT, suggesting that these mice exhibit a reduction in basal anxiety. One possibility is that altered aspects of hippocampal proliferation dynamics such as cell cycle progression or OPC proliferation due to the loss of α2-chimaerin may regulate basal anxiety levels.

A future direction will be to generate an α2-chimaerin mutant mouse *via* Tamoxifen-inducible Nestin:CreER-loxP recombination. Using this approach, we can selectively ablate α2-chimaerin in neural stem/progenitor cells in the adult hippocampus (Lagace et al., 2007). One potential outcome is that these cell-type specific knockouts would bury less marbles. If true, such data would suggest that the loss of α2-chimaerin in Nestin+ cells of the adult hippocampus impacts aspects of adult neurogenesis.

Methods

Neurosphere preparation

Primary free-floating SGZ neurospheres were prepared from P60 WT and α2 mutant mice. In short, we dissected hippocampi from three to four animals per strain, and collected the tissue in a 15mL conical tube containing ice-cold dissection media HBSS without $MgCl_2$ $CaCl_2$ containing 10mM HEPES. The isolated hippocampi were washed once with HBSS + 10mM HEPES to remove small tissue debris then the solution was replaced with 1% Tyrpsin + 0.01% DNaseI in HBSS + 10mM HEPES. The hippocampi were trypsinized in 0.025% trypsin solution for 20 minutes at 37°C, then triturated with a fire-polished nine inch glass Pasteur pipette. The cell suspension was centrifuged at 500 rpm for seven minutes at 4°C, re-suspended in 1mL of dissection media and filtered with a 40μm mesh cell strainer to remove large cellular debris. The cells where then counted in Trypan Blue to exclude dead cells and plated at 10,000 cells per 35mm well in 2mLs of self-renewal media (DMEM:F12, N2, B27, Fibroblast growth factor (20ng/mL) and Epidermal growth factor (20ng/mL)). For 10 DIV, the cell suspension was left undisturbed in the incubator (37°C/5%CO2/90% humidity) to prevent neurosphere doublet formation. After 10 DIV, we recorded the number of primary neurospheres formed in each well. To prepare primary adherent SGZ neurospheres, the cell suspension was plated on a 12mm glass coverslip coated with 50ug/uL Poly-D lysine and 200ug/uL of Fibronectin in self-renewal media. After 7 DIV the adhered cells were fixed and processed for immunocytochemistry.

BrdU injections, perfusion and brain sectioning

To evaluate SGZ proliferation we injected WT and α2-chimaerin mutant animals with 5-bromo-2'-deoxyuridine (BrdU), a synthetic thymine analog that incorporates into cellular DNA during the synthesis (S)-phase of the cell cycle (Kee et al., 2002), at (200mg/1kg of body weight). The animals were sacrificed two hours post-BrdU intraperitoneal (IP) injection to obtain a snapshot of SGZ proliferation. All BrdU-injected mice were sacrificed through a cardiac perfusion where the animal was first administered an IP injection of a 10/20 mg/mL Ketamine/Xylazine solution. After the animal was unresponsive to tail and paw pinches, we completed the cardiac perfusion by passing 5mLs of PBS followed by 5mLs of 4% PFA diluted in PBS. Physical signs of the fixation process were noted, including blood clearing of the liver, tail flinching and body stiffening. We dissected the brain and post-fixed the tissue overnight in 4% PFA at 4°C. The following day the brains were washed in PBS and mounted in 2% low-melt agar. Utilizing a VT2-12000 microtome, we collected 50μm coronal sections and placed each individual slice in a 15mm well of a 24-well cluster plate containing 1mL of PBS/well. After control and α2-chimaerin mutant slices were prepared, we anatomically matched the slices to ensure similar hippocampal sections were analyzed for the experiment. For immunostaining, we divided the slices into groups where odd numbered slices were stained with BrdU antibodies, and even numbered slices were treated with Ki67 antibodies, as Ki67 is an endogenous nuclear protein expressed during all proliferative stages of the cell cycle (Kee et al., 2002),.

Immunostaining

Coronal brain slices were blocked and permeabilized in 5% Donkey serum containing 0.1% TX-100 for two hours at 4°C. To assay BrdU+ proliferative cells, coronal brain sections were incubated in 2N HCl at 37°C for 20 minutes to denature DNA before blocking and permeabilization. The brain slices were incubated in primary antibodies overnight followed by incubation with secondary antibodies for two hours at room temperature. Afterwards, three to six coronal sections were mounted on Superfrost microscope glass slides with Fluoromount-G mounting media.

Imaging and data analysis

All immunostained hippocampi sections were imaged with a Leica multi-channel fluorescent microscope, or a Nikon A1 confocal microscope to collect Z-series images. We utilized the Cell Counter Plugin in ImageJ image processing software to count and categorize the localization of BrdU+ and Ki67+ cells throughout the dentate. We calculated the mean BrdU+ and Ki67+ cells per hippocampi that were localized in the subgranular zone, granule cell layer and molecular layer of the dentate gyrus. For statistical analysis we utilized GraphPad Prism 6.0.

Acknowledgements

Chris Valdez and Asim Beg designed the experiments presented in this chapter. Chris Valdez completed the experimental work and data analysis, and Alex Stanczyk provided technical assistance and data analysis to the work presented in this chapter.

Chapter 4

Discussion

Temporal and spatial profile of α2-chimaerin

In vertebrates, Rac1 is expressed in most cell types and its activity is critical for cytoskeletal dynamics during cell growth, migration and proliferation. Given its various functions, Rac1 activity and its regulators, GEFs and GAPs, are often altered in diseased states such carcinogenesis, where cells are transformed exhibiting expansive proliferation and invasive outgrowth (Etienne-Manneville and Hall, 2002; Schnelzer et al., 2000).

Numerous GEF and GAP isoforms have been identified in various cell types, and single cells that express multiple GEF and GAP isoforms may functionally compartmentalize these modulatory proteins to distinct subcellular regions (Bos et al., 2007; Cherfils and Zeghouf, 2013). Additionally, GEFs and GAPs can be temporally regulated, limiting expression to developmental periods or expressed continuously into adulthood to regulate a particular function (Cherfils and Zeghouf, 2013). Thus, assessing the precise spatial and temporal profile of α2-chimaerin is an important goal in better understanding the molecular and cellular mechanisms of α2-chimaerin function.

In tissue, we observed relatively high levels of α2-chimaerin protein in the brain and testis and, to a lesser extent, in the heart and lungs. We did not detect α2-chimaerin expression in the liver, kidney or spleen. To determine α2-chimaerin transcription levels

in the nervous system, we utilized the lacZ reporter cassette expressed in the α2-chimaerin mutant mouse. Using this approach, we observed a dense population of β-gal+ cells in neuronal layers of the hippocampus, corroborating a previous report which detected α2-chimaerin expression in neurons (Iwata et al., 2014). When we looked at expression in other neural cells, we observed α2-chimaerin expressed in oligodendrocyte precursor cells, but not in Schwann cells of the peripheral nervous system or astrocytes and microglia from the CNS. Taken together, these data demonstrate another layer of regulation within the nervous system.

Given that the role of α2-chimaerin in the hippocampus was a focus for this dissertation, we also evaluated the spatial and temporal distribution of α2-chimaerin among hippocampal neuronal populations. Our investigation of β-gal+ cells from the α2-chimaerin mutant mouse revealed that granule neurons may suppress α2-chimaerin as the hippocampal dentate gyrus matures and, as a result, α2-chimaerin may be limited to pyramidal neurons in the stratum pyramidale of the adult hippocampus. Consequently, one potential reason for the temporal reduction of α2-chimaerin, beginning at P6, may be due to this suppression of α2-chimaerin from the granule cell layer, suggesting that α2-chimaerin is only developmentally regulated in granule neurons (Buttery et al., 2006). While our studies suggest α2-chimaerin expression is present in granule neurons up to P25, one caveat is that the lacZ reporter only informs of the onset of gene transcription, but does not inform about protein expression (Gossler et al., 1989). Nevertheless, our data suggests that β-gal+ cells in the dentate gyrus are differentially regulated as compared to pyramidal neurons and, taken together; these findings support further inquiry into the differential expression of α2-chimaerin across neuronal subsets within

the hippocampus. More importantly, these findings may impact the interpretation of our data in characterizing the role of α2-chimaerin in various aspects of hippocampal neuronal morphology and function.

One possibility that arose from our analysis of mature primary neurons and adult brain slices, is that mature and adult hippocampal neurons may exhibit α2-chimaerin-dependent regulation of Rac1 in pyramidal neurons, but α2-chimaerin-independent regulation in granule neurons. Such a scenario could explain the slight, but statistically significant, changes in dendritic morphology and synaptic connectivity that we quantified, as we included both pyramidal and granule neurons in our analysis. Furthermore, our results may be an underrepresentation of the true impact of α2-chimaerin in the hippocampus due to the fact that we assessed hippocampal neurons as a whole (pyramidal and granule neurons) versus discrete analysis of only actively expressing α2-chimaerin neurons. The development of an α2-chimaerin antibody with immunostaining capabilities is necessary for further investigation.

Overall, our assessment of the spatial and temporal distribution of α2-chimaerin has provided new insight into α2-chimaerin expression in the hippocampus and throughout the body. In the hippocampus, our analyses suggest that α2-chimaerin may exhibit "*intrahippocampal regulation*", where it may have only a developmental role in granule neurons, but an on-going role in pyramidal neurons that persists into adulthood.

The impact of α2-chimaerin at the synapse

Most excitatory connections in the brain consist of the presynaptic axonal terminal, the postsynaptic dendritic spine and the surrounding glial cell, which together form a single synaptic connection (Araque et al., 1999). From our analysis, we reveal a

divergence from the well-documented observation that a postsynaptic spine forms a singular synapse with a single presynaptic axon terminal (Hell and Ehlers, 2008). In α2-chimaerin mutant neurons, we often detected two to three synapses on a single branched dendritic spine. This unusual phenotype is likely due to defects in the presynaptic axon terminal, the postsynaptic dendritic spine, or from both of these neuronal partners. As astrocytes do not express α2-chimaerin it is unlikely they play a role in the phenotype.

An outstanding question is *when* and *how* are atypical branched spines formed as a result of the loss of α2-chimaerin. In an attempt to explain this, we generated two working models that describes when and how irregular branched dendritic spines might be formed in the α2-chimaerin mutant hippocampus.

When are branched spines formed?

Under wild type conditions, branched spines are transiently observed during the development of neuronal connectivity and are competitively refined/pruned during developmental periods of synaptic maintenance (Figure 4.1) (Ethell and Pasquale, 2005; Petrak et al., 2005). However, upon the loss of α2-chimaerin, the intracellular processing that drives the competitive refinement to prune multiple connections on a single dendritic spine may be altered allowing atypical

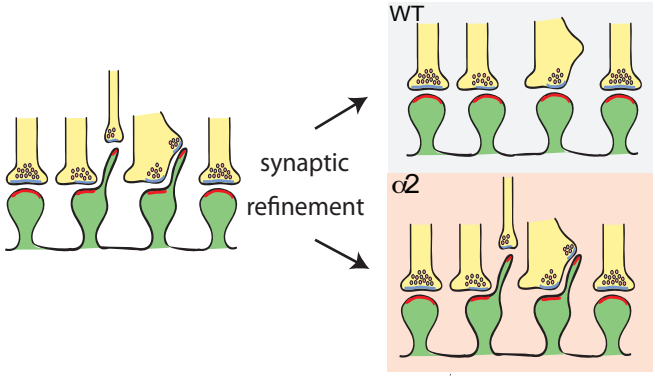

Figure 4.1 Model #1: Branched spines formed during development
Polymorphic spines are formed during development and, despite synaptic refinement, persist in the adult brain.

spines and polysynaptic connections to persist into the adult brain. Furthermore, EphR/ephrin signaling has been demonstrated to direct and regulate axonal migration; however, the loss of α2-chimaerin impacts EphR/ephrin control over this process causing aberrant synapse formation during spinal cord development that persists into the adult animal (Beg et al., 2007; Kao et al.; Kao et al., 2015). A future goal of this work is to determine if EphR/ephrin signaling targets α2-chimaerin activity to refine synapses in the hippocampus.

In the mature α2-chimaerin mutant brain, branched spines can form due to synaptic activity, which drives irregular outgrowth and polysynaptic connectivity from mushroom-shaped spines (Figure 4.2). For example, the persistent increase in synaptic strength following high frequency stimulation, also known as long-term potentiation (LTP), can cause cytoskeletal rearrangements in the dendritic spine head due to an enhancement of F-actin polymerization (Chen et al., 2007). As a result, these actin-dependent cytoskeletal changes have been found to remodel the receptor topography of the synaptic active zone (Matus, 2000).

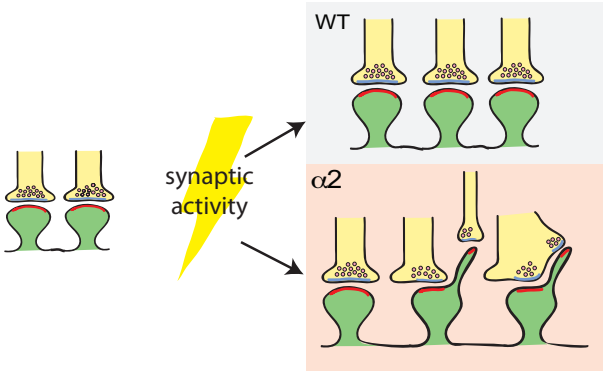

Figure 4.2 Model #2: Branched spines form as a result of synaptic activity. Polymorphic spines are formed upon synaptic activity as a result of altered Rac1 regulation at the synapse.

In this scenario, a key regulatory principle is that actin-based remodeling during synaptic connectivity must be transient in nature, because non-regulated actin polymerization would cause a continuous expansion of the dendritic spine head

resulting in a loss of the in-step and phasic structural plasticity that is coupled to activity. Under normal conditions, α2-chimaerin would provide the "*brakes*" after Rac1-GTP induced cytoskeletal re-arrangement of the dendritic spine head during synaptic activity. Upon the loss of α2-chimaerin, Rac1-GTP-mediated actin dynamics aberrantly continue after the synaptic signaling event; thereby inducing the formation of the branched spines and polysynaptic connections observed in the α2-chimaerin mutant. Our electrophysiological results suggest that, on a circuit level, these spines do not negatively affect function, and are the result of altered Rac1 regulation. However, not all neurophysiology encompasses the strengthening of synaptic connections. Instead, distinct forms of signaling such as long-term depression (LTD) can induce a persistent weakening of synaptic connections, dendritic spine shrinkage and ultimately a loss of synaptic connections (Ito, 1989). On a broad level, LTD is thought to prevent memory saturation, by depotentiating the circuit-level effects of LTP (Artola and Singer, 1993; Mulkey and Malenka, 1992). Given these parameters, one possibility is that α2-chimaerin mutant mice exhibit attenuated LTD, as high Rac1 levels may prevent the activity-induced structural collapse of dendritic spines, and thereby the reduction of synaptic connections.

How are branched spines formed?

One possibility is that polysynaptic dendritic spines are the result of a single axon that redundantly synapses on a single dendritic spine (Figure 4.3). Since α2-chimaerin expression is also lost in the dendritic spine, the postsynaptic structure compliments the aberrant presynaptic partner by developing multiple spine heads from a single dendritic protrusion; hence, the significant increase in polysynaptic and branched spines in the

α2-chimaerin mutant. Another possibility is that polysynaptic dendritic spines arise from aberrant outgrowth at the dendritic spine head that breaks away portions of the postsynaptic density thus forming connections with different afferent axon terminals (Figure 4.3).

From a mechanistic perspective, it is likely that heightened Rac1-GTP in the dendritic spine or axon drive the altered cytoskeletal dynamics represented in both of these models (Figure 4.3). Rac1 is a central regulator of dendritic architecture, and during early-stages of development Rac1-GTP is important for activating various effectors that promote initial dendrite outgrowth and branching (Govek et al., 2005). Future studies to determine when and how polymorphic dendritic spines are formed will be instrumental to our understanding of α2-chimaerin function in neurons during development, and in response to activity. Further research is required to address our working model, and combining live-imaging experiments with inducible neural activity paradigms would be an appropriated approach to address these outstanding questions.

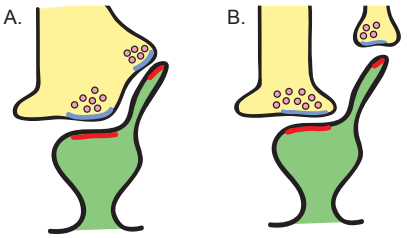

Figure 4-3 How are polysynaptic branched synapses formed?

A) Axonal terminal redundantly synapses on a single branched spine.

B) Aberrant outgrowth of the dendritic spine head synapses with multiple axonal terminals

Neuronal circuitry in α2-chimaerin mutants

Despite a simplified dendritic arbor, reduction in spine density and an increase in dysmorphic spines, α2-chimaerin mutant neurons exhibit no change in synaptic strength

following high frequency stimulation induced long-term potentiation. One possibility is that synapse density is not negatively affected in α2-chimaerin mutant hippocampal neurons. The increased synapse density in α2-chimaerin mutants can be partially explained by the significant increase in multiple synapses formed on atypical branched spines. These polymorphic spines exhibit the second highest percentage of protrusion-based synapses in the α2-chimaerin mutant, and may be functional similar to a mushroom-shaped spine. For this reason, the simplification and reduction of dendritic arbors and spines in the α2-chimaerin mutant is perhaps functionally compensated through an increase in synaptic connections that is partially attributed to polysynaptic dendritic spines.

Alpha2-chimaerin is an essential regulator of Rac1-mediated control over neuronal morphology

Our data demonstrate that α2-chimaerin mutant neurons exhibit elevated Rac1-GTP levels in hippocampal neurons, and increased polymerized F-actin in dendritic spines. For this reason, we analyzed morphological characteristics of mature α2-chimaerin mutant neurons including dendritic complexity and dendritic spine morphology. In agreement with previous reports that evaluated neuron morphology from overexpression of constituently active Rac1-GTP, we similarly observed a simplification of dendritic arborization, and an increase in abnormal dendritic spine density in α2-chimaerin mutant neurons (Govek et al., 2005; Nakayama et al., 2000; Nobes and Hall, 1995). However, we did not observe an accumulation of dendritic spines as previously reported (Hall, 1998; Luo, 2000). One possibility is that heightened Rac-GTP levels in α2-chimaerin mutants results in the accumulation of polymorphic spines as opposed to

mushroom or stubby-shaped dendritic spines. Additionally, our analysis revealed that atypical dendritic spines exhibit spatially distinct F-actin puncta localized to the multiple spine heads, demonstrating a potential physiological effect of elevated Rac1-GTP, which was previously uncharacterized until this report. Likewise, the knockdown of α1-chimaerin, also results in the increase of branched spines and loss of mushroom spines in hippocampal neurons, suggesting that α1- and α2-chimaerin negatively regulate Rac1-GTP under distinct physiological conditions that contribute to the maintenance of dendritic spine shape (Buttery and Beg et al., 2006).

EphA4/α2-chimaerin signaling at the synapse

Our laboratory, along with others, has established that α2-chimaerin is an essential intracellular effector of EphA4 surface signaling that mediates axon guidance during the assembly of spinal cord neuronal circuits (Beg et al., 2007; Iwasato et al., 2007; Wegmeyer et al., 2007a). These previous studies provided the basis of my dissertation work, investigating the role of α2-chimaerin in shaping neuronal dendritic architecture, synaptic function and behavior. One possibility, based on our results, is that α2-chimaerin may be a key intracellular regulator of Eph receptor activity at the synapse (Calo et al., 2006; Filosa et al., 2009; Fu et al., 2011).

EphA4 receptor activity can promote dendritic spine shortening and lead to the removal of AMPA receptors from the membrane (see Introduction for details pg. 14) (Fu et al., 2011; Murai et al., 2003). Alternatively, EphB signaling can promote dendritic spine stability and stabilize NMDA receptors at the synapse (see Introduction for details pg. 12) (Dalva et al., 2000; Henderson et al., 2001; Sheffler-Collins and Dalva, 2012; Takasu et al., 2002). Akin to the loss of EphA4 receptor signaling, our lab has similarly

observed an increase in surface levels of glutamate receptor ionotropic AMPA 1 (GRIA1); suggesting EphA4 synaptic signaling is attenuated in α2-chimaerin mutants preventing the removal of AMPA receptors from the synapse. Supporting this hypothesis, we have also observed that α2-chimaerin mutant mice exhibited elevated levels of the AMPA receptor subunit, GRIA1, in synaptosomal protein fractions similar to EphA4 knockout mice (Fu et al., 2011). While further experiments are required to identify and functionally characterize α2-chimaerin as an intracellular effector of EphA4 and EphB receptors at the synapse, we propose the following working model to describe the role of α2-chimaerin in synaptic Eph receptor signaling (Figure 4.4).

Based on previously published data, we predict that the SH2-domain of α2-chimaerin is critical for EphR/α2-chimaerin signaling at the synapse (Beg et al., 2007; Shi et al., 2007). At the synapse, EphB receptors can interact with Glutamate receptor ionotropic, NMDA 1 (NR1), and this complex may negatively regulate Rac1-GTP after the expansion or incorporation of receptors in the synapse. In regards to EphA signaling, α2-chimaerin may interact directly with it, and participate in actin-dependent collapse of the dendritic spine as a result of EphA4-mediated removal of AMPA receptors from the synapse (Zhou et al., 2012) (Murai et al., 2003). Our future goal would be to conduct single-cell recordings combined with time-lapse imaging of dendritic spines. These experiments will require high-speed imaging, as we will also monitor spine motility combined with electrophysiology.

Perspective on GEFs and GAPS at the synapse

Neurons express an orchestra of GEFs and GAPS to maintain precise control of Rac1 activity in dendrite branches and spines (Hall, 1998) (Nakayama et al., 2000). In

the dendrite, Rac1 functions as a gatekeeper of cytoskeletal dynamics by initiating various protein effectors that alter dendritic spine stability and morphology (Luo, 2000). Recent work has begun to unravel how GEFs and GAPs are spatially regulated to execute precise control of Rac1 in the dendrite (Um et al., 2014). For instance, a recent publication reported that the T-lymphoma invasion and metastasis-inducing protein 1-GEF (Tiam1-GEF) and Breakpoint Cluster Region-GAP (BCR-GAP) complex together and translocate to the membrane in response to synaptic activity (Um et al., 2014). As a result, leading questions in the field are (1) how are various GEFs and GAPs regulated in neurons? (2) What are the different receptors that regulate GEF and GAP activity at the synapse?

Overall, these biological questions suggest that there is precise, positive and negative control of Rac1 at each individual dendritic spine. We propose that when multiple GEFs and GAPs, or different cell-surface receptors are altered, the result can culminate into unique phenotypes that are often observed in Autism Spectrum Disorder (ASD) (Durand et al., 2011) (Williams et al., 1980). Perhaps the lack of dynamic control over Rac1-mediated pathways may be a leading cause of structural and functional defects in ASD.

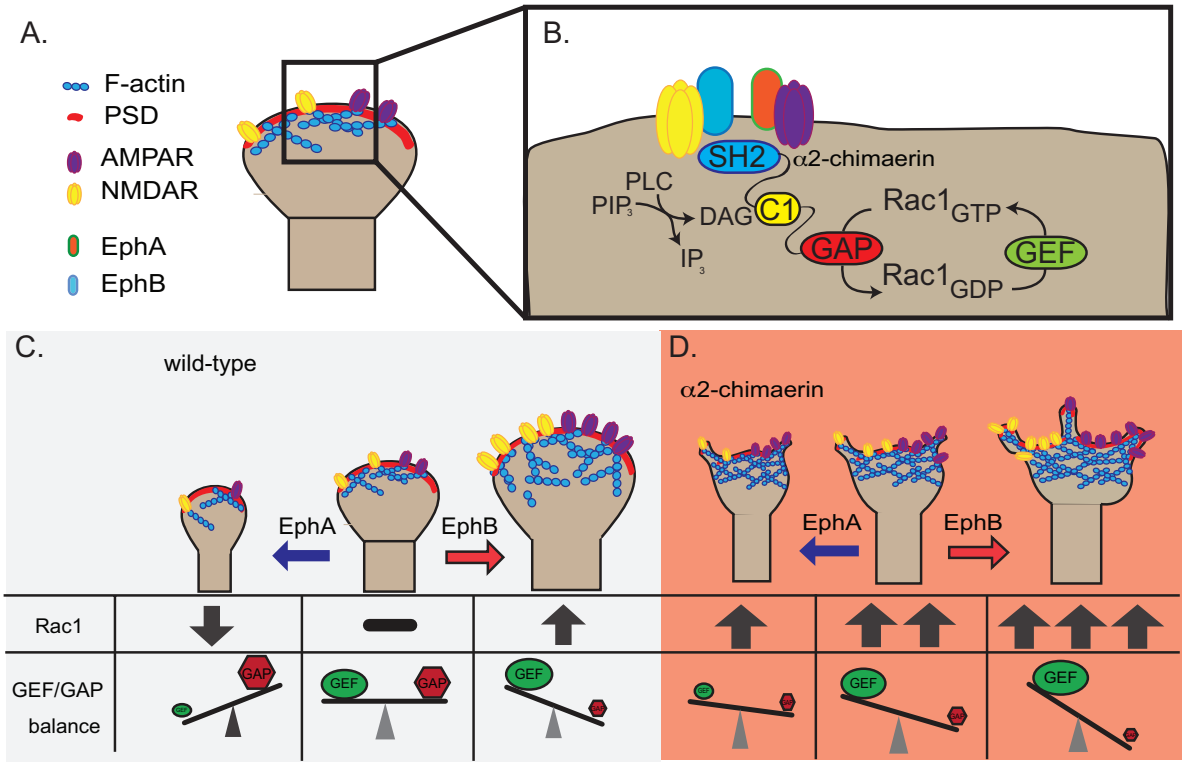

Figure 4.4 Working model demonstrating the role of α2-chimaerin in Eph receptor signaling at the synapse

A-B) At the dendritic spine, α2-chimaerin may directly interact with synaptic receptors or with Eph receptors to regulate Rac1-GTP.

C) In wild type neurons, synaptic activity can drive EphB receptor signaling to promote expansion of the dendritic spine head and the incorporation of additional AMPA and NMDA receptors. Alternatively, EphA4 signaling promotes the shortening of dendritic spines and the removal of synaptic receptors from the membrane. Both Eph receptors can activate GEFs/GAPs, and modulate the balance of Rac1-GTP at the synapse.

D) In the α2-chimaerin mutant, Rac1-GTP levels are heightened at baseline and upon EphB signaling, GEFs further potentiate Rac-GTP leading to irregular dendritic spine head outgrowth and incorporation of synaptic receptors. Upon EphA signaling, the loss of α2-chimaerin protein effector signaling prevents the shrinkage of dendritic spines, and the removal of synaptic receptors from the membrane.

Alpha2-chimaerin expression in the adult hippocampus and potential role in adult neurogenesis

We took advantage of the β-gal reporter in α2-chimaerin mutant mice to identify what cellular populations would otherwise express α2-chimaerin protein. While we identified β-gal+ neurons in the pyramidal and granule cell layers from P1-P25, we, interestingly, observed a selective loss of β-gal+ neurons from the granule cell layer at P60. What would drive the selective loss of β-gal+ neurons from the granule cell layer of the adult hippocampus?

While both cell layers consist of post-mitotic neurons, the dentate gyrus exhibits a neural stem cell niche, known as the subgranular zone (SGZ), localized between the hilus and the granule cell layer (Eriksson et al., 1998). In the SGZ, stem cells generate neuronal progenitors that give rise to adult born neurons, which migrate into the GCL, differentiate and replace existing granule cells (Gage, 2002). In the adult rat hippocampus approximately 2,000 neuronal progenitors are born a day, and proliferation rates can be influenced by exercise or anxiety (Cameron et al., 1993; Van Praag et al., 2005). Despite the birth rate of adult-born neurons, the granular layer does not continuously expand throughout the animal's lifespan. Instead, there is a balance between birth of adult born neurons and apoptosis of existing neurons (Gage, 2002). For this reason, a working model is that the selective loss of β-gal+ cells from the adult granule cell layer may be due to the turnover of β-gal+ developmentally derived neurons with the replacement of β-gal- adult born granule neurons, due to neurogenesis in the SGZ.

This model suggests that α2-chimaerin promoter activity is developmentally regulated in the GCL and no longer targeted in adult born granule neurons (Mizuno et al., 2004). In such a scenario, several questions arise: 1) If α2-chimaerin is not expressed in adult born neurons, then what Rac-GAP takes its place? 2) What are the genomic and proteomic differences between an adult born and a developmentally born neuron? 3) Would an adult born neuron in an α2-chimaerin mutant mouse also ignore ephrin-A1 repulsive signaling (Beg et al., 2007; Kao et al., 2015)? While these questions propose experiments that are out of the scope of this dissertation, the preliminary data that supports further investigation originated from the efforts put forth in completing this dissertation.

Appendix 1

Spillover Transmission is mediated by the Excitatory GABA Receptor LGC-35 in *C. elegans*

Abstract

Under most circumstances γ-aminobutyric acid (GABA) activates chloride-selective channels and thereby inhibits neuronal activity. Here, we identify a GABA receptor in the nematode *Caenorhabditis elegans* that conducts cations and is therefore excitatory. Expression in *Xenopus* oocytes demonstrates that LGC-35 is a homopentameric cation-selective receptor of the cys-loop family exclusively activated by GABA. Phylogenetic analysis suggests that LGC-35 evolved from GABA-A receptors, but the pore-forming domain contains novel molecular determinants that confer cation selectivity. LGC-35 is expressed in muscles, and directly mediates sphincter muscle contraction in the defecation cycle in hermaphrodites, and spicule eversion during mating in the male. In the locomotory circuit, GABA release directly activates chloride channels on the muscle to cause muscle relaxation. However, GABA spillover at these synapses activates LGC-35 receptors localized on acetylcholine motor neurons, which in turn cause muscles to contract, presumably to drive wave propagation along the body. These studies demonstrate that both direct and indirect excitatory GABA signaling play important roles in regulating neuronal circuit function and behavior in *C. elegans*.

Introduction

The family of cysteine-loop ligand-gated ion channels (cys-loop LGICs) mediate rapid neurotransmission and consists of four major receptor types: acetylcholine, serotonin, glycine, and GABA receptors. These receptors are comprised of five subunits arranged to form a central ion-conducting pore (Thompson et al., 2010). Each subunit is composed of an extracellular ligand-binding domain (LBD), a cysteine-loop motif (C-X_{13}-C), four transmembrane domains (M1-M4), and a large intracellular loop connecting M3 to M4. Typically, cation conductance mediates excitation and anion conductance mediates inhibition.

The *Caenorhabditis elegans (C. elegans)* genome encodes ~102 cys-loop receptor subunits, making it the largest and most diverse known eukaryotic cys-loop superfamily (Jones and Sattelle, 2008). As in vertebrates, there are classical excitatory acetylcholine and inhibitory GABA receptors. However, *C. elegans* employs an arsenal of unusual cys-loop receptor subtypes, including: inhibitory anion-selective receptors gated by acetylcholine, choline, serotonin, dopamine, tyramine, and octopamine; and excitatory cation-selective receptors activated by GABA, betaine and protons (Bamber et al., 1999a; Beg et al., 2008; Beg and Jorgensen, 2003a; Jones and Sattelle, 2008; Peden et al., 2013; Pirri et al., 2009; Putrenko et al., 2005; Ranganathan et al., 2000; Ringstad et al., 2009; Yassin et al., 2001). This diversity adds tremendous flexibility, as each transmitter can be excitatory, inhibitory, or have mixed-action within the same tissue depending on the dedicated or combinatorial expression of particular receptor subtypes. Importantly, only a fraction of cys-loop receptors have been characterized in

C. elegans, suggesting that new modes of neurotransmission within this simple organism have yet to be identified.

Over twenty years ago, a strategy was designed to identify genes required for GABA function in *C. elegans* (McIntire et al., 1993a). Three major GABA-dependent behavioral phenotypes were identified using genetic and laser ablation techniques: locomotion, foraging, and defecation (McIntire et al., 1993b). During locomotion and foraging, GABA acts to relax body muscles via GABA-activated chloride channels and thereby helps generate a sinusoidal wave along the body axis (Bamber et al., 1999b). By contrast, GABA stimulates enteric muscle contraction during defecation via the GABA-gated cation channel EXP-1 (Beg and Jorgensen, 2003b; McIntire et al., 1993b). The enteric muscles comprise the intestinal, anal depressor, and sphincter muscles. Although EXP-1 is required for intestinal and anal depressor muscle contraction, it is neither expressed in, nor required for, sphincter muscle contraction (Beg and Jorgensen, 2003b). Importantly, GABA is the primary neurotransmitter released on the enteric muscles, suggesting that an unidentified GABA receptor mediates sphincter muscle contraction (White et al., 1986a).

Here, we demonstrate that *lgc-35* encodes a homopentameric excitatory GABA-gated cation channel that is required for diverse modes of neuromuscular transmission. Our findings demonstrate that LGC-35 mediates sphincter muscle contraction, is expressed in a subset of acetylcholine motor neurons where it functions as a spillover receptor to modulate locomotory behavior, and is involved in male-specific copulatory muscle contraction. Together, our data show that excitatory GABA signaling is not a

specialized mode of signaling confined to enteric muscle function, but plays a broader role in the modulation of neuronal circuits in *C. elegans*.

Results

LGC-35 is a GABA-gated Cation-Selective Receptor

We identified *lgc-35* (*l*igand-*g*ated *c*hannel-*35*) by searching the *C. elegans* genome for *exp-1* homologs. LGC-35 is most closely related to the excitatory GABA receptor EXP-1 (53% identity) and contains the canonical motif (C-X_{13}-C) that defines the cys-loop superfamily (Figure A.1A-B). LGC-35 contains highly conserved amino acid residues within the putative GABA binding pocket and transmembrane domains (Figure A.1C, data not shown). The LGC-35 M2 domain region, which lines the ion channel pore and determines ion selectivity, is nearly identical to the cation-selective EXP-1 receptor (Figure A.1D). The pore domain seems to have arisen by deletion of the proline, alanine, and arginine residues (PAR motif) that are critical for chloride ion selectivity in ionotropic GABA receptors, but does not otherwise resemble the cation permeable pore found in acetylcholine and serotonin-gated ion channels (Figure A.1D) (Beg and Jorgensen, 2003b; Keramidas et al., 2000). This unusual channel family is confined to nematodes; homologs of LGC-35 and EXP-1 are not readily identified in other phyla (see Methods).

To determine whether LGC-35 can form a functional GABA receptor, we expressed complementary RNA (cRNA) in *Xenopus laevis* oocytes and tested for receptor activity using two-electrode voltage clamp recordings. Application of a panel of ligands revealed that LGC-35-expressing oocytes evoked whole-cell currents in response to GABA, but not other ligands; water-injected oocytes did not respond to

GABA (Figure A.2A, data not shown). LGC-35 was activated in a dose-dependent manner by GABA, with a median effective concentration (EC_{50}) of ~15 μM (Figure A.2).

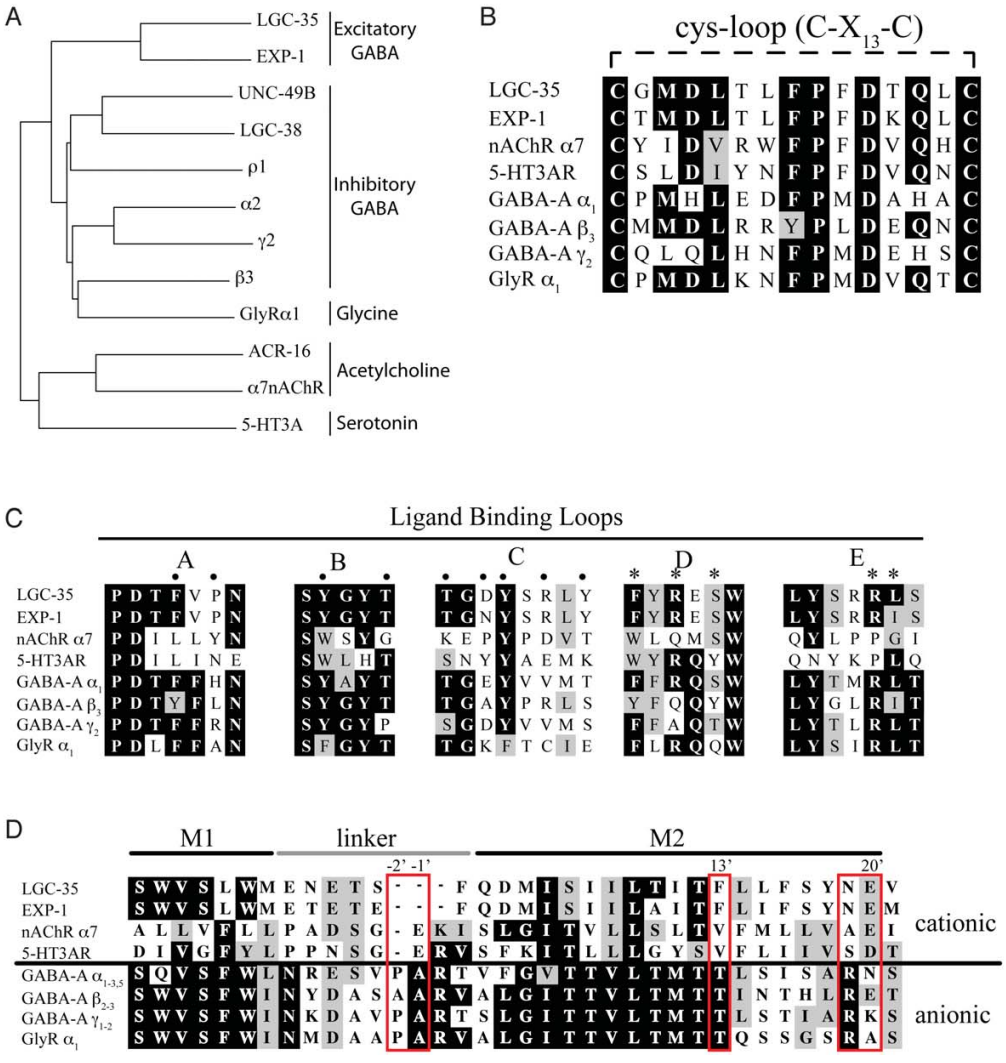

Figure A.1 *lgc-35* encodes for a cys-loop GABA receptor

(A) Phylogenetic tree of human and C. elegans cys-loop LGICs. Alignments were performed using clustalX and the tree was generated by the 'neighbor-joining' bootstrap method. LGC-35 is most closely related to the cation selective GABA receptor EXP-1. Genbank Accession Numbers: C. elegans Sequences: UNC-49B (CAC42346.1), ACR-16 (P48180.1), LGC-38 (CCD63396.1); Human Sequences: GABRA2 (P47869.2), GABRG2 (P18507.2), GABRB3 (P28472.1), GABRR1 (P24046.2), GLYRA1 (CAA36257.1), CHNRA7 (P36544.5), 5HT3A (NP_000860.2).

(B) Protein alignment showing the conserved C-X13-C motif present in all cys-loop LGICs.

(C) Protein sequence alignment of the ligand-binding loops in ionotropic cys-loop receptors. Alignments were made with clustalX. Residues implicated in GABA binding by a1 (asterisks, loops D and E) and b2 (black circles, loops A, B, C) subunits are indicated (Amin and Weiss, 1993; Beg and Jorgensen, 2003b; Boileau et al., 1999; Boileau et al., 2002; Sigel et al., 1992; Wagner and Czajkowski, 2001; Westh-Hansen et al., 1999; White et al., 1986b).

(D) Alignment of the M2 region shows that LGC-35 is nearly identical to EXP-1. Residues determining ion selectivity are boxed in red and numbered.

To determine LGC-35 ion selectivity, we substituted extracellular ions and measured the reversal potentials of agonist-evoked responses. In control solution, the GABA-dependent current reversed at -11 mV, similar to the non-selective cation channel, EXP-1 (-5 mV), and significantly different from the UNC-49B GABA receptor (-30 mV), a chloride selective channel (Figure A.2D, Control, solid black line) (Bamber et al., 1999b; Beg and Jorgensen, 2003b). Replacement of extracellular chloride with gluconate did not markedly shift the reversal potential (-13 mV). Additionally, agonist-evoked inward current was not abolished, suggesting that LGC-35 is not permeable to anions (Figure A.2D, Cl^- free, blue line). In contrast, replacement of extracellular sodium with *N*-methyl-D-glucamine (NMDG) shifted the reversal potential to -77mV, near the predicted potassium equilibrium potential in *Xenopus laevis* oocytes (Weber,

1999), and abolished GABA-evoked inward whole-cell currents (Figure A.2D, Na^+ free, red line). Lastly, when extracellular sodium was replaced with equimolar potassium, robust inward currents were observed with a reversal potential of +6 mV (Figure A.2D, K^+, green line), demonstrating that LGC-35 is permeable to both sodium and potassium. Taken together, the electrophysiological data demonstrate that LGC-35 is a GABA-gated non-selective cation channel.

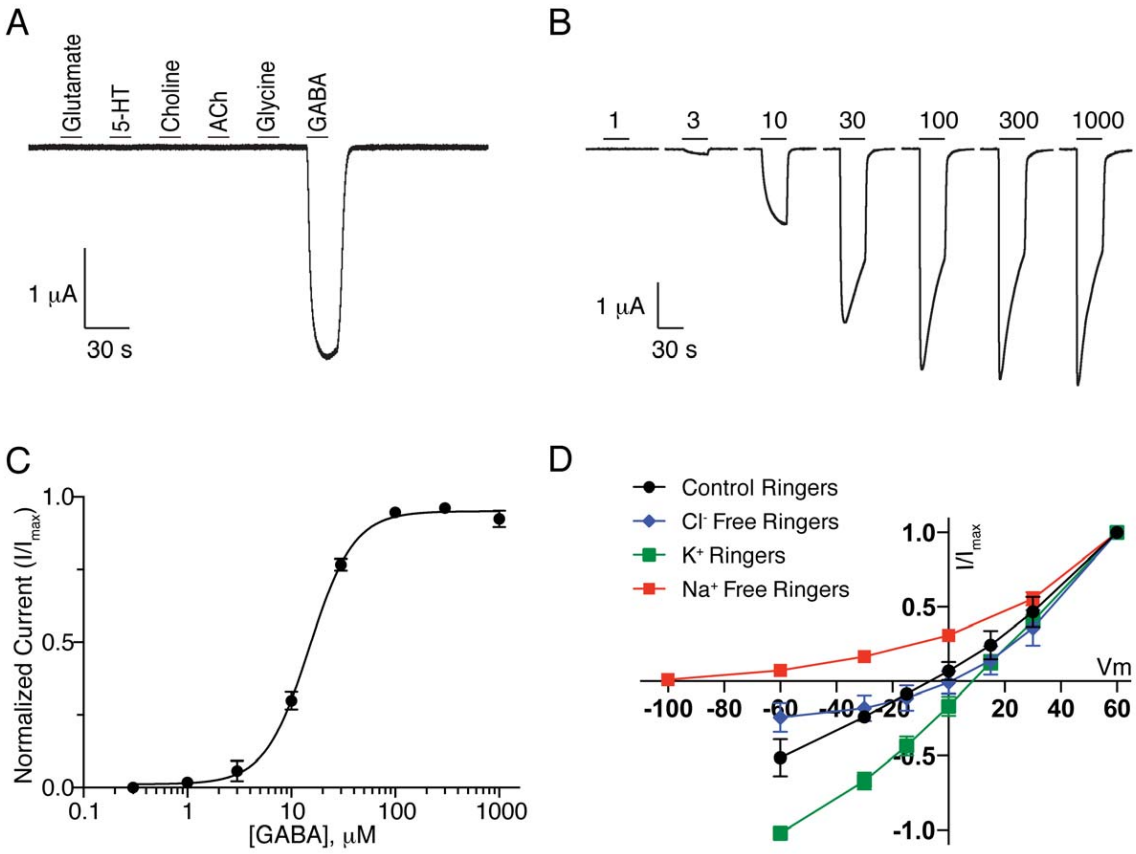

Figure A.2 LGC-35 is a GABA-gated cation channel

(A) Whole cell currents recorded from Xenopus laevis oocytes expressing LGC-35 in response to 1mM: glutamate, serotonin (5-HT), choline, acetylcholine, glycine and GABA (black bar is 10 second application of ligand). Only GABA application evoked whole cell currents in LGC-35 expressing oocytes.

(B) Representative traces of LGC-35 dose response experiments (Black bar denotes 1-1000 μM GABA application, 30 seconds).

(C) Dose response curve for LGC-35 expressing oocytes. Oocytes expressing LGC-35 were voltage-clamped at -60 mV and GABA was bath-applied in series (1-1000 μM) for 5 seconds. Points indicate mean current value normalized to maximum value. For LGC-35 receptors, EC50 = 15.04 ± 1.04 μM and Hill coefficient = 1.9 ± (n =26). Error bars represent s.e.m.

(D) Current-voltage relations of LGC-35-expressing oocytes. I-V curves determined in control Ringers solution (Erev = -10.86 ± 1.15 mV, n = 12, black), Cl- free Ringers (Erev = -12.94 ± 2.79 mV, n = 8, blue), and Na+ Free Ringer (Erev = -76.85 ± 0.65 mV, n = 7, red), K+ Ringers (Erev = 6.35 ± 1.26 mV, n = 7, green). Each point represents the mean ± s.d.

LGC-35 localization

To identify cells expressing *lgc-35*, we built a transcriptional reporter using the ~3kb *lgc-35* promoter attached to the coding region of a red fluorescent protein (P*lgc-35*::TagRFP). Reporter expression was observed in a subset of ventral cord motor neurons and head interneurons (Figure A.3A). To visualize LGC-35 protein localization, we made a translational fusion with the coding sequence of green fluorescent protein (GFP) inserted into the cytoplasmic loop between M3-M4 in a 7.6 kb *lgc-35* genomic fragment (LGC-35::GFP) (Figure A.3B, 4A). The TagRFP transcriptional reporter and translational GFP-tagged fusion protein exhibited similar cellular distributions, with some important exceptions (Figure A.3A-B). In both reporter lines, we observed expression in a subset of ventral cord motor neurons (VA, VB, DA, DB) (Figure A.3A-B), the motor neuron PDA (Figure A.3F), the tail interneurons DVA and PVT (Figure A.3F), the head interneurons AIY and AVD (Figure A.3C-D), and in the head mesodermal cell (Figure A.3C). However, the LGC-35::GFP construct, which includes the introns, exhibited

robust expression in the sphincter muscle (Figure A.3E), and all of the acetylcholine ventral cord motor neurons except the AS and VC class of neurons (Figure A.3B and Fig3-5A). The LGC-35::GFP fusion protein was localized to the plasma membrane as expected, but fluorescence was also observed in the cytoplasm probably due to transgene overexpression (Figure A.3F and Figure A.5A). These data suggest that regulatory elements within the *lgc-35* introns are necessary for cell-type specific expression.

To determine the function of *lgc-35* in these cells we characterized two different mutant alleles disrupting the *lgc-35* gene. *lgc-35(tm1444)* is a ~1.3 kb deletion of the first five exons that removes the extracellular GABA binding domains and cys-loop, and thus likely represents a null allele (Figure A.4A). To verify that *lgc-35(tm1444)* is a null allele, we generated a second deletion allele *(ox469)* that eliminates the entire gene using the MosDEL technique (Frøkjær-Jensen et al., 2010) (Figure A.4A).

LGC-35 mediates contraction of the sphincter muscle

Expression of LGC-35 in the sphincter muscle suggested that this receptor could play a role in defecation (Figure A.3E). The defecation motor program in the adult hermaphrodite is a stereotyped behavior initiated approximately every 50 seconds when the animal is feeding (Croll, 1975; Liu and Thomas, 1994; Thomas, 1990). The motor program begins with a posterior body contraction, followed by an anterior body contraction and ends with contraction of the enteric muscles (Emc). The EXP-1 excitatory GABA receptor mediates contraction of the intestinal and anal depressor muscles; mutants lacking this gene exhibit a significant reduction in enteric muscle contractions (Emc/cycle) compared to control animals (Figure A.4B, wild-type = 99% vs.

exp-1 = 31% Emc/cycle, *p<0.0001*). However, the defect in *exp-1* mutants is milder than complete loss of GABA function, suggesting that a second GABA receptor may be involved. Specifically, mutations in *unc-25*, which encodes the biosynthetic enzyme for GABA, glutamic acid decarboxylase, cause a severe defect in enteric muscle contractions (Figure A.4B, *exp-1* = 31% vs. *unc-25* = 8.7% Emc/cycle, *p<0.0001*).

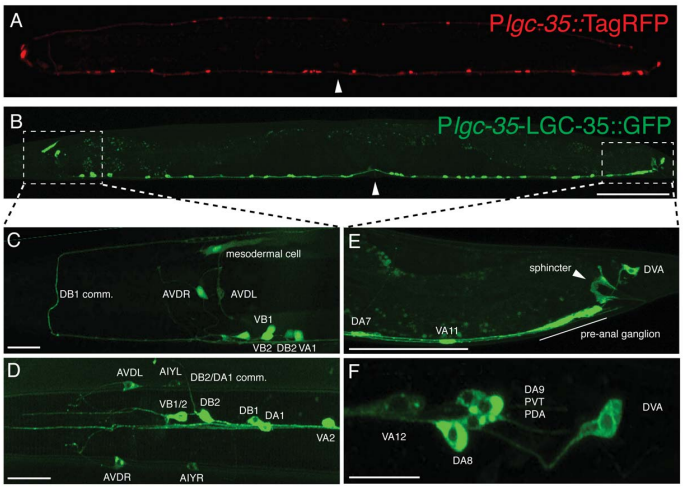

Figure A.3 LGC-35 is expressed in the sphincter and a subset of ventral cord motor neurons
(A) Transcriptional reporter. Plgc-35::TagRFP is expressed in a subset of VA, VB, and DB acetylcholine motor neurons anterior to the vulva, and in a subset of VA and DA acetylcholine motor neurons posterior to the vulva. Note that this construct lacks introns.
(B) Translational reporter. LGC-35::GFP is expressed in all acetylcholine motor neurons (VA, VB, DA, DB), except the AS and VC class. Note that this construct includes all introns.

(C) Plgc-35::TagRFP (pseudocolored green) expression in the adult nerve ring. In addition to the ventral cord motor neurons, lgc-35 is expressed in the AVD neurons and the head mesodermal cell.

(D) LGC-35::GFP expression is observed in the AIY and AVD interneurons and commissural (comm.) processes.

(E) Close-up of posterior hermaphrodite tail region. LGC-35::GFP sphincter muscle expression is denoted by white arrowhead.

(F) High magnification of the hermaphrodite tail. LGC-35::GFP is expressed in DVA, PDA and PVT neurons. Scale bars = 100mm (A-B); 10mm (C-F). Images are lateral views of an adult hermaphrodite, anterior is to the left. Arrowhead marks the location of the vulva, white boxes in panel B mark the imaged areas in panels C-F.

To determine if the LGC-35 receptor contributes to enteric muscle contractions we generated double mutants. Mutants lacking both receptors (*lgc-35 exp-1*) exhibited decreased enteric muscle contractions compared to *exp-1* single mutants (Figure A.4B, *exp-1* = 31% vs. *lgc-35(tm1444) exp-1* = 12% or *lgc-35(ox469) exp-1* = 13% Emc/cycle, *p< 0.0001*) and were not significantly different than *unc-25* single mutants (Figure A.4B, *lgc-35(tm1444) exp-1 p=0.24 or lgc-35(ox469) exp-1 p=0.06*). Additionally, RNA interference knockdown of *lgc-35* recapitulated the genetic loss-of-function experiments (Figure A.4B). Finally, LGC-35::GFP transgene expression in the double mutant rescued defecation to *exp-1* single mutant levels demonstrating the enhanced phenotype was specifically due to the loss of *lgc-35* (Figure A.4B, *exp-1* = 31% vs. *lgc-35(tm1444) exp-1;Ex[*LGC-35::GFP*] = 29%* Emc/cycle, *p=0.81*). These findings demonstrate that LGC-35 and EXP-1 together mediate GABA-dependent enteric muscle contraction.

The enteric muscles are coupled by gap junctions and appear to contract almost simultaneously. However, analysis of the related nematode *Oscheius myriophila* and high-speed videos of *C. elegans* indicates that there is a distinct order to the contraction (J. Delafield-Butt and E. Jorgensen, personal communication). The intestinal muscles contract first and fill the rectum with intestinal fluid. Contraction of the sphincter muscle seals the rectum, preventing reflux. Once the intestine is sealed, contraction of the anal depressor muscle opens the anus, and gut contents are expelled. Due to the close temporal activation of the enteric muscles, it is difficult to observe contraction of the sphincter muscle when the intestinal and anal depressor muscle contractions are present. Therefore, we used the *exp-1* mutant background to specifically isolate

sphincter muscle contraction because these mutants rarely exhibit intestinal and anal depressor contractions. High-speed video analysis revealed sphincter muscle contraction in *exp-1* mutants (Movie 4.1, n=12), confirming that EXP-1 is not required for this muscle contraction. By contrast, in *lgc-35 exp-1* double mutants, the sphincter muscle did not contract, and the rare expulsions that occurred were explosive, uncoordinated and were not accompanied by sphincter muscle contraction (n=15, Movie 4.2). These behavioral data demonstrate that LGC-35 specifically mediates GABA-induced contraction of the sphincter muscle and contributes to the contraction of all enteric muscles during the defecation motor program (Figure A.4C).

Movie 4.1
exp-1(ox276)

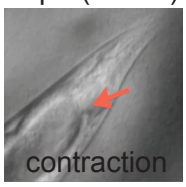

Movie A.1 Visualizing sphincter muscle contraction in exp-1(ox276) mutants

Sphincter contraction with no expulsion. exp-1(ox276) mutant recorded during a non-expulsive cycle. The sphincter contracts (red arrow) after the posterior body contraction in the absence of exp-1 mediated anal depressor contraction and expulsion (n = 12).

Movie 4.2
lgc-36(tm1444)exp-1(ox276)

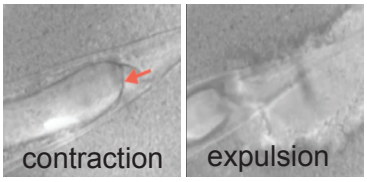

Movie A.2 Sphincter muscle does not contract in lgc-35 mutants

In lgc-35(tm1444) exp-1(ox276) double mutants, expulsions rarely occurred and were explosive. Sphincter contraction was never observed (red arrow, n =15). This video is recorded during an expulsive cycle, the posterior intestine swells and the rectum fills with food. The sphincter is passive and flaccid. The anal depressor contracts and opens the anus. The sphincter fails to contract and the gut contents explode from the anus.

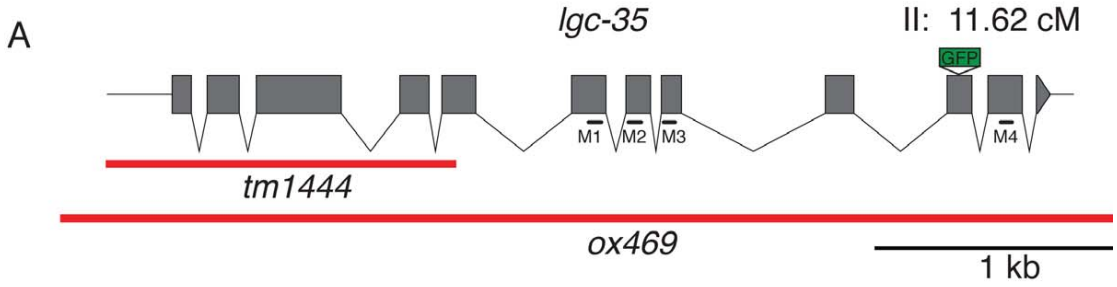
A
lgc-35
II: 11.62 cM
GFP
M1
M2
M3
M4
tm1444
ox469
1 kb

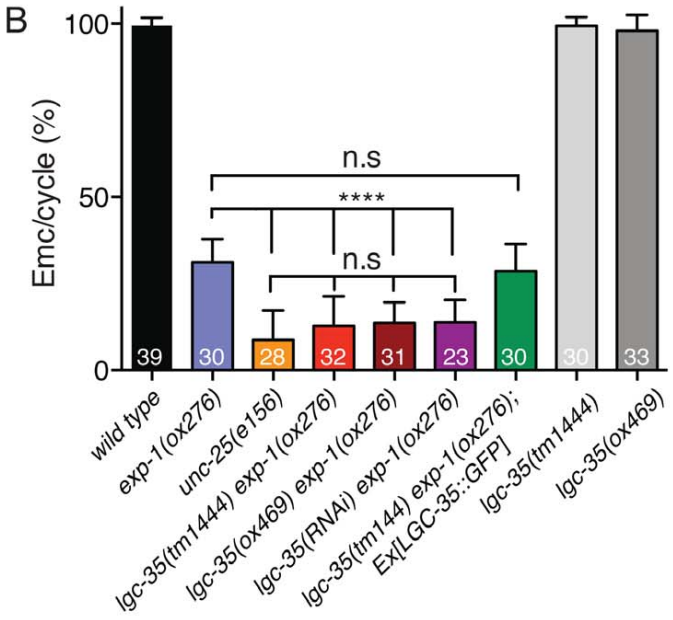
B
100
50
0
Emc/cycle (%)
n.s
****
n.s
39
30
28
32
31
23
30
30
33
wild type
exp-1(ox276)
unc-25(e156)
lgc-35(tm1444) exp-1(ox276)
lgc-35(ox469) exp-1(ox276)
lgc-35(RNAi) exp-1(ox276)
lgc-35(tm144) exp-1(ox276);
Ex[LGC-35::GFP]
lgc-35(tm1444)
lgc-35(ox469)

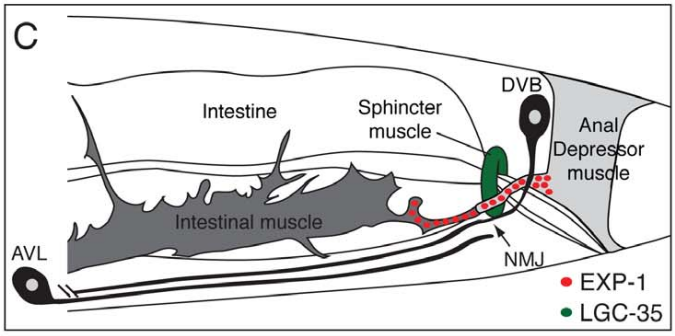
C
Intestine
Sphincter muscle
DVB
Anal Depressor muscle
Intestinal muscle
AVL
NMJ
EXP-1
LGC-35

Figure A.4 lgc-35 mediates contraction of the sphincter muscle

(A) Exon-intron structure of the lgc-35 genomic locus. The deletion extent for each allele is marked by red bars. Black bars mark transmembrane domain (M1-M4) location. The GFP insertion site is shown.

(B) lgc-35(tm1444 or ox469) exp-1(ox276) double mutants are more defective in enteric muscle contractions than exp-1(ox276) mutants alone. Enteric muscle contractions per posterior body contraction were scored to determine successful enteric muscle contractions per defecation cycle (Emc/cycle). Eleven defecation cycles were scored from young adult hermaphrodites for each genotype. The strain lgc-35(tm1444) exp-1(ox276); Ex[LGC-35::GFP] contains an extrachromosomal genomic lgc-35::gfp rescuing array (oxEx1291). Percentage of Emc/Cycle (mean ± s.e.m.): wild-type = 99.5 ± 0.36%, exp-1(ox276) = 31.2 ± 1.2%, unc-25(e156) = 8.68 ± 1.6%, lgc-35(tm1444) exp-1(ox276) =12.7 ± 1.53%, lgc-35(ox469) exp-1(ox276) =13.65 ± 1.06%, lgc-35(RNAi) exp-1(ox276) = 13.74 ± 1.4, lgc-35(tm1444) exp-1(ox276); Ex[LGC-35::GFP] = 28.6 ± 1.4%, lgc-35(tm1444) = 99.3 ± 0.46%, lgc-35(ox469) = 97.9 ± 0.79%, One-way ANOVA with Tukey post-hoc was used for multiple comparison, ****p<0.0001, n.s. = not significant. Error bars are s.e.m. The number of animals scored for each genotype is shown at the bottom of each bar.

(C) Schematic model of the enteric muscles. Red circles mark clustered EXP-1 receptors at the AVL/DVB synapse. The sphincter muscle is colored green to illustrate diffuse and non-clustered LGC-35 expression. Figure adapted from (Beg and Jorgensen, 2003b).

GABA spillover stimulates acetylcholine release in the locomotory circuit

To confirm that *lgc-35* is expressed in the acetylcholine motor neurons, we created double transgenic animals in which the ventral cord acetylcholine motor neurons express the fluorescent protein mCherry under the control of the *acr-2* promoter (P*acr-2*::mCherry). *acr-2* is expressed in VA, VB, DA, and DB acetylcholine motor neurons (Jospin et al., 2009). In P*lgc-35*::LGC-35::GFP; P*acr-2*::mCherry double transgenics, co-localization of fluorescent reporter proteins was observed, verifying that *lgc-35* is expressed in these acetylcholine motor neurons (Figure A.5A). To determine if *lgc-35* is expressed in GABA motor neurons, P*lgc-35*::LGC-35::GFP expressing animals were crossed into a strain expressing the fluorescent protein mCherry under the control of the *unc-47* promoter (P*unc-47*::mCherry), which labels all 26 GABA motor neurons

(Jin et al., 1999). We observed no co-localization between *lgc-35* and *unc-47* expression in these animals, confirming that LGC-35 is expressed in ventral cord acetylcholine, but not GABA motor neurons (Figure A.5B).

Both diffuse and punctate localization of the LGC-35::GFP translational fusion protein was observed in the dorsal and ventral nerve cords and in the acetylcholine motor neuron cell bodies (Figs.3-3A and Figure A.5A and C). To determine if LGC-35 is juxtaposed to GABA synapses, we labeled the synaptic vesicle protein synaptobrevin with TagRFP in GABA neurons (P*unc-47*::SNB-1::TagRFP). Synaptobrevin distribution was punctate, marking GABA neuromuscular junctions along the nerve cord (Bamber et al., 1999b). LGC-35::GFP puncta were not juxtaposed to GABA synapses but were rather localized to intersynaptic regions along the nerve cord between the GABA synapses (Figure A.5C). These data suggest that GABA spillover from GABA neuromuscular junctions activates LGC-35 on acetylcholine motor axons.

The presence of LGC-35 on acetylcholine motor neurons suggests that GABA stimulates acetylcholine release onto muscles and that there may be deficits in acetylcholine transmission in the absence of LGC-35. To determine if acetylcholine release is decreased in the absence of LGC-35, we assayed the sensitivity of *lgc-35* mutants to aldicarb, an acetylcholinesterase inhibitor (Mahoney et al., 2006).

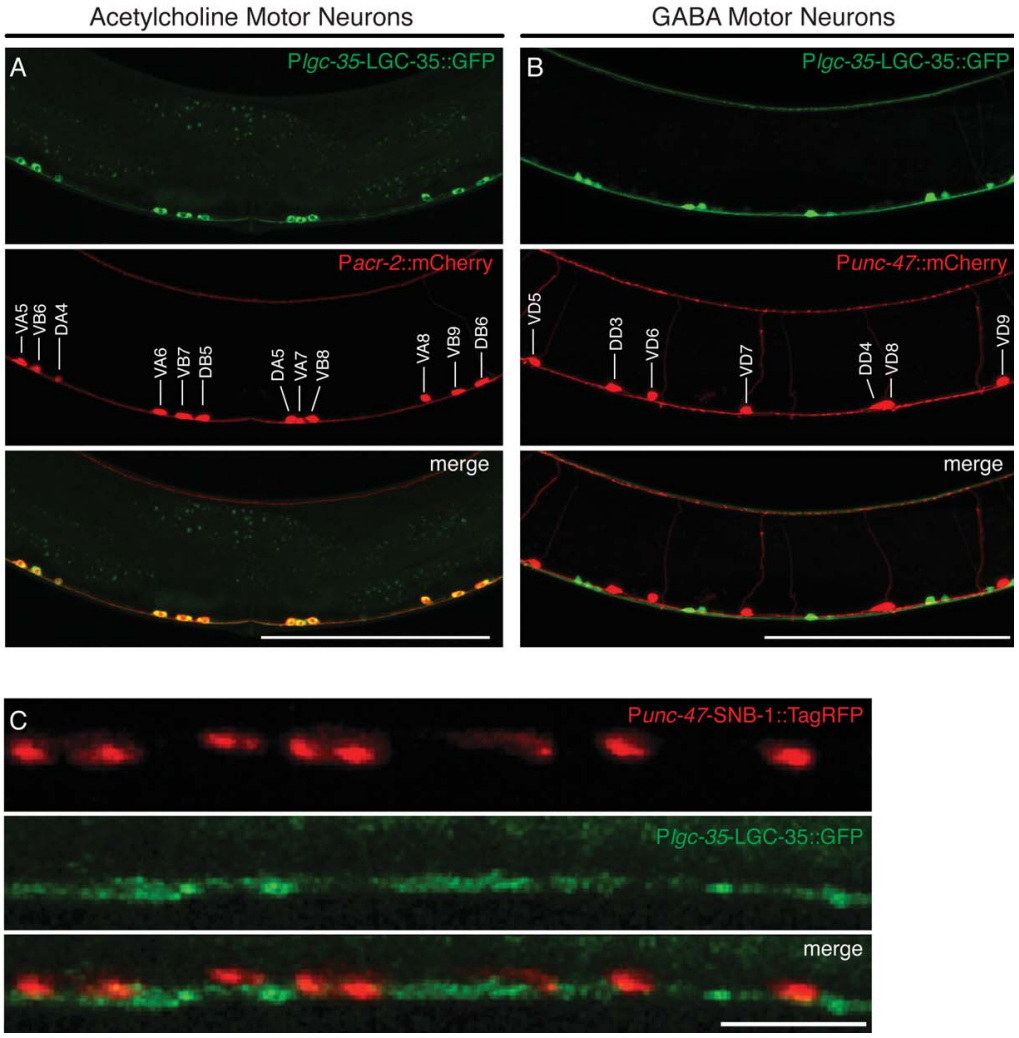

Figure A.5 lgc-35 is expressed in ventral cord acetylcholine motor neurons

A, Lateral view of LGC-35::GFP expression in Pacr-2::mCherry background. Co-localization is seen in all acr-2-expressing acetylcholine motor neurons (DA, DB, VA, VB). Lateral view of the vulva region of an adult hermaphrodite, anterior is to the left and dorsal is up. The acetylcholine motor neurons are labeled in the middle panel.

B, Lateral view of LGC-35::GFP motor neuron expression in Punc-47::mCherry background. LGC-35::GFP (green) is not localized to GABA motor neurons (red). Lateral view of the vulva region of an adult hermaphrodite, anterior is to the left and dorsal is up. The GABA motor neurons are labeled in the middle panel.

C, LGC-35::GFP is localized to intersynaptic regions. Punc-47::SNB-1::TagRFP (red, top panel) co-injected with Plgc-35::LGC-35:GFP (green, middle panel). Lateral view of the dorsal cord. Scale bars = 100mm (A-B); 10mm (C).

Both *lgc-35* mutant strains were resistant to aldicarb, suggesting a presynaptic defect in neuronal excitability or neurotransmitter release (Figure A.6A). To demonstrate that this phenotype was specifically due to loss of LGC-35, we rescued the sensitivity to aldicarb by transgenic expression of LGC-35::GFP (Figure A.6A). These pharmacological data indicate a decrease in acetylcholine transmission at neuromuscular junctions in the mutants. To determine if this decrease in neurotransmission affects locomotion, we performed thrashing assays in liquid. *lgc-35* mutants not only exhibited a significant decrease in the number of body bends, but also displayed uncoordinated body bending compared to wild- type controls (Figure A.6B, data not shown). These phenotypes were rescued by transgene expression of LGC-35::GFP (Figure A.6B), suggesting that loss of LGC-35 results in an imbalance in the excitation to inhibition ratio within the locomotor circuit.

To determine the function of *lgc-35* in locomotory behavior, we analyzed *lgc-35* mutants crawling on agar using a computerized worm tracker. Animals were evaluated under high magnification during normal, unstimulated movement on food. *lgc-35* mutants spent comparable amounts of time moving forward and backward compared to wild-type controls (data not shown). However, the animals moved faster and the amplitude of body bends was increased in *lgc*-35 mutants; both phenotypes were rescued by transgene expression of LGC-35::GFP (Figure A.6C-D). Together, these data suggest that *lgc-35* functions in motor neurons to regulate animal locomotion.

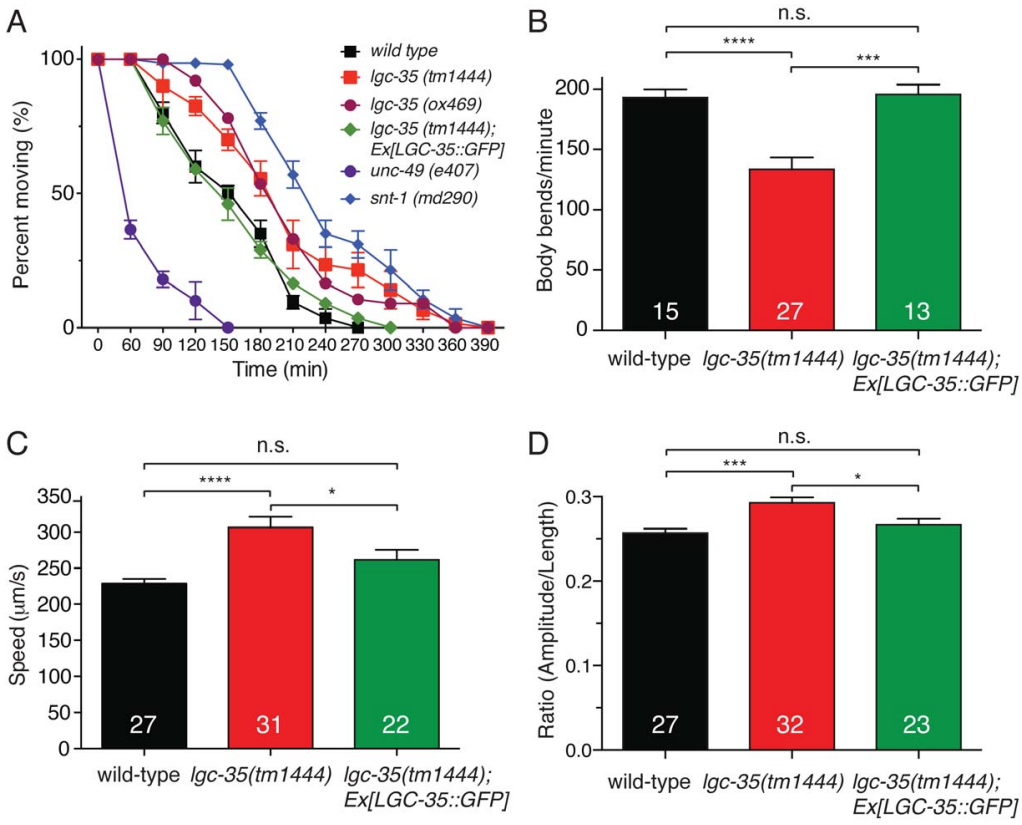

Figure A.6 lgc-35 mutants have altered locomotion and neuromuscular transmission

(A) lgc-35 mutants are resistant to aldicarb, an acetylcholinesterase inhibitor. lgc-35 mutants (tm1444 and ox469) are resistant to the paralyzing effects of aldicarb compared to wild-type. A known hypersensitive mutant unc-49(e407), and resistant mutant snt-1(md290) were used as controls. Data are mean ± s.e.m., n=30 animals, 3 plates per genotype. Aldicarb resistance in lgc-35(tm1444) mutants is rescued by LGC-35::GFP transgene expression.

(B) Liquid thrash assays were used to assess neuromuscular transmission and coordination. lgc-35(tm1444) mutants exhibited a significant decrease in the number of body bends per minute compared to wild-type controls: lgc-35(tm1444) = 133 ± 9.7 vs. wild-type = 193 ± 6.9, ****p<0.0001, which was rescued by LGC-35::GFP transgene expression: lgc-35(tm1444); Ex[LGC-35::GFP] = 195 ± 7.9, p=0.64 compared to the wild-type, ***p=0.0003 compared to lgc-35(tm1444).

(C) lgc-35 mutants move with increased speed compared to the wild-type controls: lgc-35(tm1444) = 306 mm/s vs. wild-type = 229 mm/s ,****p<0.0001. This increase is rescued by transgenic expression of LGC-35::GFP (262 mm/s vs. wild-type (p= 0.19), and *p=0.039 compared to lgc-35(tm1444) mutants).

(D) lgc-35(tm1444) mutants exhibit an increased body bend amplitude compared to the wild-type controls: lgc-35(tm1444) = 0.29 vs. wild-type = 0.25, ***p=0.0002. This increase in lgc-35(tm1444) mutants is rescued by transgenic expression of LGC-35::GFP (0.26 mm, p=0.57, compared to the wild-type, *p=0.012 compared to lgc-35(tm1444) mutants). The body bend amplitude ratio (Amplitude/Length) is shown. One-way ANOVA with Tukey post hoc analysis was used for multiple comparison and the p-values are indicated for each condition. Not significant (n.s) is p>0.05. The number of animals tested for each genotype or assay is shown at the bottom of each bar.

LGC-35 is involved in male spicule eversion

After hatching, larval *C. elegans* hermaphrodites and males are largely indistinguishable. However, in the fourth larval stage (L4), male-specific neurons and copulatory muscles are generated and the enteric muscles are extensively remodeled. Specifically, the anal depressor attaches to the spicule protractor and the sphincter muscle becomes enlarged and attaches to the dorsal surface of the body wall. We generated males expressing either transcriptional or translational GFP fusions to determine if *lgc-35* is expressed in male-specific muscles and neurons. In contrast to hermaphrodites, *lgc-35* is not expressed in any of the male enteric muscles, including the sphincter muscle, suggesting that it does not play a role in defecation in adult males (Figure A.7A-B). Like hermaphrodites, adult males expressed *lgc-35* in acetylcholine motor neurons, the head mesodermal cell, and in the head interneurons AIY and AVD (data not shown). In the male tail, *lgc-35* is expressed in sensory rays 2, 3, 4, 5 and 9, the SPV neurons and the oblique muscles (Figure A.7A-C).

Consistent with this expression pattern, GABA neurons are known to innervate these cells. The vesicular GABA transporter (*unc-47*) is expressed in the male specific PCB, PCC post-cloacal sensilla neurons and the SPC proprioceptive motor neurons (Figure A.7C-D). Interestingly, in addition to expressing the GABA transporter, these motor neurons also express the vesicular acetylcholine transporter UNC-17 (Garcia et al., 2001) (Figure A.7D). It is likely that these sensory-motor neurons redundantly use GABA and acetylcholine to induce muscle contraction during copulation (Jarrell et al., 2012). The SPC neurons make chemical synapses directly with the spicule muscles and presumably act via a different GABA receptor than LGC-35 (Figure A.7D). The

PCB and PCC neurons make chemical synapses with the LGC-35-expressing oblique muscles (Figure A.7D). During intromission, the post-cloacal PCB and PCC neurons mediate insertion of the spicules into the vulva by initially stimulating oblique muscle contraction. In turn, the oblique muscles transduce the signals to the spicule-associated sex muscles through electrical junctions (Garcia et al., 2001; Jarrell et al., 2012; Liu and Sternberg, 1995; Liu et al., 2011) (Figure A.7D).

The expression of LGC-35 in male-specific muscles and neurons suggests the receptor might play a role in male mating. We assayed mating efficiency by placing single males with four wild-type hermaphrodites and then removed the male after four time points (1, 3, 6, and 24 hours). With the exception of the 6 hour time point, *lgc-35(tm1444) him-8(e1489)* double mutants males were not significantly different than control *him-8(e1489)* single mutants males for the percentage of cross progeny sired (Figure A.7E); nor was male potency in aged animals affected in *lgc-35* mutants. Specifically, single males, aged 1-6 days, were paired with a young adult *pha-1(ts)* hermaphrodite and the presence of any cross progeny was scored three days later. The virility of *lgc-35* males diminished at a similar rate as control males over six days (Figure A. 7F), suggesting that *lgc-35* does not play an overt role in male mating ability or potency.

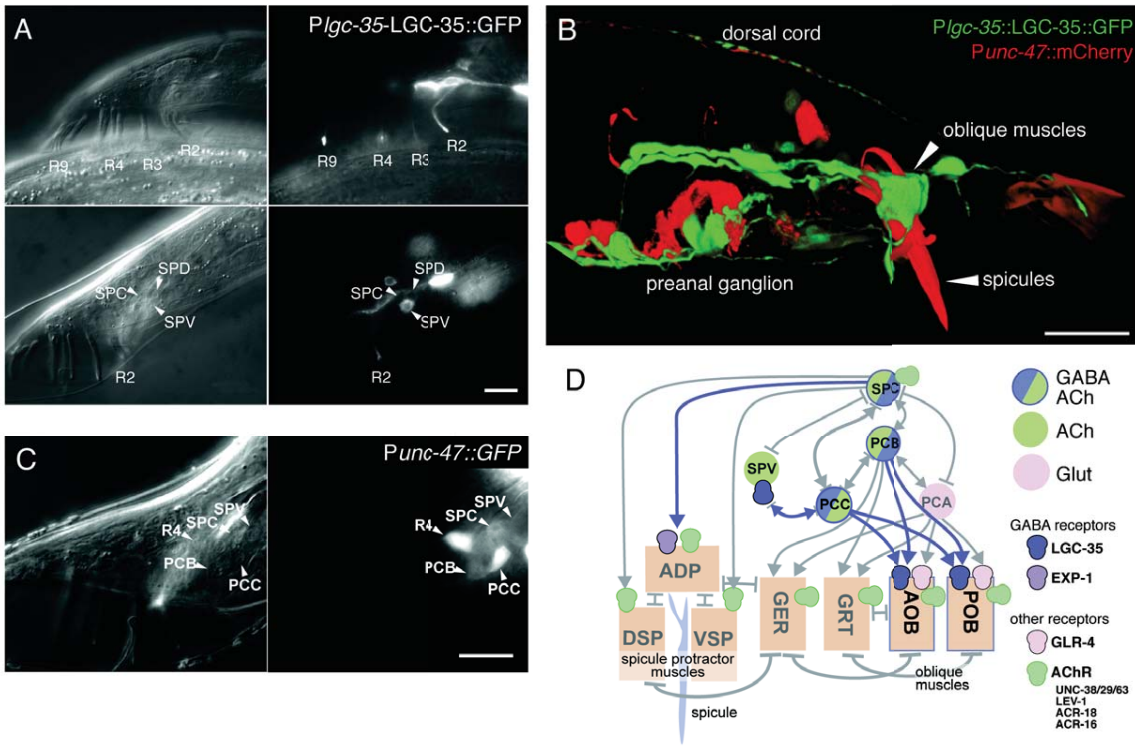
A
Plgc-35-LGC-35::GFP
R9
R4
R3
R2
SPD
SPC
SPV
B
dorsal cord
Plgc-35::LGC-35::GFP
Punc-47::mCherry
oblique muscles
preanal ganglion
spicules
C
Punc-47::GFP
R4
PCB
PCC
D
SPC
PCB
SPV
PCC
PCA
ADP
GER
GRT
AOB
POB
DSP
VSP
spicule protractor muscles
oblique muscles
spicule
GABA
ACh
Glut
GABA receptors
LGC-35
EXP-1
other receptors
GLR-4
AChR
UNC-38/29/63
LEV-1
ACR-18
ACR-16
E
him-8(e1489)
lgc-35(tm1444); him-8(e1489)
% Cross Progeny
Hours Mated
F
him-5(e1490)
lgc-35(tm1444); him-8(e1489)
% males that can sire progeny
Days
G
% Spicule Eversion (48hrs)
****
n.s.
*
Wild type
him-8(e1489)
lgc-35(tm1444)
unc-49(e407)
lgc-35(tm1444); unc-49(e407)
lgc-35(tm1444); unc-49(e407); Ex[LGC-35::GFP]

Figure A.7 LGC-35 is expressed in male specific muscles and neurons and is involved in spicule eversion

(A) Nomarski (left panels) and fluorescence (right panels) images of LGC-35::GFP expression in the male. The top panels show LGC-35::GFP expression in rays (R) 2,3,4, and 9 (Ray 5 expression not shown). The bottom panels show LGC-35::GFP expression in ray 2, the SPV neurons, and possibly the SPD neuron.

(B) Confocal image of a transgenic male expressing Plgc-35::LGC-35::GFP and Punc-47::mCherry. Arrows indicate spicules and oblique muscles.

(C) Male cloacal neurons express the GABA vesicular transporter gene unc-47. Nomarski (left panel) and fluorescence (middle panel) images of the lateral tail of Punc-47::GFP expressing in an oxIs12 him-5(e1490) male. The PCC neurons strongly express the transgene, whereas weak expression can be detected in the PCB postcloacal sensilla neurons and the SPC proprioceptive neurons.

(D) Panel depicts an abbreviated connectome of the post-cloacal sensilla neurons and the male sex muscles. Lines with arrows or bars depict chemical or electrical connections, respectively. Muscles in the male cloacal region: AOB, POB, anterior and posterior oblique; GER, GRT, gubernaculum erector and retractor; DSP, VSP dorsal and ventral spicule protractor; ADP anal depressor.

(E) lgc-35 mating ability. There is no difference in cross progeny number between lgc-35(tm1444) him-8(e1489) double mutants vs. him-8(e1489) single mutant controls for a single males performance at 1, 3, and 24-hour timepoints ($p>0.05$, n=4 plates/time point/genotype). There was a significant difference at the 6-hour timepoint ($p=0.037$, n=4 plates/time point/genotype).

(F) lgc-35 mating potency. There is no difference between lgc-35(tm1444) him-8(e1489) vs. him-5(e1490) male mating potency measured by the percent of males that can sire progeny over time (Fisher exact test, n= 20 males/genotype/day).

(G) Spicule eversion. An everted spicule refers to spicules permanently everted from the body cavity of adult male at 48 hours. All animals are in a him-8(e1489) background. Spicule eversion is not different in wild-type males (5.7% ± 2.8, n=70) compared to him-8(e1489) controls (9.83% ± 3.8, n=61, $p>0.05$). lgc-35(tm1444) mutants (1.58% ± 1.5, n=63) have significantly fewer everted spicules compared to him-8(e1489) controls (*$p<0.05$). unc-49(e407) mutants (40.4% ± 6.8, n=52) exhibit significantly increased spicule eversion compared to him-8(e1489) controls (****$p<0.0001$). The enhanced spicule eversion phenotype in unc-49(e407) mutants is suppressed by loss of lgc-35 (lgc-35(tm1444) unc-49(e407) (1.22% ± 1.1, n=82), ****$p<0.0001$). Suppression of spicule eversion in lgc-35(tm1444) unc-49(e407) mutants was reversed by microinjection of a LGC-35::GFP rescuing construct (34.1% ± 7.23, n=44). One-way ANOVA with Tukey post-hoc was used for multiple comparisons. Data are mean ± s.e.m., Scale bar, 10mM.

To determine whether there were more subtle defects in the male, we examined spicule extension and retraction between mating events. During periods between sex, the male generally keeps his spicules inside his tail. However, at a low probability, he will spontaneously protract his spicules during defecation (Garcia and Sternberg, 2003). In rare cases, the spicules become permanently everted in adult wild-type males (5.7% everted) or from the strain *him-8,* which produces males at high frequency (9.8% everted) (Figure A.7G). Spicule eversion is significantly reduced by the loss of the excitatory GABA receptor LGC-35 compared to *him-8* controls (1.6% everted in *lgc-35; him-8*, $p<0.05$) (Figure A.7G). By contrast, spicule eversion is greatly exacerbated by the loss of the inhibitory GABA receptor UNC-49 compared to *him-8* controls (40.4% everted spicules in *unc-49; him-8, p<0.0001*) (Figure A.7G). Moreover, loss of *lgc-35* completely suppressed the everted spicule phenotype observed in *unc-49* mutants (1.2% in *lgc-35; unc-49; him-8*) and suppression of spicule eversion was reversed by transgene expression of LGC-35::GFP (34.1% in *lgc-35; unc-49; him-8; Ex[*LGC-35::GFP*]*) (Figure A.7G). Taken together, these data suggest that inhibitory GABA signaling inhibits spicule extension, whereas excitatory GABA signaling stimulates spicule extension, probably via GABA inputs into the spicule-associated muscles, which is in part formed from remodeled enteric muscles during the L4 stage.

Discussion

We found that the GABA receptor LGC-35 acts as an excitatory ion channel at the sphincter muscle in hermaphrodites, at the spicule protractor in males and on acetylcholine motor neurons involved in locomotion. We discuss these results in regard to the structure and evolution of ligand-gated ion channels, the relationship of EXP-1,

and LGC-35 in the control of muscle contraction, and finally the role of LGC-35 in spillover transmission between motor neurons.

How did LGC-35 acquire cation-selectivity?

How did GABA-gated cation channels evolve? Phylogenetic analysis demonstrates that these receptors are more closely related to other GABA receptors than they are to acetylcholine or serotonin receptors (Figure A.1A and C). However, the M2 domain is divergent from other cation channels indicating that there are multiple solutions for generating cation permeability (Figure A.1D).

Mutational studies have demonstrated that pore geometry, size and electrostatic charge are critical features that determine cys-loop receptor ion-selectivity (Jensen et al., 2005b). Changes in three residues are sufficient to convert ion selectivity of GABA and glycine receptors from anions to cations: 1) a deletion of the -2' proline (P-2'D), 2) a glutamate substitution at the -1' position (A-1'E), and 3) a hydrophobic valine substitution at the 13' position (T13'V) (Jensen et al., 2005a; Jensen et al., 2002; Keramidas et al., 2000; Wotring et al., 2003). The reciprocal changes have also been demonstrated to convert the cation-selective nicotinic acetylcholine and serotonin receptors to anion-selective (Corringer et al., 1999; Galzi et al., 1992; Gunthorpe and Lummis, 2001). Significantly, the single A-1'E point mutation is sufficient to make the glycine receptor (GlyRa1) permeable to cations (Keramidas et al., 2002), while the reverse mutation (E-1'A) renders the serotonin (5-HT3A) receptor non-selective (Gunthorpe and Lummis, 2001).

LGC-35 has several features that differ from canonical inhibitory cys-loop receptors and may explain cation-selectivity: 1) a significantly shorter linker region that

lacks the conserved PAR motif present in the majority of anion-selective receptors that may alter pore diameter and geometry (Jensen et al., 2005b), 2) a hydrophobic phenylalanine at the 13' position, which is a hydrophilic threonine in anion-selective receptors (Keramidas et al., 2000), and 3) a negatively charged glutamate residue at the extracellular ring of charge, a position that is predominantly positive in anion channels (19') and negative in cation channels (20') (Imoto et al., 1988) (Figure A.1D). Surprisingly, LGC-35 does not contain the critical negative charge at the -1' position. Instead, the closest residue is a neutral serine. One model is that phosphorylation of the -3' serine may provide the negative electrostatic environment that favors cation-selectivity. Interestingly, the analogous residue in EXP-1 is a negatively charged glutamate residue, suggesting that charge in this position may play an important role in conferring cation-selectivity. Alternatively, the ETS motif in LGC-35 may substitute for the PAR motif present in anionic-channels and provide the electrostatics for cation permeability (Jones and Sattelle, 2008; Wotring and Weiss, 2008). Together, these observations suggest that LGC-35 evolved a novel strategy for cation-permeability and that the molecular and electrostatic requirements for ion-selectivity may be more flexible than previously appreciated.

Enteric muscle contraction

The enteric muscles are comprised of two intestinal muscles, the sphincter and anal depressor muscle; contraction of these muscles during the defecation cycle is mediated by the GABA motor neurons AVL and DVB (McIntire et al., 1993b; White et al., 1986a) (Figure A.4C). Contraction of the intestinal and anal depressor muscles is mediated by the GABA-gated cation channel EXP-1 (Beg and Jorgensen, 2003b;

McIntire et al., 1993a; Thomas, 1990) and the sphincter muscle contraction is mediated by LGC-35 (this manuscript) (Figure A.4C). Contraction of these muscles is ordered from anterior to posterior. First the intestinal muscles contract and fill the rectum with gut contents (EXP-1-mediated); second, the sphincter muscle contracts to seal the intestine and prevent reflux (LGC-35-mediated); third, the anal depressor lifts the roof of the anus (EXP-1-mediated) and turgor pressure collapses the rectum driving expulsion. Because the enteric muscles are connected by gap junctions, the presence of either one of these receptors is able to stimulate some muscle contractions. Only by eliminating both receptors are contractions eliminated, fully recapitulating the defecation phenotype of mutants lacking the biosynthetic enzyme for GABA (Jin et al., 1999).

Why are two GABA-gated cation channels (LGC-35 and EXP-1) needed for enteric muscle contraction? One possibility is that differences in receptor localization and desensitization coordinate the proper timing and length of each muscle contraction. EXP-1 is less sensitive to GABA (~27mM), rapidly desensitizing and highly clustered at the AVL/DVB neuromuscular junction (Beg and Jorgensen, 2003b), whereas LGC-35 is more sensitive to GABA (~15mM), desensitizes slowly and is diffusely expressed in the sphincter muscle, with no apparent clustering or enrichment at the synapse (Figure A.4C). These properties suggest that synaptic signaling from AVL and DVB motor neurons rapidly activates the intestinal muscles via EXP-1, while spillover transmission onto LGC-35 causes a prolonged sphincter muscle contraction safeguarding against reflux of the expellant during opening of the anus. In addition, the inhibitory GABA receptor isoform UNC-49B is expressed in the sphincter muscle but not in the anal depressor or intestinal muscles (Bamber et al., 1999b). Sphincter relaxation is

important for defecation in adult males, but there is not an apparent role in hermaphrodites (Reiner and Thomas, 1995).

Spicule Eversion and Mating

Lack of inhibitory inputs into male specific muscles mediated by the GABA–gated chloride channel UNC-49 causes the spicules to extend, become permanently everted and hang from the cloaca. This phenotype is likely due to an excess of excitatory inputs into these muscles caused by loss of inhibitory input. Because loss of the excitatory GABA receptor LGC-35 suppresses this phenotype, it is likely that GABA acts to stimulate the spicule protractor muscle. Surprisingly, loss of LGC-35 did not result in a significant defect in male mating ability or potency in *lgc-35* mutants. It is possible that *exp-1* and *lgc-35* provide overlapping functions but the contribution from *exp-1* is essential because it is required for male mating (E. Jorgensen, unpublished). Alternatively, *lgc-35* GABA signaling might be redundant with acetylcholine signaling. Surprisingly the PCC, PCB and SPC neurons express vesicular transporters for both GABA and acetylcholine, and the target oblique muscles express both the GABA receptor LGC-35 and acetylcholine receptor subunits (UNC-38, UNC-63, UNC-29, LEV-1, ACR-16, and ACR-18) (Liu et al., 2011). The release of two transmitters violates Dale's principle of 'one neuron: one transmitter' (Eccles et al., 1954), but there are now several examples of transmitter corelease (Hnasko and Edwards, 2012) and even an example of GABA and acetylcholine corelease (Lee et al., 2010).

GABA acts in spillover neurotransmission on locomotory motor neurons

In *C. elegans*, GABA receptors mostly act at neuromuscular junctions (Schuske et al., 2004). Here, we find that the excitatory GABA receptor LGC-35 is expressed in the sphincter muscle and also in the acetylcholine motor neurons. The loss of excitatory GABA input into the acetylcholine motor neurons leads to decreased acetylcholine output, observed as an aldicarb-resistant phenotype in *lgc-35* mutants. These excitatory GABA inputs are both direct and indirect.

There are some direct synaptic contacts between the ventral VD GABA motor neurons and the ventral acetylcholine motor neurons that are observed in the wiring diagram (Chen et al., 2006). However, they are a minor component of the output of these motor neurons; for example, the VD3 GABA motor neuron forms 23 synapses to ventral body muscle, but only 2 synapses each to VA3 and VB2 (Chen et al., 2006). Moreover, the DD neurons for the most part do not have similar inputs into the DA and DB motor neurons. This connectivity appears counterproductive: GABA release will simultaneously inhibit muscle contraction directly via UNC-49 and indirectly drive muscle contraction by stimulating acetylcholine release. However, it is likely that these direct inputs serve to initiate a rebound of the acetylcholine motor neurons to reverse the flexure during locomotion. Consistent with this model, *lgc-35* mutants exhibit exaggerated bending in liquid or on solid surfaces, likely due to an inability to reverse ipsilateral relaxation that leads to flexures of greater amplitude.

The dominant inputs from GABA neurons to acetylcholine neurons are not via direct inputs but rather through indirect inputs, mediated by spillover transmission. In addition to receiving direct inputs from GABA neurons, LGC-35 is largely distributed on

acetylcholine axons between GABA neuromuscular junctions; in other words LGC-35 is not juxtaposed to GABA release sites but rather is found between them. As expected for a receptor that is distant to a release site, LGC-35 exhibits increased sensitivity to GABA compared to the inhibitory GABA receptor on muscles juxtaposed to the release site (LGC-35 EC_{50} = 15 mM; UNC-49 EC_{50} = 44 mM) (Bamber et al., 1999b). In addition, unlike other GABA neurons in the worm, the ventral cord GABA motor neurons do not express the GABA transporter SNF-11 (Mullen et al., 2006), nor do they show GABA uptake activity (McIntire et al., 1993a). In the absence of rapid clearance, GABA spillover along the motor neurons will activate the acetylcholine motor neurons.

Spillover transmission is not unique to nematodes. There are examples in vertebrate circuits where neurotransmission has indirect components (Nishiyama and Linden, 2007). In these circuits, spillover transmission may function to modify direct synaptic signaling. For example, climbing fibers in the mouse cerebellum make thousands of direct excitatory synaptic contacts with their primary target Purkinje cells. These same climbing fibers also communicate with inhibitory cerebellar basket and stellate interneurons exclusively by spillover transmission (Szapiro and Barbour, 2007). Additionally, inhibitory golgi-granule cell communication in the cerebellum is predominantly mediated by spillover transmission (Rossi and Hamann, 1998). Together, these data and our findings reveal that spillover transmission adds an additional layer of complexity to neuronal circuits and underscores that simply mapping synaptic connectivity cannot describe how behavioral output is encoded at the circuit level.

Material and Methods

Strains

For all experiments, the Bristol N2 strain was used as the wild-type control. Worms were grown at 22°C on NGM plates seeded with *E. coli* OP50 or HB101. EG4787 *lgc-35(tm1444)* II, a deletion mutation removing the first five exons of *lgc-35*, was obtained from the Japan National BioResource project and outcrossed six times. To obtain a second null allele of *lgc-35*, the MosDEL technique was used to generate the targeted deletion EG6027 *lgc-35(ox469)* II (Frøkjær-Jensen et al., 2010). Briefly, the *Mos1* transposon in *lgc-35(ttTi13013) II* was remobilized causing a break in the DNA, which was repaired by a template encompassing a deletion of *lgc-35*. The following strains were used for experiments described in this work: JT6 *exp-1(sa6)* II, EG276 *exp-1(ox276)* II, EG4920 *unc-25(e156)* III, EG7856 *unc-49(e407)* III, EG3328 *exp-1(ox276)* II; *unc-49(e407)* III, and CB1489 *him-8(e1489)* IV. The following strains were generated for the experiments described in this work: EG4563 *lgc-35(tm1444) exp-1(ox276)* II, EG4869 *lgc-35(tm1444) exp-1(ox276)* II; *unc-49(e407)* III, EG5035 *lgc-35(tm1444) exp-1(ox276)* II; *lin-15(n765ts)* X, EG5377 *lgc-35(tm1444)* II*; him-8(e1489)* IV, EG5330 *exp-1(ox276) lgc-35(tm1444) II; oxEx129 [*P*lgc-35::*LGC-35::GFP*,* P*sur-5::GFP, lin-15(+)],* EG7253 *lgc-35(tm1444) II; oxEx1291[*P*lgc-35*::LGC-35::GFP, P*sur-5*::GFP, *lin-15(+)]*, and EG5331 *lgc-35(tm1444) II; unc-49(e407) III; him-8(e1489) IV; oxEx1328 [*P*lgc-35*::LGC-35::GFP*::let858-UTR,* P*sur-5:GFP, lin-15(+)].*

Sequences

Orthologs of LGC-35 found in nematode species include: *C. japonica* (JA09778, 87% identity), *C. brenneri* (CN11371, 76% identity), *C. briggsae* (CB18417, 71%

identity), and *P. pacificus* (PP42968, 58% identity), and in the parasitic nematodes *Ascaris suum* (ERG83865.1, 43% identity), *Brugia malayi* (XP_001900837.1, 48% identity), *Loa loa* (XP_003137178.1, 47% identity), and *Onchocera volvulus* (OVOC9886, 41% identity).

Transcriptional fusion

A 7.6 kb genomic fragment including ~3 kb upstream sequence, the 3.54 kb Y46G5A.26 (*lgc-35*) open reading frame, and 1.0 kb downstream sequence was PCR amplified and cloned into the vector pCR2.1 (Invitrogen) to generate pAB12. To generate the transcriptional reporters, a 2.9kb *lgc-35* promoter fragment was PCR amplified from pAB12 using primers containing attB4 and attB1 sites. The promoter fragment with flanking sites was recombined into pDONR P4-P1R (Invitrogen) using the BP recombination reaction to make pMJ50. The EGFP transcriptional reporter pMJ52 (P*lgc-35*::EGFP::*let-858* terminator) was made by recombining pMJ50, pGH115, and ADA-126 in a multisite LR reaction into pDEST R4-R3 (Invitrogen). The TagRFP transcriptional reporter pMJ53 (P*lgc-35*::TagRFP::*let-858* terminator) was made by recombining pMJ50, pRH142, ADA-126 in a multisite LR reaction into pDEST R4-R3 (Invitrogen). Sequencing and restriction digests confirmed correct construction of all reporter constructs. The two transcriptional reporters, pMJ52 and pMJ53, were separately injected at 20 ng/µL with 80 ng/µL of pEK1(*lin-15*+) into *lin-15(n765ts)* animals to generate *oxEx1314*(pMJ52) and *oxEx1315*(pMJ53).

Translational GFP fusion

To determine protein localization, GFP was inserted into the open reading frame of LGC-35 within the intracellular loop between M3-M4. To generate pAB10, an in-frame translational LGC-35::GFP fusion plasmid, an XmaI/AgeI restriction fragment from pPD102.22 containing the EGFP coding region was ligated to AgeI linearized pAB12. Sequencing confirmed that the EGFP insertion site was in-frame within pAB10. pAB10 was injected at 30ng/µL with pEK1(*lin-15*+) at 30 ng/µL and 1kb+ DNA Ladder at 40 ng/µL into *lin-15(n765ts*) animals to generate *oxEx1253*. An additional translational reporter was generated using the gateway system. LGC-35::GFP from pAB10 was PCR amplified using primers containing attB1 and attB2 sites. The PCR product was recombined with attP1 and attP2 sites into pDONR P1-P2R (Invitrogen) using the BP recombination reaction to make pMJ51 (LGC-35::GFP). An EGFP translational reporter, pMJ54 (P*lgc-35*::LGC-35::GFP-*let-858* terminator), was made by recombining pMJ50, pMJ51, ADA-126 in a multisite LR reaction into pDEST R4-R3 (Invitrogen).

Cell Identification

To determine if LGC-35 protein is expressed in acetylcholine motor neurons (VA,VB, DA, DB), an injection mix of 30 ng/µL of pAB10, 2.5 ng/µL of pCFJ90, 30 ng/µL of *Pacr-2*::mCherry and 37.5 ng/µL of 1Kb+ DNA Ladder (Invitrogen) was injected into wild-type animals to generate *aabEx13.* To determine if LGC-35 is expressed in GABA motor neurons (DD and VD) 30 ng/µL of pAB10, 30 ng/µL of pGH21 and 40 ng/µL of pEK1(*lin-15*+) were injected into *lin-15(n765ts)* animals to generate *oxEx1224*. Cell identifications were made from young adult hermaphrodite animals using the vulva as a landmark for orientation. Sequencing and restriction digests confirmed correct construction for all

constructs. Standard microinjection techniques were used to generate all transgenic strains (Mello et al., 1991). Strains were imaged on a Pascal LSM5 confocal microscope (Carl Zeiss) or Nikon A1R confocal.

Lgc-35 rescue constructs

Rescue of *lgc-35(tm1444)* mutants was achieved by injecting 15 ng/µL of pMJ54, 5 ng/µL of P*sur-5*::GFP, and 80 ng/µL of pEK1 generating the array *oxEx1291*.

RNAi

RNA interference (RNAi) was performed by feeding (Kamath et al., 2003). Ten adult gravid hermaphrodites were placed on RNAi bacteria and allowed to lay eggs for six hours before being removed. RNAi plates were grown at room temperature until eggs grew into adults (2-3 days). Ten F1 young adult animals were scored for defecation cycle steps from each genotype as previously described (Thomas, 1990).

Behavioral Assay

Defecation

To determine enteric muscle contractions (Emc) per defecation cycle, animals were scored for a positive enteric muscle contraction following a posterior body contraction (Emc /Pboc). Each animal was observed for eleven cycles and fifteen animals were scored for each genotype. Animals were raised and scored at room temperature (22°C) on OP50 bacteria.

High-speed video

Contraction of the intestinal muscles occurs on a millisecond time scale. To observe contraction of the intestinal muscle, videos were recorded at 60 frames per second at

400X total magnification. The raw data was converted to an AVI file and slowed to 5 frames a second to manage the large size of these files. The videos were edited to capture the expulsion step for qualitative analysis.

Worm tracking

Worm movement was analyzed by filming *lgc-35(tm1444),* or *lgc-35(tm1444) oxEx1291,* or wild-type (N2) animals. Each genotype was raised and filmed at room temperature (22°C) on OP50 bacteria on standard NGM plates. Young adult worms were picked individually and placed briefly on an intermediate NGM plate until clear of residual bacteria. An individual animal was then placed on a test plate of room temperature NGM agar and allowed to move for one minute before filming. Each animal was filmed for a single 30-second duration. Worm movement was filmed using a Leica MS 5 microscope, a Prior Scientific OptiScan II moving stage and a CCD Firewire camera (Sony XCD-V60). Worm locomotion was analyzed using the Track-A-Worm software platform (Wang and Wang, 2013).

Aldicarb

We determined sensitivity to aldicarb, an acetylcholine esterase inhibitor, by measuring the onset of paralysis after exposure to 1 mM of aldicarb as previously described (Mahoney et al., 2006). Thirty worms were placed on an NGM plate treated with aldicarb and screened for paralysis. Conditions were repeated in triplicate.

Thrash Assay

Locomotor defects were quantified by counting the number of body thrashes in 100ml of liquid M9 media at room temperature for a 2-minute interval (Miller et al., 1996). Single animals were placed into an agarose coated well of a 96 well plate and allowed to

acclimate for 2 minutes prior to recording. Animals were recorded using a Leica IC80HD camera for 2 minutes. The total number of body bends was counted offline by slowing videos to one-quarter speed using ImageJ. A blinded scorer counted the total number of body bends and divided this number by two to yield a bodybend/minute count.

Spicule eversion and rescue

To determine if spicule eversion and retraction was functional, males were scored for functional spicules (spicules that could retract into the body after attempting to mate over time). Spicules that were permanently everted and were unable to retract into the body were scored as nonfunctional. Ten young adult males and hermaphrodites were fed on an OP50 plate for 24 hours. At 24 hours, a new group of ten virgin hermaphrodites were introduced and the older hermaphrodites were removed in order to increase mating attempts. At 48 hours, the males' spicules were scored for functionality. *him-8(e1489)* was the control strain and all genotypes were in a *him-8(e1489)* background to maintain males in the population.

Rescue of *lgc-35(tm14444)* II; *unc-49(e407)* III; *him-8(e1489)* IV mutants was achieved by injecting 15 ng/µL of pMJ54, 5 ng/µL of pTG96, and 80ng/µl EK1(*lin-15*+) into triple mutants animals generating the array *oxEx1328*.

Male mating

Male mating efficiency was assessed as previously described (Hodgkin, 1983). One young adult male was placed on a NGM plate seeded with HB101 with four young adult wild-type hermaphrodites. Males were removed at different time intervals (1, 3, 6, and 24 hours). At day three and four, plates were blinded for genotype and were

scored by eye for cross progeny. All male genotypes tested were in a *him-8(e1489)* background.

To determine if males could sire progeny over time 120 L4 *lgc-35(tm1444)* II; *him-8(e1489)* IV males and 120 L4 *him-5(e1490)* males were separated into populations of 20 worms per plate. Each day for 6 days, 20 adult males were tested for mating potency. Mating potency was measured by pairing a single male with a single 24-hour old virgin adult *pha-1(ts)* hermaphrodite on a plate containing a 10mm OP50 lawn. Mating plates were incubated at 20°C and scored after three days for the presence of at least one cross progeny.

Electrophysiology

LGC-35 cDNA isolation: To determine the full-length mRNA of *lgc-35*, wild-type poly-A+ selected RNA was subjected to reverse-transcription and polymerase chain reaction (RT-PCR). The 5' end of the gene was determined using circular RACE (Maruyama et al., 1995), and the 3' end of the gene was predicted by sequence analysis of the genome based on predictions that had homology to the fourth transmembrane domain of EXP-1. Full-length cDNAs were isolated by designing oligonucleotide primers to the 5' and 3' untranslated regions of Y46G5A.26. PCR products were cloned into the pCR2.1 TA cloning vector (Invitrogen) and cDNAs were sequenced to obtain full-length error-free clones (Applied Biosystems).

Xenopus oocyte expression: A SpeI /XhoI fragment containing the full-length *lgc-35* cDNA, including the 5' and 3' UTRs, was cloned into the SpeI/XhoI sites of pSGEM (courtesy of M. Hollmann), creating plasmid pAB08. Capped RNA was prepared using the T7 mMessage mMachine kit (Ambion). *Xenopus* oocytes were collected and

injected with 10 ng of cRNA and two-electrode voltage clamp recordings were performed 2-5 days post injection.

Dose-response and ion selectivity experiments: The standard bath solution for dose-response and control I-V experiments was Ringer's (in mM): 115 NaCl, 2.5 KCl, 1.8 $CaCl_2$, 10 HEPES (pH 7.2 NaOH). For dose-response experiments, each oocyte was subjected to a five-second application of GABA (1-1000 mM) with 2 minutes of wash between applications. Ion selectivity experiments and data analysis were performed as previously described (Beg and Jorgensen, 2003b). All recording were done at room temperature. We used 3M KCl-filled electrodes with a resistance between 1-3 MΩ. A 3M KCl agar bridge was used to minimize liquid junction potentials, and all liquid junction potentials arising at the tip of the recording electrode were corrected online.

Statistical Analysis

Statistical analyses were performed using GraphPad Prism 6. Two-tailed unpaired Student's t-tests were performed to determine the difference between two genotypes (p <0.05 was considered significant). One-way ANOVA with Tukey post-hoc test was used for comparison involving more than two groups. Data are reported as mean ± s.e.m. unless otherwise noted and all experiments were performed blind to the observer.

Acknowledgements

The work presented in this chapter was designed and completed by Meghan Jobson, Chris Valdez, Jann Gardner, L.Rene Garcia, Erik Jorgensen, and Asim Beg. Meghan Jobson, Chris Valdez, Jann Gardner, L.Rene Garcia, Erik Jorgensen, and Asim Beg analyzed the data presented in this chapter, and L.Rene Garcia and Erik Jorgensen contributed unpublished reagents/analytic tools. M. Wayne Davis and

Gunther Hollopeter provided expert technical assistance using the MosDEL technique; Rob Hobson for providing plasmids and reagents; Jonathan Delafield Butt for assisting with high-speed video analysis; Shawn Xu for the Pacr-2::mCherry plasmid; Rob Weymouth for providing *Xenopus* oocytes; Georgina Nicholl for cRNA preparation, oocyte injections, and preliminary data; and Patrick Mac for critical reading of the manuscript. Some strains were provided by the Caenorhabditis Genetics Center, which is funded by the National Institutes of Health Office of Research Infrastructure Programs (P40 OD010440). The *lgc-35(tm1444)* allele was provided by the Japan National BioResource Project, and the transposon insertion strain *lgc-35(ttTi13013)* was provided by the NemaGENETAG consortium. This work was supported by the Alfred P. Sloan Foundation, The Hartwell Foundation (to Asim Beg), and the National Institutes of Health (to Erik Jorgensen).

References

Alonso, A., and Hernán, M.A. (2008). Temporal trends in the incidence of multiple sclerosis A systematic review. Neurology *71*, 129-135.

Alonso-Nanclares, L., Gonzalez-Soriano, J., Rodriguez, J.R., and DeFelipe, J. (2008). Gender differences in human cortical synaptic density. Proceedings of the National Academy of Sciences *105*, 14615-14619.

Alvarez-Buylla, A., and García-Verdugo, J.M. (2002). Neurogenesis in adult subventricular zone. The Journal of neuroscience *22*, 629-634.

Amin, J., and Weiss, D.S. (1993). GABAA receptor needs two homologous domains of the & beta;-subunit for activation by GABA but not by pentobarbital.

Anagnostaras, S.G., Gale, G.D., and Fanselow, M.S. (2001). Hippocampus and contextual fear conditioning: recent controversies and advances. Hippocampus *11*, 8-17.

Antion, M.D., Christie, L.A., Bond, A.M., Dalva, M.B., and Contractor, A. (2010). Ephrin-B3 regulates glutamate receptor signaling at hippocampal synapses. Molecular and cellular neurosciences *45*, 378-388.

Aoki, K., Nakamura, T., and Matsuda, M. (2004). Spatio-temporal regulation of Rac1 and Cdc42 activity during nerve growth factor-induced neurite outgrowth in PC12 cells. Journal of Biological Chemistry *279*, 713-719.

Aoto, J., Ting, P., Maghsoodi, B., Xu, N., Henkemeyer, M., and Chen, L. (2007). Postsynaptic ephrinB3 promotes shaft glutamatergic synapse formation. The Journal of neuroscience *27*, 7508-7519.

Araque, A., Parpura, V., Sanzgiri, R.P., and Haydon, P.G. (1999). Tripartite synapses: glia, the unacknowledged partner. Trends in neurosciences *22*, 208-215.

Artola, A., and Singer, W. (1993). Long-term depression of excitatory synaptic transmission and its relationship to long-term potentiation. Trends in neurosciences *16*, 480-487.

Bacchelli, E., Blasi, F., Biondolillo, M., Lamb, J.A., Bonora, E., Barnby, G., Parr, J., Beyer, K.S., Klauck, S.M., and Poustka, A. (2003). Screening of nine candidate genes

for autism on chromosome 2q reveals rare nonsynonymous variants in the cAMP-GEFII gene. Molecular psychiatry *8*, 916-924.

Bai, Y., Xiang, X., Liang, C., and Shi, L. (2015). Regulating Rac in the Nervous System: Molecular Function and Disease Implication of Rac GEFs and GAPs. BioMed research international *2015*.

Bamber, B.A., Beg, A.A., Twyman, R.E., and Jorgensen, E.M. (1999a). The Caenorhabditis elegans unc-49 locus encodes multiple subunits of a heteromultimeric GABA receptor. The Journal of neuroscience *19*, 5348-5359.

Bamber, B.A., Beg, A.A., Twyman, R.E., and Jorgensen, E.M. (1999b). The Caenorhabditis elegans unc-49 locus encodes multiple subunits of a heteromultimeric GABA receptor. In The Journal of neuroscience : the official journal of the Society for Neuroscience, pp. 5348-5359.

Bashaw, G.J., and Klein, R. (2010). Signaling from axon guidance receptors. Cold Spring Harbor perspectives in biology *2*, a001941.

Beg, A.A., Ernstrom, G.G., Nix, P., Davis, M.W., and Jorgensen, E.M. (2008). Protons act as a transmitter for muscle contraction in C. elegans. Cell *132*, 149-160.

Beg, A.A., and Jorgensen, E.M. (2003a). EXP-1 is an excitatory GABA-gated cation channel. Nature neuroscience *6*, 1145-1152.

Beg, A.A., and Jorgensen, E.M. (2003b). EXP-1 is an excitatory GABA-gated cation channel. In Nature neuroscience, pp. 1145-1152.

Beg, A.A., Sommer, J.E., Martin, J.H., and Scheiffele, P. (2007). alpha2-Chimaerin is an essential EphA4 effector in the assembly of neuronal locomotor circuits. Neuron *55*, 768-778.

Bhatt, D.H., Zhang, S., and Gan, W.-B. (2009). Dendritic spine dynamics. Annu Rev Physiol *71*, 261-282.

Bloodgood, B.L., and Sabatini, B.L. (2005). Neuronal activity regulates diffusion across the neck of dendritic spines. Science *310*, 866-869.

Boileau, A.J., Evers, A.R., Davis, A.F., and Czajkowski, C. (1999). Mapping the Agonist Binding Site of the GABAAReceptor: Evidence for a β-Strand. The Journal of neuroscience *19*, 4847-4854.

Boileau, A.J., Newell, J.G., and Czajkowski, C. (2002). GABAA Receptor β2Tyr97 and Leu99 Line the GABA-binding Site INSIGHTS INTO MECHANISMS OF AGONIST AND ANTAGONIST ACTIONS. Journal of Biological Chemistry *277*, 2931-2937.

Borgius, L., Nishimaru, H., Caldeira, V., Kunugise, Y., Low, P., Reig, R., Itohara, S., Iwasato, T., and Kiehn, O. (2014). Spinal glutamatergic neurons defined by EphA4

signaling are essential components of normal locomotor circuits. The Journal of neuroscience : the official journal of the Society for Neuroscience *34*, 3841-3853.

Bos, J.L., Rehmann, H., and Wittinghofer, A. (2007). GEFs and GAPs: critical elements in the control of small G proteins. Cell *129*, 865-877.

Bourne, J.N., and Harris, K.M. (2008). Balancing structure and function at hippocampal dendritic spines. Annual review of neuroscience *31*, 47-67.

Bourne, J.N., and Harris, K.M. (2011). Coordination of size and number of excitatory and inhibitory synapses results in a balanced structural plasticity along mature hippocampal CA1 dendrites during LTP. Hippocampus *21*, 354-373.

Brown, M., Jacobs, T., Eickholt, B., Ferrari, G., Teo, M., Monfries, C., Qi, R.Z., Leung, T., Lim, L., and Hall, C. (2004). α2-Chimaerin, cyclin-dependent kinase 5/p35, and its target collapsin response mediator protein-2 are essential components in semaphorin 3A-induced growth-cone collapse. The Journal of neuroscience *24*, 8994-9004.

Buttery and Beg, P., Beg, A.A., Chih, B., Broder, A., Mason, C.A., and Scheiffele, P. (2006). The diacylglycerol-binding protein alpha1-chimaerin regulates dendritic morphology. Proceedings of the National Academy of Sciences of the United States of America *103*, 1924-1929.

Buttery, P., Beg, A.A., Chih, B., Broder, A., Mason, C.A., and Scheiffele, P. (2006). The diacylglycerol-binding protein alpha1-chimaerin regulates dendritic morphology. Proceedings of the National Academy of Sciences of the United States of America *103*, 1924-1929.

Caceres, A., Payne, M.R., Binder, L.I., and Steward, O. (1983). Immunocytochemical localization of actin and microtubule-associated protein MAP2 in dendritic spines. Proceedings of the National Academy of Sciences *80*, 1738-1742.

Cahill, M.E., Xie, Z., Day, M., Photowala, H., Barbolina, M.V., Miller, C.A., Weiss, C., Radulovic, J., Sweatt, J.D., and Disterhoft, J.F. (2009). Kalirin regulates cortical spine morphogenesis and disease-related behavioral phenotypes. Proceedings of the National Academy of Sciences *106*, 13058-13063.

Calo, L., Cinque, C., Patane, M., Schillaci, D., Battaglia, G., Melchiorri, D., Nicoletti, F., and Bruno, V. (2006). Interaction between ephrins/Eph receptors and excitatory amino acid receptors: possible relevance in the regulation of synaptic plasticity and in the pathophysiology of neuronal degeneration. Journal of neurochemistry *98*, 1-10.

Cameron, H.A., Woolley, C.S., McEwen, B.S., and Gould, E. (1993). Differentiation of newly born neurons and glia in the dentate gyrus of the adult rat. Neuroscience *56*, 337-344.

Canty, A.J., Greferath, U., Turnley, A.M., and Murphy, M. (2006). Eph tyrosine kinase receptor EphA4 is required for the topographic mapping of the corticospinal tract. Proceedings of the National Academy of Sciences *103*, 15629-15634.

Canty, A.J., and Murphy, M. (2008). Molecular mechanisms of axon guidance in the developing corticospinal tract. Progress in neurobiology *85*, 214-235.

Carlisle, H.J., and Kennedy, M.B. (2005). Spine architecture and synaptic plasticity. Trends in neurosciences *28*, 182-187.

Carmeliet, P., and Tessier-Lavigne, M. (2005). Common mechanisms of nerve and blood vessel wiring. Nature *436*, 193-200.

Catchpole, T., and Henkemeyer, M. (2011). EphB2 tyrosine kinase-dependent forward signaling in migration of neuronal progenitors that populate and form a distinct region of the dentate niche. The Journal of neuroscience : the official journal of the Society for Neuroscience *31*, 11472-11483.

Cazalets, J.-R., Borde, M., and Clarac, F. (1995). Localization and organization of the central pattern generator for hindlimb locomotion in newborn rat. The Journal of neuroscience *15*, 4943-4951.

Chan, W.-M., Miyake, N., Zhu-Tam, L., Andrews, C., and Engle, E.C. (2011). Two novel CHN1 mutations in 2 families with Duane retraction syndrome. Archives of ophthalmology *129*, 649-652.

Chen, B.L., Hall, D.H., and Chklovskii, D.B. (2006). Wiring optimization can relate neuronal structure and function. Proceedings of the National Academy of Sciences of the United States of America *103*, 4723-4728.

Chen, L.Y., Rex, C.S., Casale, M.S., Gall, C.M., and Lynch, G. (2007). Changes in synaptic morphology accompany actin signaling during LTP. The Journal of neuroscience : the official journal of the Society for Neuroscience *27*, 5363-5372.

Cherfils, J., and Zeghouf, M. (2013). Regulation of small GTPases by GEFs, GAPs, and GDIs. Physiological reviews *93*, 269-309.

Chumley, M.J., Catchpole, T., Silvany, R.E., Kernie, S.G., and Henkemeyer, M. (2007). EphB receptors regulate stem/progenitor cell proliferation, migration, and polarity during hippocampal neurogenesis. The Journal of neuroscience : the official journal of the Society for Neuroscience *27*, 13481-13490.

Cline, H.T. (2001). Dendritic arbor development and synaptogenesis. Current opinion in neurobiology *11*, 118-126.

Cohen, N.R., Taylor, J.S.H., Scott, L.B., Guillery, R.W., Soriano, P., and Furley, A.J.W. (1998). Errors in corticospinal axon guidance in mice lacking the neural cell adhesion molecule L1. Current Biology *8*, 26-33.

Coonan, J.R., Greferath, U., Messenger, J., Hartley, L., Murphy, M., Boyd, A.W., Dottori, M., Galea, M.P., and Bartlett, P.F. (2001). Development and reorganization of corticospinal projections in EphA4 deficient mice. Journal of Comparative Neurology *436*, 248-262.

Corringer, P.J., Bertrand, S., Galzi, J.L., Devillers-Thiery, A., Changeux, J.P., and Bertrand, D. (1999). Mutational analysis of the charge selectivity filter of the alpha7 nicotinic acetylcholine receptor. Neuron *22*, 831-843.

Croll, N.A. (1975). Behavioural analysis of nematode movement. Adv Parasitol *13*, 71-122.

Dailey, M.E., and Smith, S.J. (1996). The Dynamics of Dendritic Structure in Developing Hippocampal Slices. J Neurosci *12*, 2983-2994.

Dalva, M.B., Takasu, M.A., Lin, M.Z., Shamah, S.M., Hu, L., Gale, N.W., and Greenberg, M.E. (2000). EphB receptors interact with NMDA receptors and regulate excitatory synapse formation. Cell *103*, 945-956.

David, S., and Lacroix, S. (2003). Molecular approaches to spinal cord repair. Annual review of neuroscience *26*, 411-440.

Davidson, R.J. (2002). Anxiety and affective style: role of prefrontal cortex and amygdala. Biological psychiatry *51*, 68-80.

De Rubeis, S., He, X., Goldberg, A.P., Poultney, C.S., Samocha, K., Cicek, A.E., Kou, Y., Liu, L., Fromer, M., and Walker, S. (2014). Synaptic, transcriptional and chromatin genes disrupted in autism. Nature *515*, 209-215.

Deacon, R.M. (2006). Digging and marble burying in mice: simple methods for in vivo identification of biological impacts. NATURE PROTOCOLS-ELECTRONIC EDITION- *1*, 122.

Deng, W., Aimone, J.B., and Gage, F.H. (2010). New neurons and new memories: how does adult hippocampal neurogenesis affect learning and memory? Nature Reviews Neuroscience *11*, 339-350.

DeRespinis, P.A., Caputo, A.R., Wagner, R.S., and Guo, S. (1993). Duane's retraction syndrome. Survey of ophthalmology *38*, 257-288.

Dickson, B.J. (2002). Molecular mechanisms of axon guidance. Science *298*, 1959-1964.

Dobson, C.B., Villagra, F., Clowry, G.J., Smith, M., Kenwrick, S., Donnai, D., Miller, S., and Eyre, J.A. (2001). Abnormal corticospinal function but normal axonal guidance in human L1CAM mutations. Brain *124*, 2393-2406.

Dokmanovic, M., Hirsch, D.S., Shen, Y., and Wu, W.J. (2009). Rac1 contributes to trastuzumab resistance of breast cancer cells: Rac1 as a potential therapeutic target for the treatment of trastuzumab-resistant breast cancer. Molecular cancer therapeutics *8*, 1557-1569.

Donatelle, J.M. (1977). Growth of the corticospinal tract and the development of placing reactions in the postnatal rat. Journal of Comparative Neurology *175*, 207-231.

Dottori, M., Hartley, L., Galea, M., Paxinos, G., Polizzotto, M., Kilpatrick, T., Bartlett, P.F., Murphy, M., Köntgen, F., and Boyd, A.W. (1998). EphA4 (Sek1) receptor tyrosine kinase is required for the development of the corticospinal tract. Proceedings of the National Academy of Sciences *95*, 13248-13253.

Douglas, R.J., and Martin, K.A.C. (2004). Neuronal circuits of the neocortex. Annu Rev Neurosci *27*, 419-451.

Duman, J.G., Mulherkar, S., Tu, Y.-K., Cheng, J., and Tolias, K.F. (2015). Mechanisms for spatiotemporal regulation of Rho-GTPase signaling at synapses. Neuroscience letters.

Dumont, J.P.C., and Robertson, R.M. (1986). Neuronal circuits: an evolutionary perspective. Science *233*, 849-853.

Dunaevsky, A., Tashiro, A., Majewska, A., Mason, C., and Yuste, R. (1999). Developmental regulation of spine motility in the mammalian central nervous system. Proceedings of the National Academy of Sciences of the United States of America *96*, 13438-13443.

Durand, C.M., Perroy, J., Loll, F., Perrais, D., Fagni, L., Bourgeron, T., Montcouquiol, M., and Sans, N. (2011). SHANK3 mutations identified in autism lead to modification of dendritic spine morphology via an actin-dependent mechanism. Molecular psychiatry.

Eberhart, J., Barr, J., O'Connell, S., Flagg, A., Swartz, M.E., Cramer, K.S., Tosney, K.W., Pasquale, E.B., and Krull, C.E. (2004). Ephrin-A5 exerts positive or inhibitory effects on distinct subsets of EphA4-positive motor neurons. The Journal of neuroscience *24*, 1070-1078.

Ebert, D.H., and Greenberg, M.E. (2013). Activity-dependent neuronal signalling and autism spectrum disorder. Nature *493*, 327-337.

Eccles, J.C., Fatt, P., and Koketsu, K. (1954). Cholinergic and inhibitory synapses in a pathway from motor-axon collaterals to motoneurones. J Physiol *126*, 524-562.

Eichenbaum, H., Dudchenko, P., Wood, E., Shapiro, M., and Tanila, H. (1999). The hippocampus, memory, and place cells: is it spatial memory or a memory space? Neuron *23*, 209-226.

Endl, E., and Gerdes, J. (2000). The Ki-67 protein: fascinating forms and an unknown function. Experimental cell research *257*, 231-237.

Engle, E.C. (2010). Human genetic disorders of axon guidance. Cold Spring Harbor perspectives in biology *2*, a001784.

Eriksson, P.S., Perfilieva, E., Björk-Eriksson, T., Alborn, A.-M., Nordborg, C., Peterson, D.A., and Gage, F.H. (1998). Neurogenesis in the adult human hippocampus. Nature medicine *4*, 1313-1317.

Ethell, I.M., and Pasquale, E.B. (2005). Molecular mechanisms of dendritic spine development and remodeling. Progress in neurobiology *75*, 161-205.

Etienne-Manneville, S., and Hall, A. (2002). Rho GTPases in cell biology. Nature *420*, 629-635.

Evarts, E.V. (1981). Role of motor cortex in voluntary movements in primates. Comprehensive Physiology.

Feng, G., Mellor, R.H., Bernstein, M., Keller-Peck, C., Nguyen, Q.T., Wallace, M., Nerbonne, J.M., Lichtman, J.W., and Sanes, J.R. (2000). Imaging neuronal subsets in transgenic mice expressing multiple spectral variants of GFP. Neuron *28*, 41-51.

Ferguson, B., Matyszak, M.K., Esiri, M.M., and Perry, V.H. (1997). Axonal damage in acute multiple sclerosis lesions. Brain *120*, 393-399.

Fiala, J.C., Feinberg, M., Popov, V., and Harris, K.M. (1998). Synaptogenesis via dendritic filopodia in developing hippocampal area CA1. The Journal of neuroscience : the official journal of the Society for Neuroscience *18*, 8900-8911.

Fiala, J.C., Spacek, J., and Harris, K.M. (2002). Dendritic spine pathology: cause or consequence of neurological disorders? Brain Res Brain Res Rev *39*, 29-54.

Filosa, A., Paixao, S., Honsek, S.D., Carmona, M.A., Becker, L., Feddersen, B., Gaitanos, L., Rudhard, Y., Schoepfer, R., Klopstock, T.*, et al.* (2009). Neuron-glia communication via EphA4/ephrin-A3 modulates LTP through glial glutamate transport. Nature neuroscience *12*, 1285-1292.

Finger, J.H., Bronson, R.T., Harris, B., Johnson, K., Przyborski, S.A., and Ackerman, S.L. (2002). The netrin 1 receptors Unc5h3 and Dcc are necessary at multiple choice points for the guidance of corticospinal tract axons. The Journal of neuroscience *22*, 10346-10356.

Fischer, M., Kaech, S., Knutti, D., and Matus, A. (1998). Rapid actin-based plasticity in dendritic spines. Neuron *20*, 847-854.

Fischer, M., Kaech, S., Wagner, U., Brinkhaus, H., and Matus, A. (2000). Glutamate receptors regulate actin-based plasticity in dendritic spines. Nature neuroscience *3*, 887-894.

Franklin, R.J.M. (2002). Why does remyelination fail in multiple sclerosis? Nature Reviews Neuroscience *3*, 705-714.

Frøkjær-Jensen, C., Davis, M.W., Hollopeter, G., Taylor, J., Harris, T.W., Nix, P., Lofgren, R., Prestgard-Duke, M., Bastiani, M., Moerman, D.G.*, et al.* (2010). Targeted gene deletions in C. elegans using transposon excision. In Nature methods.

Fu, A.K., Hung, K.W., Fu, W.Y., Shen, C., Chen, Y., Xia, J., Lai, K.O., and Ip, N.Y. (2011). APC(Cdh1) mediates EphA4-dependent downregulation of AMPA receptors in homeostatic plasticity. Nature neuroscience *14*, 181-189.

Gage, F.H. (2002). Neurogenesis in the adult brain. The Journal of Neuroscience *22*, 612-613.

Gale, N.W., Holland, S.J., Valenzuela, D.M., Flenniken, A., Pan, L., Ryan, T.E., Henkemeyer, M., Strebhardt, K., Hirai, H., and Wilkinson, D.G. (1996). Eph receptors and ligands comprise two major specificity subclasses and are reciprocally compartmentalized during embryogenesis. Neuron *17*, 9-19.

Galzi, J.L., Devillers-Thiery, A., Hussy, N., Bertrand, S., Changeux, J.P., and Bertrand, D. (1992). Mutations in the channel domain of a neuronal nicotinic receptor convert ion selectivity from cationic to anionic. Nature *359*, 500-505.

Garcia, L.R., Mehta, P., and Sternberg, P.W. (2001). Regulation of distinct muscle behaviors controls the C. elegans male's copulatory spicules during mating. In Cell, pp. 777-788.

Garcia, L.R., and Sternberg, P.W. (2003). Caenorhabditis elegans UNC-103 ERG-like potassium channel regulates contractile behaviors of sex muscles in males before and during mating. The Journal of neuroscience : the official journal of the Society for Neuroscience *23*, 2696-2705.

Gerlai, R. (2001). Eph receptors and neural plasticity. Nature reviews Neuroscience *2*, 205-209.

Goodman, C.S., and Shatz, C.J. (1993). Developmental mechanisms that generate precise patterns of neuronal connectivity. Cell *72*, 77-98.

Goodman, C.S., and Tessier-Lavigne, M. (1997). Molecular mechanisms of axon guidance and target recognition. Molecular and cellular approaches to neural development, 108-178.

Gossler, A., Joyner, A.L., Rossant, J., and Skarnes, W.C. (1989). Mouse embryonic stem cells and reporter constructs to detect developmentally regulated genes. Science *244*, 463-465.

Govek, E.-E., Newey, S.E., and Van Aelst, L. (2005). The role of the Rho GTPases in neuronal development. Genes & development *19*, 1-49.

Gray, E.G. (1959). Electron microscopy of synaptic contacts on dendrite spines of the cerebral cortex. Nature *183*, 1592-1593.

Guan, K.-L., and Rao, Y. (2003). Signalling mechanisms mediating neuronal responses to guidance cues. Nature Reviews Neuroscience *4*, 941-956.

Gunthorpe, M.J., and Lummis, S.C. (2001). Conversion of the ion selectivity of the 5-HT(3a) receptor from cationic to anionic reveals a conserved feature of the ligand-gated ion channel superfamily. The Journal of biological chemistry *276*, 10977-10983.

Hall, A. (1998). Rho GTPases and the actin cytoskeleton. Science *279*, 509-514.

Hall, C., Michael, G.J., Cann, N., Ferrari, G., Teo, M., Jacobs, T., Monfries, C., and Lim, L. (2001). α2-chimaerin, a Cdc42/Rac1 regulator, is selectively expressed in the rat embryonic nervous system and is involved in neuritogenesis in N1E-115 neuroblastoma cells. The Journal of Neuroscience *21*, 5191-5202.

Hall, C., Monfries, C., Smith, P., Lim, H.H., Kozma, R., Ahmed, S., Vanniasingham, V., Leung, T., and Lim, L. (1990). Novel human brain cDNA encoding a 34,000 M r protein n-chimaerin, related to both the regulatory domain of protein kinase C and BCR, the product of the breakpoint cluster region gene. Journal of molecular biology *211*, 11-16.

Hall, C., Sin, W.C., Teo, M., Michael, G.J., Smith, P., Dong, J.M., Lim, H.H., Manser, E., Spurr, N.K., and Jones, T.A. (1993). Alpha 2-chimerin, an SH2-containing GTPase-activating protein for the ras-related protein p21rac derived by alternate splicing of the human n-chimerin gene, is selectively expressed in brain regions and testes. Molecular and cellular biology *13*, 4986-4998.

Handley, S.L. (1991). Evaluation of marble-burying behavior as a model of anxiety. Pharmacology Biochemistry and Behavior *38*, 63-67.

Harris, K.M. (1999). Structure, development, and plasticity of dendritic spines. Current opinion in neurobiology *9*, 343-348.

Harris, K.M., F.E., J., and B., T. (1992). Three-Dimensional Structure of Dendritic Spines and Synapses in Rat Hippocampus (CAI) at Postnatal Day 15 and Adult Ages: Implications for the Maturation of Synaptic Physiology and Long-term Potentiation. The Journal of neuroscience : the official journal of the Society for Neuroscience *12*, 2685-2705.

Heasman, S.J., and Ridley, A.J. (2008). Mammalian Rho GTPases: new insights into their functions from in vivo studies. Nature reviews Molecular cell biology *9*, 690-701.

Hebb, D.O. (1949). The organization of behavior (New York: Wiley).

Hell, J.W., and Ehlers, M.D. (2008). Structural and functional organization of the synapse (Springer Science & Business Media).

Henderson, J.T., Georgiou, J., Jia, Z., Robertson, J., Elowe, S., Roder, J.C., and Pawson, T. (2001). The receptor tyrosine kinase EphB2 regulates NMDA-dependent synaptic function. Neuron *32*, 1041-1056.

Henkemeyer, M., Itkis, O.S., Ngo, M., Hickmott, P.W., and Ethell, I.M. (2003). Multiple EphB receptor tyrosine kinases shape dendritic spines in the hippocampus. The Journal of cell biology *163*, 1313-1326.

Herrera, R., and Shivers, B.D. (1994). Expression of α1‐chimaerin (rac‐1 GAP) alters the cytoskeletal and adhesive properties of fibroblasts. Journal of cellular biochemistry *56*, 582-591.

Hnasko, T.S., and Edwards, R.H. (2012). Neurotransmitter corelease: mechanism and physiological role. Annu Rev Physiol *74*, 225-243.

Hodgkin, J. (1983). Male Phenotypes and Mating Efficiency in CAENORHABDITIS ELEGANS. In Genetics, pp. 43-64.

Holder, N., Cooke, J., and Brennan, C. (1998). MINI‐REVIEW The Eph receptor tyrosine kinases and the ephrins–roles in nervous system development. European Journal of Neuroscience *10*, 405-408.

Hollyday, M., and Hamburger, V. (1977). An autoradiographic study of the formation of the lateral motor column in the chick embryo. Brain research *132*, 197-208.

Honkura, N., Matsuzaki, M., Noguchi, J., Ellis-Davies, G.C.R., and Kasai, H. (2008). The subspine organization of actin fibers regulates the structure and plasticity of dendritic spines. Neuron *57*, 719-729.

Hotchkiss, M.G., Miller, N.R., Clark, A.W., and Green, W.R. (1980). Bilateral Duane's retraction syndrome: a clinical-pathologic case report. Archives of ophthalmology *98*, 870-874.

Huang, G.J., Bannerman, D., and Flint, J. (2008). Chronic fluoxetine treatment alters behavior, but not adult hippocampal neurogenesis, in BALB/cJ mice. Molecular psychiatry *13*, 119-121.

Huber, A.B., Kolodkin, A.L., Ginty, D.D., and Cloutier, J.-F. (2003). Signaling at the growth cone: ligand-receptor complexes and the control of axon growth and guidance. Annual review of neuroscience *26*, 509-563.

IMGSAC, I.M.G.S.o.A.C. (2001). A Genomewide Screen for Autism: Strong Evidence for Linkage to Chromosomes 2q, 7q, and 16p. American Journal of Human Genetics *69*, 570-581.

Imoto, K., Busch, C., Sakmann, B., Mishina, M., Konno, T., Nakai, J., Bujo, H., Mori, Y., Fukuda, K., and Numa, S. (1988). Rings of negatively charged amino acids determine the acetylcholine receptor channel conductance. Nature *335*, 645-648.

Ito, M. (1989). Long-term depression. Annual review of neuroscience *12*, 85-102.

Iwasato, T., Katoh, H., Nishimaru, H., Ishikawa, Y., Inoue, H., Saito, Y.M., Ando, R., Iwama, M., Takahashi, R., and Negishi, M. (2007). Rac-GAP α-chimerin regulates motor-circuit formation as a key mediator of EphrinB3/EphA4 forward signaling. Cell *130*, 742-753.

Iwata, R., Matsukawa, H., Yasuda, K., Mizuno, H., Itohara, S., and Iwasato, T. (2015). Developmental RacGAP α2-Chimaerin Signaling Is a Determinant of the Morphological Features of Dendritic Spines in Adulthood. The Journal of Neuroscience *35*, 13728-13744.

Iwata, R., Ohi, K., Kobayashi, Y., Masuda, A., Iwama, M., Yasuda, Y., Yamamori, H., Tanaka, M., Hashimoto, R., Itohara, S.*, et al.* (2014). RacGAP α2-Chimaerin Function in Development Adjusts Cognitive Ability in Adulthood. Cell Reports *8*, 1257-1264.

Izquierdo, I., and Medina, J.H. (1997). Memory formation: the sequence of biochemical events in the hippocampus and its connection to activity in other brain structures. Neurobiology of learning and memory *68*, 285-316.

Jackman, N., Ishii, A., and Bansal, R. (2009). Oligodendrocyte development and myelin biogenesis: parsing out the roles of glycosphingolipids. Physiology *24*, 290-297.

Jakeman, L.B., Chen, Y., Lucin, K.M., and McTigue, D.M. (2006). Mice lacking L1 cell adhesion molecule have deficits in locomotion and exhibit enhanced corticospinal tract sprouting following mild contusion injury to the spinal cord. European Journal of Neuroscience *23*, 1997-2011.

Jarrell, T.A., Wang, Y., Bloniarz, A.E., Brittin, C.A., Xu, M., Thomson, J.N., Albertson, D.G., Hall, D.H., and Emmons, S.W. (2012). The connectome of a decision-making neural network. Science *337*, 437-444.

Jensen, M.L., Pedersen, L.N., Timmermann, D.B., Schousboe, A., and Ahring, P.K. (2005a). Mutational studies using a cation-conducting GABAA receptor reveal the selectivity determinants of the Cys-loop family of ligand-gated ion channels. Journal of neurochemistry *92*, 962-972.

Jensen, M.L., Schousboe, A., and Ahring, P.K. (2005b). Charge selectivity of the Cys-loop family of ligand-gated ion channels. Journal of neurochemistry *92*, 217-225.

Jensen, M.L., Timmermann, D.B., Johansen, T.H., Schousboe, A., Varming, T., and Ahring, P.K. (2002). The beta subunit determines the ion selectivity of the GABAA receptor. The Journal of biological chemistry *277*, 41438-41447.

Jiao, J.-w., Feldheim, D.A., and Chen, D.F. (2008). Ephrins as negative regulators of adult neurogenesis in diverse regions of the central nervous system. Proceedings of the National Academy of Sciences *105*, 8778-8783.

Jin, Y., Jorgensen, E., Hartwieg, E., and Horvitz, H.R. (1999). The Caenorhabditis elegans gene unc-25 encodes glutamic acid decarboxylase and is required for synaptic transmission but not synaptic development. In The Journal of neuroscience : the official journal of the Society for Neuroscience, pp. 539-548.

Jobson and Valdez, M.A., Valdez, C.M., Gardner, J., Garcia, L.R., Jorgensen, E.M., and Beg, A.A. (2015). Spillover Transmission Is Mediated by the Excitatory GABA Receptor LGC-35 in C. elegans. The Journal of Neuroscience *35*, 2803-2816.

Jones, A.K., and Sattelle, D.B. (2008). The cys-loop ligand-gated ion channel gene superfamily of the nematode, Caenorhabditis elegans. In Invert Neurosci, pp. 41-47.

Jospin, M., Qi, Y.B., Stawicki, T.M., Boulin, T., Schuske, K.R., Horvitz, H.R., Bessereau, J.-L., Jorgensen, E.M., and Jin, Y. (2009). A neuronal acetylcholine receptor regulates the balance of muscle excitation and inhibition in Caenorhabditis elegans. In PLoS Biol, pp. e1000265.

Kaech, S., and Banker, G. (2006). Culturing hippocampal neurons. Nature protocols *1*, 2406-2415.

Kamai, T., Yamanishi, T., Shirataki, H., Takagi, K., Asami, H., Ito, Y., and Yoshida, K.-I. (2004). Overexpression of RhoA, Rac1, and Cdc42 GTPases is associated with progression in testicular cancer. Clinical cancer research *10*, 4799-4805.

Kamath, R.S., Fraser, A.G., Dong, Y., Poulin, G., Durbin, R., Gotta, M., Kanapin, A., Le Bot, N., Moreno, S., Sohrmann, M.*, et al.* (2003). Systematic functional analysis of the Caenorhabditis elegans genome using RNAi. Nature *421*, 231-237.

Kao, T.-J., Law, C., and Kania, A. Eph and ephrin signaling: lessons learned from spinal motor neurons (Elsevier).

Kao, T.-J., Nicholl, G.C.B., Johansen, J.A., Kania, A., and Beg, A.A. (2015). α2-Chimaerin Is Required for Eph Receptor-Class-Specific Spinal Motor Axon Guidance and Coordinate Activation of Antagonistic Muscles. The Journal of Neuroscience *35*, 2344-2357.

Katz, L.C., and Shatz, C.J. (1996). Synaptic activity and the construction of cortical circuits. Science *274*, 1133-1138.

Kayser, M.S., Nolt, M.J., and Dalva, M.B. (2008). EphB receptors couple dendritic filopodia motility to synapse formation. Neuron *59*, 56-69.

Kee, N., Sivalingam, S., Boonstra, R., and Wojtowicz, J.M. (2002). The utility of Ki-67 and BrdU as proliferative markers of adult neurogenesis. Journal of neuroscience methods *115*, 97-105.

Kennedy, M.B., Beale, H.C., Carlisle, H.J., and Washburn, L.R. (2005). Integration of biochemical signalling in spines. Nature reviews Neuroscience *6*, 423-434.

Keramidas, A., Moorhouse, A.J., French, C.R., Schofield, P.R., and Barry, P.H. (2000). M2 Pore Mutations Convert the Glycine Receptor Channel from Being Anion- to Cation-Selective. In Biophysical Journal, pp. 247-259.

Keramidas, A., Moorhouse, A.J., Pierce, K.D., Schofield, P.R., and Barry, P.H. (2002). Cation-selective mutations in the M2 domain of the inhibitory glycine receptor channel reveal determinants of ion-charge selectivity. J Gen Physiol *119*, 393-410.

Khodosevich, K., Watanabe, Y., and Monyer, H. (2011). EphA4 preserves postnatal and adult neural stem cells in an undifferentiated state in vivo. Journal of cell science *124*, 1268-1279.

Klein, R. (2004). Eph/ephrin signaling in morphogenesis, neural development and plasticity. Current opinion in cell biology *16*, 580-589.

Koleske, A.J. (2013). Molecular mechanisms of dendrite stability. Nature Reviews Neuroscience *14*, 536-550.

Korobova, F., and Svitkina, T. (2010). Molecular architecture of synaptic actin cytoskeleton in hippocampal neurons reveals a mechanism of dendritic spine morphogenesis. Mol Biol Cell *21*, 165-176.

Kuhlmann, T., Miron, V., Cuo, Q., Wegner, C., Antel, J., and Brück, W. (2008). Differentiation block of oligodendroglial progenitor cells as a cause for remyelination failure in chronic multiple sclerosis. Brain *131*, 1749-1758.

Kullander, K., Croll, S.D., Zimmer, M., Pan, L., McClain, J., Hughes, V., Zabski, S., DeChiara, T.M., Klein, R., and Yancopoulos, G.D. (2001). Ephrin-B3 is the midline barrier that prevents corticospinal tract axons from recrossing, allowing for unilateral motor control. Genes & development *15*, 877-888.

Kullander, K., and Klein, R. (2002). Mechanisms and functions of Eph and ephrin signalling. Nature reviews Molecular cell biology *3*, 475-486.

Lagace, D.C., Whitman, M.C., Noonan, M.A., Ables, J.L., DeCarolis, N.A., Arguello, A.A., Donovan, M.H., Fischer, S.J., Farnbauch, L.A., and Beech, R.D. (2007). Dynamic contribution of nestin-expressing stem cells to adult neurogenesis. The Journal of neuroscience *27*, 12623-12629.

Lanuza, G.M., Gosgnach, S., Pierani, A., Jessell, T.M., and Goulding, M. (2004). Genetic identification of spinal interneurons that coordinate left-right locomotor activity necessary for walking movements. Neuron *42*, 375-386.

Lee, S., Kim, K., and Zhou, Z.J. (2010). Role of ACh-GABA cotransmission in detecting image motion and motion direction. Neuron *68*, 1159-1172.

Liang, X., Draghi, N.A., and Resh, M.D. (2004). Signaling from integrins to Fyn to Rho family GTPases regulates morphologic differentiation of oligodendrocytes. The Journal of neuroscience *24*, 7140-7149.

Lim, H.H., Michael, G.J., Smith, P., Lim, L., and Hall, C. (1992). Developmental regulation and neuronal expression of the mRNA of rat n-chimaerin, a p21rac GAP: cDNA sequence. Biochem J *287*, 415-422.

Liu, D.W., and Thomas, J.H. (1994). Regulation of a periodic motor program in C. elegans. In The Journal of neuroscience : the official journal of the Society for Neuroscience, pp. 1953-1962.

Liu, K.S., and Sternberg, P.W. (1995). Sensory regulation of male mating behavior in Caenorhabditis elegans. In Neuron, pp. 79-89.

Liu, Y., LeBeouf, B., Guo, X., Correa, P.A., Gualberto, D.G., Lints, R., and Garcia, L.R. (2011). A cholinergic-regulated circuit coordinates the maintenance and bi-stable states of a sensory-motor behavior during Caenorhabditis elegans male copulation. PLoS Genet *7*, e1001326.

Longair, M.H., Baker, D.A., and Armstrong, J.D. (2011). Simple Neurite Tracer: open source software for reconstruction, visualization and analysis of neuronal processes. Bioinformatics *27*, 2453-2454.

Luo, L. (2000). Rho GTPases in neuronal morphogenesis. Nature reviews Neuroscience *1*, 173-180.

Ma, X.-M., Kiraly, D.D., Gaier, E.D., Wang, Y., Kim, E.-J., Levine, E.S., Eipper, B.A., and Mains, R.E. (2008). Kalirin-7 is required for synaptic structure and function. The Journal of Neuroscience *28*, 12368-12382.

Machacek, M., Hodgson, L., Welch, C., Elliott, H., Pertz, O., Nalbant, P., Abell, A., Johnson, G.L., Hahn, K.M., and Danuser, G. (2009). Coordination of Rho GTPase activities during cell protrusion. Nature *461*, 99-103.

Mahoney, T.R., Luo, S., and Nonet, M.L. (2006). Analysis of synaptic transmission in Caenorhabditis elegans using an aldicarb-sensitivity assay. In Nature protocols, pp. 1772-1777.

Maletic-Savatic, M., Malinow, R., and Svoboda, K. (1999). Rapid dendritic morphogenesis in CA1 hippocampal dendrites induced by synaptic activity. Science *283*, 1923-1927.

Maren, S. (2001). Neurobiology of Pavlovian fear conditioning. Annual review of neuroscience *24*, 897-931.

Marland, J.R.K., Pan, D., and Buttery, P.C. (2011). Rac GTPase-activating protein (Rac GAP) α1-Chimaerin undergoes proteasomal degradation and is stabilized by diacylglycerol signaling in neurons. Journal of Biological Chemistry *286*, 199-207.

Martinez, L.A., and Tejada-Simon, M.V. (2011). Pharmacological inactivation of the small GTPase Rac1 impairs long-term plasticity in the mouse hippocampus. Neuropharmacology *61*, 305-312.

Maruyama, I.N., Rakow, T.L., and Maruyama, H.I. (1995). cRACE: a simple method for identification of the 5' end of mRNAs. Nucleic Acids Res *23*, 3796-3797.

Matsuzaki, M., Ellis-Davies, G.C., Nemoto, T., Miyashita, Y., Iino, M., and Kasai, H. (2001). Dendritic spine geometry is critical for AMPA receptor expression in hippocampal CA1 pyramidal neurons. Nature neuroscience *4*, 1086-1092.

Matus, A. (2000). Actin-based plasticity in dendritic spines. Science *290*, 754-758.

McAllister, A.K. (2000). Cellular and molecular mechanisms of dendrite growth. Cerebral cortex *10*, 963-973.

McEchron, M.D., Bouwmeester, H., Tseng, W., Weiss, C., and Disterhoft, J.F. (1998). Hippocampectomy disrupts auditory trace fear conditioning and contextual fear conditioning in the rat. Hippocampus *8*, 638-646.

McIntire, S.L., Jorgensen, E., and Horvitz, H.R. (1993a). Genes required for GABA function in Caenorhabditis elegans. In Nature, pp. 334-337.

McIntire, S.L., Jorgensen, E., Kaplan, J., and Horvitz, H.R. (1993b). The GABAergic nervous system of Caenorhabditis elegans. In Nature, pp. 337-341.

Meijering, E. (2010). Neuron tracing in perspective. Cytometry Part A *77A*, 693-704.

Mello, C.C., Kramer, J.M., Stinchcomb, D., and Ambros, V. (1991). Efficient gene transfer in C.elegans: extrachromosomal maintenance and integration of transforming sequences. Embo J *10*, 3959-3970.

Michaelson, D., Abidi, W., Guardavaccaro, D., Zhou, M., Ahearn, I., Pagano, M., and Philips, M.R. (2008). Rac1 accumulates in the nucleus during the G2 phase of the cell cycle and promotes cell division. The Journal of cell biology *181*, 485-496.

Micheva, K.D., Busse, B., Weiler, N.C., O'Rourke, N., and Smith, S.J. (2010). Single-synapse analysis of a diverse synapse population: proteomic imaging methods and markers. Neuron *68*, 639-653.

Miller, K.G., Alfonso, A., Nguyen, M., Crowell, J.A., Johnson, C.D., and Rand, J.B. (1996). A genetic selection for Caenorhabditis elegans synaptic transmission mutants. Proceedings of the National Academy of Sciences of the United States of America *93*, 12593-12598.

Ming, G.-l., and Song, H. (2011). Adult neurogenesis in the mammalian brain: significant answers and significant questions. Neuron *70*, 687-702.

Miyake, N., Chilton, J., Psatha, M., Cheng, L., Andrews, C., Chan, W.-M., Law, K., Crosier, M., Lindsay, S., and Cheung, M. (2008). Human CHN1 mutations hyperactivate α2-chimaerin and cause Duane's retraction syndrome. Science *321*, 839-843.

Mizuno, T., Yamashita, T., and Tohyama, M. (2004). Chimaerins act downstream from neurotrophins in overcoming the inhibition of neurite outgrowth produced by myelin‐associated glycoprotein. Journal of neurochemistry *91*, 395-403.

Mori, T., Buffo, A., and Götz, M. (2005). The novel roles of glial cells revisited: the contribution of radial glia and astrocytes to neurogenesis. Current topics in developmental biology *69*, 67-99.

Mulkey, R.M., and Malenka, R.C. (1992). Mechanisms underlying induction of homosynaptic long-term depression in area CA1 of the hippocampus. Neuron *9*, 967-975.

Mullen, G.P., Mathews, E.A., Saxena, P., Fields, S.D., McManus, J.R., Moulder, G., Barstead, R.J., Quick, M.W., and Rand, J.B. (2006). The Caenorhabditis elegans snf-11 gene encodes a sodium-dependent GABA transporter required for clearance of synaptic GABA. Mol Biol Cell *17*, 3021-3030.

Murai, K.K., Nguyen, L.N., Irie, F., Yamaguchi, Y., and Pasquale, E.B. (2003). Control of hippocampal dendritic spine morphology through ephrin-A3/EphA4 signaling. Nature neuroscience *6*, 153-160.

Nakamura, F., Kalb, R.G., and Strittmatter, S.M. (2000). Molecular basis of semaphorin-mediated axon guidance. Journal of neurobiology *44*, 219-229.

Nakayama, A.Y., Harms, M.B., and Luo, L. (2000). Small GTPases Rac and Rho in the maintenance of dendritic spines and branches in hippocampal pyramidal neurons. The Journal of neuroscience : the official journal of the Society for Neuroscience *20*, 5329-5338.

Niell, C.M., Meyer, M.P., and Smith, S.J. (2004). In vivo imaging of synapse formation on a growing dendritic arbor. Nature neuroscience *7*, 254-260.

Nielsen, J.A., Maric, D., Lau, P., Barker, J.L., and Hudson, L.D. (2006). Identification of a novel oligodendrocyte cell adhesion protein using gene expression profiling. The Journal of neuroscience *26*, 9881-9891.

Nishiyama, H., and Linden, D.J. (2007). Pure spillover transmission between neurons. Nature neuroscience *10*, 675-677.

Nobes, C.D., and Hall, A. (1995). Rho, rac, and cdc42 GTPases regulate the assembly of multimolecular focal complexes associated with actin stress fibers, lamellipodia, and filopodia. Cell *81*, 53-62.

Noguchi, J., Matsuzaki, M., Ellis-Davies, G.C.R., and Kasai, H. (2005). Spine-neck geometry determines NMDA receptor-dependent Ca 2+ signaling in dendrites. Neuron *46*, 609-622.

Nudo, R.J., and Masterton, R.B. (1990). Descending pathways to the spinal cord, III: Sites of origin of the corticospinal tract. The Journal of comparative neurology *296*, 559-583.

Nugent, A.A., Kolpak, A.L., and Engle, E.C. (2012). Human disorders of axon guidance. Current opinion in neurobiology *22*, 837-843.

Oh, D., Han, S., Seo, J., Lee, J.R., Choi, J., Groffen, J., Kim, K., Cho, Y.S., Choi, H.S., Shin, H.*, et al.* (2010). Regulation of synaptic Rac1 activity, long-term potentiation maintenance, and learning and memory by BCR and ABR Rac GTPase-activating proteins. The Journal of neuroscience : the official journal of the Society for Neuroscience *30*, 14134-14144.

Okabe, S., Miwa, A., and Okado, H. (2001). Spine formation and correlated assembly of presynaptic and postsynaptic molecules. The Journal of neuroscience : the official journal of the Society for Neuroscience *21*, 6105-6114.

Pasquale, E.B. (2008). Eph-ephrin bidirectional signaling in physiology and disease. Cell *133*, 38-52.

Peden, A.S., Mac, P., Fei, Y.-J., Castro, C., Jiang, G., Murfitt, K.J., Miska, E.A., Griffin, J.L., Ganapathy, V., and Jorgensen, E.M. (2013). Betaine acts on a ligand-gated ion channel in the nervous system of the nematode C. elegans. Nature neuroscience *16*, 1794-1801.

Penzes, P., Beeser, A., Chernoff, J., Schiller, M.R., Eipper, B.A., Mains, R.E., and Huganir, R.L. (2003). Rapid induction of dendritic spine morphogenesis by trans-synaptic ephrinB-EphB receptor activation of the Rho-GEF kalirin. Neuron *37*, 263-274.

Penzes, P., Cahill, M.E., Jones, K.A., VanLeeuwen, J.E., and Woolfrey, K.M. (2011). Dendritic spine pathology in neuropsychiatric disorders. Nature neuroscience *14*, 285-293.

Penzes, P., and Jones, K.A. (2008). Dendritic spine dynamics–a key role for kalirin-7. Trends in neurosciences *31*, 419-427.

Petrak, L.J., Harris, K.M., and Kirov, S.A. (2005). Synaptogenesis on mature hippocampal dendrites occurs via filopodia and immature spines during blocked synaptic transmission. Journal of Comparative Neurology *484*, 183-190.

Pirri, J.K., McPherson, A.D., Donnelly, J.L., Francis, M.M., and Alkema, M.J. (2009). A tyramine-gated chloride channel coordinates distinct motor programs of a Caenorhabditis elegans escape response. Neuron *62*, 526-538.

Porter, R., and Lemon, R. (1993). Corticospinal function and voluntary movement (Oxford University Press, USA).

Portera-Cailliau, C., Pan, D.T., and Yuste, R. (2003). Activity-regulated dynamic behavior of early dendritic protrusions: Evidence for different types of dendritic filopodia. Journal of Neuroscience *23*, 7129-7142.

Putrenko, I., Zakikhani, M., and Dent, J.A. (2005). A family of acetylcholine-gated chloride channel subunits in Caenorhabditis elegans. Journal of Biological Chemistry *280*, 6392-6398.

Ramakers, G.J.A. (2002). Rho proteins, mental retardation and the cellular basis of cognition. Trends in neurosciences *25*, 191-199.

Ranganathan, R., Cannon, S.C., and Horvitz, H.R. (2000). MOD-1 is a serotonin-gated chloride channel that modulates locomotory behaviour in C. elegans. Nature *408*, 470-475.

Raynaud, F., Janossy, A., Dahl, J., Bertaso, F., Perroy, J., Varrault, A., Vidal, M., Worley, P.F., Boeckers, T.M., and Bockaert, J. (2013). Shank3-Rich2 interaction regulates AMPA receptor recycling and synaptic long-term potentiation. The Journal of Neuroscience *33*, 9699-9715.

Reiner, D.J., and Thomas, J.H. (1995). Reversal of a muscle response to GABA during C. elegans male development. The Journal of neuroscience : the official journal of the Society for Neuroscience *15*, 6094-6102.

Revest, J.M., Dupret, D., Koehl, M., Funk-Reiter, C., Grosjean, N., Piazza, P.V., and Abrous, D.N. (2009). Adult hippocampal neurogenesis is involved in anxiety-related behaviors. Molecular psychiatry *14*, 959-967.

Ringstad, N., Abe, N., and Horvitz, H.R. (2009). Ligand-gated chloride channels are receptors for biogenic amines in C. elegans. Science *325*, 96-100.

Risi, S., Zhang, J., Taarnby, R., Greve, P., Piskur, J., Liapis, A., and Togelius, J. (2014). The case for a mixed-initiative collaborative neuroevolution approach. arXiv preprint arXiv:14080998.

Rogan, M.T., Stäubli, U.V., and LeDoux, J.E. (1997). Fear conditioning induces associative long-term potentiation in the amygdala. Nature *390*, 604-607.

Rossi, D.J., and Hamann, M. (1998). Spillover-mediated transmission at inhibitory synapses promoted by high affinity alpha6 subunit GABA(A) receptors and glomerular geometry. Neuron *20*, 783-795.

Saint-Amant, L., and Drapeau, P. (2001). Synchronization of an embryonic network of identified spinal interneurons solely by electrical coupling. Neuron *31*, 1035-1046.

Schaefer, A., Reinhard, N.R., and Hordijk, P.L. (2014). Toward understanding RhoGTPase specificity: structure, function and local activation. Small GTPases *5*, 1-11.

Schafe, G.E., Nader, K., Blair, H.T., and LeDoux, J.E. (2001). Memory consolidation of Pavlovian fear conditioning: a cellular and molecular perspective. Trends in neurosciences *24*, 540-546.

Schnelzer, A., Prechtel, D., Knaus, U., Dehne, K., Gerhard, M., Graeff, H., Harbeck, N., Schmitt, M., and Lengyel, E. (2000). Rac1 in human breast cancer: overexpression, mutation analysis, and characterization of a new isoform, Rac1b. Oncogene *19*, 3013-3020.

Schuske, K., Beg, A.A., and Jorgensen, E.M. (2004). The GABA nervous system in C. elegans. In Trends in neurosciences, pp. 407-414.

Segal, M., and Andersen, P. (2000). Dendritic spines shaped by synaptic activity. Current opinion in neurobiology *10*, 582-586.

Serini, G., and Bussolino, F. (2004). Common cues in vascular and axon guidance. Physiology *19*, 348-354.

Sheffler-Collins, S.I., and Dalva, M.B. (2012). EphBs: an integral link between synaptic function and synaptopathies. Trends in neurosciences *35*, 293-304.

Shi, L., Fu, W.Y., Hung, K.W., Porchetta, C., Hall, C., Fu, A.K., and Ip, N.Y. (2007). Alpha2-chimaerin interacts with EphA4 and regulates EphA4-dependent growth cone collapse. Proceedings of the National Academy of Sciences of the United States of America *104*, 16347-16352.

Sigel, E., Baur, R., Kellenberger, S., and Malherbe, P. (1992). Point mutations affecting antagonist affinity and agonist dependent gating of GABAA receptor channels. Embo J *11*, 2017.

Squire, L.R. (1992). Memory and the hippocampus: a synthesis from findings with rats, monkeys, and humans. Psychological review *99*, 195.

Stanford, W.L., Cohn, J.B., and Cordes, S.P. (2001). Gene-trap mutagenesis: past, present and beyond. Nature reviews Genetics *2*, 756-768.

Stevens, C.F. (1998). A million dollar question: does LTP= memory? Neuron *20*, 1-2.

Stoeckli, E.T., and Landmesser, L.T. (1998). Axon guidance at choice points. Current opinion in neurobiology *8*, 73-79.

Szapiro, G., and Barbour, B. (2007). Multiple climbing fibers signal to molecular layer interneurons exclusively via glutamate spillover. Nature neuroscience *10*, 735-742.

Takasu, M.A., Dalva, M.B., Zigmond, R.E., and Greenberg, M.E. (2002). Modulation of NMDA receptor-dependent calcium influx and gene expression through EphB receptors. Science *295*, 491-495.

Takebayashi, H., Yoshida, S., Sugimori, M., Kosako, H., Kominami, R., Nakafuku, M., and Nabeshima, Y.-i. (2000). Dynamic expression of basic helix-loop-helix Olig family members: implication of Olig2 in neuron and oligodendrocyte differentiation and identification of a new member, Olig3. Mechanisms of development *99*, 143-148.

Tashiro, A., Minden, A., and Yuste, R. (2000). Regulation of dendritic spine morphology by the rho family of small GTPases: antagonistic roles of Rac and Rho. Cerebral cortex *10*, 927-938.

Taupin, P. (2007). BrdU immunohistochemistry for studying adult neurogenesis: paradigms, pitfalls, limitations, and validation. Brain research reviews *53*, 198-214.

Thomas, J.H. (1990). Genetic analysis of defecation in Caenorhabditis elegans. In Genetics, pp. 855-872.

Thompson, A.J., Lester, H.A., and Lummis, S.C.R. (2010). The structural basis of function in Cys-loop receptors. Quarterly reviews of biophysics *43*, 449-499.

Tolias, K.F., Bikoff, J.B., Burette, A., Paradis, S., Harrar, D., Tavazoie, S., Weinberg, R.J., and Greenberg, M.E. (2005). The Rac1-GEF Tiam1 couples the NMDA receptor to the activity-dependent development of dendritic arbors and spines. Neuron *45*, 525-538.

Tolias, K.F., Bikoff, J.B., Kane, C.G., Tolias, C.S., Hu, L., and Greenberg, M.E. (2007). The Rac1 guanine nucleotide exchange factor Tiam1 mediates EphB receptor-dependent dendritic spine development. Proceedings of the National Academy of Sciences *104*, 7265-7270.

Tolias, K.F., Duman, J.G., and Um, K. (2011). Control of synapse development and plasticity by Rho GTPase regulatory proteins. Progress in neurobiology *94*, 133-148.

Turrigiano, G.G. (1999). Homeostatic plasticity in neuronal networks: the more things change, the more they stay the same. Trends in neurosciences *22*, 221-227.

Turrigiano, G.G., and Nelson, S.B. (2000). Hebb and homeostasis in neuronal plasticity. Current opinion in neurobiology *10*, 358-364.

Um, K., Niu, S., Duman, J.G., Cheng, J.X., Tu, Y.-K., Schwechter, B., Liu, F., Hiles, L., Narayanan, A.S., and Ash, R.T. (2014). Dynamic control of excitatory synapse development by a Rac1 GEF/GAP regulatory complex. Developmental cell *29*, 701-715.

Van de Ven, T.J., VanDongen, H.M., and VanDongen, A.M. (2005). The nonkinase phorbol ester receptor alpha 1-chimerin binds the NMDA receptor NR2A subunit and regulates dendritic spine density. The Journal of neuroscience : the official journal of the Society for Neuroscience *25*, 9488-9496.

Van Praag, H., Shubert, T., Zhao, C., and Gage, F.H. (2005). Exercise enhances learning and hippocampal neurogenesis in aged mice. The Journal of Neuroscience *25*, 8680-8685.

Wagner, D.A., and Czajkowski, C. (2001). Structure and dynamics of the GABA binding pocket: a narrowing cleft that constricts during activation. The Journal of Neuroscience *21*, 67-74.

Wang, S.J., and Wang, Z.W. (2013). Track-a-worm, an open-source system for quantitative assessment of C. elegans locomotory and bending behavior. PloS one *8*, e69653.

Weber, W. (1999). Ion currents of Xenopus laevis oocytes: state of the art. In Biochimica et biophysica acta, pp. 213-233.

Wegmeyer, H., Egea, J., Rabe, N., Gezelius, H., Filosa, A., Enjin, A., Varoqueaux, F., Deininger, K., Schnütgen, F., and Brose, N. (2007a). EphA4-dependent axon guidance is mediated by the RacGAP α2-chimaerin. Neuron *55*, 756-767.

Wegmeyer, H., Egea, J., Rabe, N., Gezelius, H., Filosa, A., Enjin, A., Varoqueaux, F., Deininger, K., Schnütgen, F., Brose, N.*, et al.* (2007b). EphA4-Dependent Axon Guidance Is Mediated by the RacGAP α2-Chimaerin. Neuron *55*, 756-767.

Westh-Hansen, S.E., Witt, M.R., Dekermendjian, K., Liljefors, T., Rasmussen, P.B., and Nielsen, M. (1999). Arginine residue 120 of the human GABAA receptor α1, subunit is essential for GABA binding and chloride ion current gating. Neuroreport *10*, 2417-2421.

White, J.G., Southgate, E., Thomson, J.N., and Brenner, S. (1986a). The structure of the nervous system of the nematode Caenorhabditis elegans. In Philos Trans R Soc Lond, B, Biol Sci, pp. 1-340.

White, J.G., Southgate, E., Thomson, J.N., and Brenner, S. (1986b). The structure of the nervous system of the nematode Caenorhabditis elegans: the mind of a worm. Phil Trans R Soc Lond *314*, 1-340.

Wiens, K.M., Lin, H., and Liao, D. (2005). Rac1 induces the clustering of AMPA receptors during spinogenesis. The Journal of neuroscience : the official journal of the Society for Neuroscience *25*, 10627-10636.

Williams, R.S., Hauser, S.L., Purpura, D.P., DeLong, G.R., and Swisher, C.N. (1980). Autism and mental retardation: neuropathologic studies performed in four retarded persons with autistic behavior. Archives of Neurology *37*, 749-753.

Wotring, V.E., Miller, T.S., and Weiss, D.S. (2003). Mutations at the GABA receptor selectivity filter: a possible role for effective charges. J Physiol *548*, 527-540.

Wotring, V.E., and Weiss, D.S. (2008). Charge scan reveals an extended region at the intracellular end of the GABA receptor pore that can influence ion selectivity. J Gen Physiol *131*, 87-97.

Xie, Z., Srivastava, D.P., Photowala, H., Kai, L., Cahill, M.E., Woolfrey, K.M., Shum, C.Y., Surmeier, D.J., and Penzes, P. (2007). Kalirin-7 controls activity-dependent structural and functional plasticity of dendritic spines. Neuron *56*, 640-656.

Xu, N.-J., Sun, S., Gibson, J.R., and Henkemeyer, M. (2011). A dual shaping mechanism for postsynaptic ephrin-B3 as a receptor that sculpts dendrites and synapses. Nature neuroscience *14*, 1421-1429.

Yassin, L., Gillo, B., Kahan, T., Halevi, S., Eshel, M., and Treinin, M. (2001). Characterization of the deg-3/des-2 receptor: a nicotinic acetylcholine receptor that mutates to cause neuronal degeneration. Molecular and Cellular Neuroscience *17*, 589-599.

Yoshida, Y., Han, B., Mendelsohn, M., and Jessell, T.M. (2006). PlexinA1 signaling directs the segregation of proprioceptive sensory axons in the developing spinal cord. Neuron *52*, 775-788.

Yüksel, D., de Xivry, J.-J.O., and Lefèvre, P. (2010). Review of the major findings about Duane retraction syndrome (DRS) leading to an updated form of classification. Vision research *50*, 2334-2347.

Yuste, R. (2010). Dendritic spines (MIT Press).

Zhang, H., and Macara, I.G. (2006). The polarity protein PAR-3 and TIAM1 cooperate in dendritic spine morphogenesis. Nature cell biology *8*, 227-237.

Zhang, W., and Benson, D.L. (2000). Development and molecular organization of dendritic spines and their synapses. Hippocampus *10*, 512-526.

Zhang, W., and Benson, D.L. (2001). Stages of synapse development defined by dependence on F-actin. The Journal of Neuroscience *21*, 5169-5181.

Zhao, C., Deng, W., and Gage, F.H. (2008). Mechanisms and functional implications of adult neurogenesis. Cell *132*, 645-660.

Zhou, L., Jones, E.V., and Murai, K.K. (2012). EphA signaling promotes actin-based dendritic spine remodeling through slingshot phosphatase. Journal of Biological Chemistry *287*, 9346-9359.

Zoghbi, H.Y., and Bear, M.F. (2012). Synaptic Dysfunction in Neurodevelopmental Disorders Associated with Autism and Intellectual Disabilities. Cold Spring Harbor Perspectives in Biology *4*.